SYNCHRONIZATION, CHANNEL ESTIMATION AND DETECTION FOR ULTRA-WIDEBAND SYSTEMS

by

Ersen Ekrem

B. S., Electrical and Electronics Engineering, Boğaziçi University, 2006

Submitted to the Institute for Graduate Studies in
Science and Engineering in partial fulfillment of
the requirements for the degree of
Master of Science

Graduate Program in Electrical and Electronics Engineering
Boğaziçi University
2007

ACKNOWLEDGEMENTS

First of all, I would like to thank my thesis supervisor Prof. Dr. Hakan Deliç who introduced me to wireless communications and taught the research discipline. His thinking style and comments shortened my way.

I would like to thank Dr. Mutlu Koca for his supervision throughout this thesis. His valuable comments improved the quality of this thesis.

I would like to thank members of thesis jury, Prof. Ayşın Baytan Ertüzün and Dr. Fatih Alagöz, for their attentions to my thesis.

I am also so grateful to Dr. M. Kıvanç Mıhçak for not only his attendance to my thesis jury but also his friendship, support and encouragement. My future plans are shaped at his hands.

The long and painful hours spent on this thesis became an entertainment with the help of my friends: Cumhur Ozan Yalçın, Barış Özgül, Özgür Dalkılıç, Onur Özyeşil, and Ekin Şahin. I am sure that I could not find any friendlier colleagues.

I would appreciate two dear friends with them friendship and loyalty found its reflection on my life: Burak Eskici and Osman Kaytazoğlu.

Lastly, I would thank my family, mom and sister. They are always like lighthouses to find my direction in the world.

This thesis was supported by TÜBİTAK EEEAG under grants 105E034 and 105E077. The ideas, views and conclusions expressed herein do not represent the official view of TÜBİTAK.

ABSTRACT

SYNCHRONIZATION, CHANNEL ESTIMATION AND DETECTION FOR ULTRA-WIDEBAND SYSTEMS

Timing acquisition and synchronization of *ultra-wideband* UWB signals within nanosecond accuracy pose a major impediment. Noise is assumed to be *additive white Gaussian noise* (AWGN) in all of the works in spite of that impulsive noise in indoor environments. Therefore, we propose two robust acquisition algorithms. These receivers rely on robust estimation techniques and *transmitted reference* (TR) methodology. Then, the algorithms are extended to multiuser environments by assuming *multiuser interference* (MUI) as a white Gaussian *random variable* (r.v.) invoking *central limit theorem* (CLT).

The another point about synchronization of UWB signals is the multiuser synchronization under *intersymbol interference* (ISI). Two iterative synchronization algorithms are proposed for chip-level interleaved UWB signals subject to ISI and MUI. One of the algorithms is blind and the other is data-aided both of which are *soft input soft output* (SISO) devices. Moreover, data-aided approach uses the training sequence to form an initial estimate of the *a posteriori probabilities* (APPs) of the time-delays.

Another challenge for UWB is the channel estimation due to high number of parameters to be estimated. Most of the attention is devoted to non-coherent demodulation or *frequency-domain* (FD) techniques due to their low-complexities. But most of the works do not present a detailed comparison of *time-domain* (TD) and FD channel estimation and assume that noise is AWGN. Therefore, the robust FD and TD recursive channel estimators are presented with their convergence analysis. Moreover, robust detectors are designed and their probability of error performance is investigated.

ÖZET

ULTRA GENİŞ BANT SİSTEMLER İÇİN EŞZAMANLAMA, KANAL KESTİRİMİ VE SEZİM

Ultra geniş bant (UGB) nanosaniye uzunluğunda darbeler kullandığından dolayı, sinyalin bu hassasiyetle edinimi UGB için önemli bir sorun teşkil etmektedir. Tüm bu çalışmalarda gürültü *toplanabilir beyaz Gauss gürültüsü* (TBGG) kabul edilmiştir. Oysaki UGB nin de başlıca uygulama alanı olan bina içi ortamlarda gürültü dürtün gürültü niteliği kazanmaktadır. Dolayısıyla, gürbüz sinyal ediniciler tasarlanmıştır. Bu sinyal ediniciler gürbüz kestirim yöntemleri ve *gönderilen referans* (GR) mantığına dayanmaktadır. Daha sonra gürbüz sinyal ediniciler, *çoklu kullanıcı girişimini* (ÇKG) beyaz Gauss gürültü kabul ederek çoklu erişim ortamlarına da uygulanmıştır.

Diğer bir nokta ise çoklu kullanıcıların *simgelerarası girişim* (SG) altında eşzamanlanmasıdır. Hem SG hem de ÇKG ye maruz kalmış, yonga düzeyinde serpiştirilmiş UGB sinyaller için döngülü eşzamanlama yöntemleri önerilmiştir. Bunlardan biri kör diğeri ise veri yardımlı olmakla birlikte her ikisi de doğrudan yumuşak bilgi üzerinde çalışıp yumuşak bilgi üretmektedirler. Veri yardımlı yöntem, eğitim dizisinden gecikme zamanları hakkında yumuşak başlangıç bilgileri çıkarıp performans kazancı sağlamaktadır.

UGB için diğer bir güçlük ise parametre sayısının fazlalılığı nedeniyle kanal kestirimidir. Bu sebeple araştırmaların çoğu ya evre uyumsuz yapılara yönelmiş yada *frekans düzleminde* (FD) çözümü aramışlardır. Fakat FD de kanal kestirimine odaklanan çalışmalarda FD ile *zaman düzleminin* (ZD) ayrıntılı bir karşılaştırması sunulmamış ve çalışmalarda gürültü TBGG olarak kabul edilmiştir. Gürbüz özyineli FD ve ZD kanal kestiricileri sunulmuş, yakınsama analizleri yapılmıştır. Gürbüz FD ve ZD seziciler tasarlanmış, kanal kestirim hataları da hesaba katılarak BHO ları türetilmiştir.

TABLE OF CONTENTS

LIST OF FIGURES

LIST OF TABLES

LIST OF SYMBOLS/ABBREVIATIONS

$\lfloor\ \rfloor$	Integer floor operation
$\|\ \|$	Absolute value
$\|\|\ \|\|$	L-2 norm
$*$	Linear convolution
$\star$	Circular convolution
$\odot$	Hadamard product
$()^T$	Transpose
$()^{-1}$	Inverse
$()^*$	Complex conjugate
$x \doteq y$	x and y differ by a multiplicative constant
$\mathbf{0}_k$	$k \times 1$ column vector with all zero entries
a	Bias of minimum mean square error estimator
$\text{APP}(b_u(i))$	A posteriori probability of uth user's ith bit
$\text{APP}(s_u(i))$	A posteriori probability of uth user's ith chip
$\text{APP}^b(m_u = l)$	A posteriori probability of uth user's time-delay obtained blindly
$\text{APP}^t(m_u = l)$	A posteriori probability of uth user's time-delay obtained via training sequence
$\arg\max$	Argument of maximum
$\arg\min$	Argument of minimum
B	Bandwidth
$b(n)$	nth information bit for single user links
$\mathcal{B}_{i,l}^u$	The chips corresponding to ith bit of uth user given that time-delay is l
$b_u(n)$	nth information bit of uth user
$c(i)$	ith time-hopping code for single user links
$\mathbf{C}$	Covariance matrix of the chips at the output of the channel
C_g	Energy of the received frame
$\hat{C}_{g,avg}$	Channel gain estimate obtained via averaged template

$\hat{C}^{\ell}_{g,avg}$	Channel gain estimate at the ℓth step of estimation via averaged template
$\hat{C}_{g,ss}$	Channel gain estimate obtained via successive sampling
$\hat{C}^{\ell}_{g,ss}$	Channel gain estimate at the ℓth step of estimation via successive sampling
$c_u(n)$	nth time-hopping code of uth user
$\mathbf{C}_s$	Covariance matrix of chips
$\mathbf{C}^u_\alpha$	Covariance matrix of the output of uth user's data-aided synchronization block
$\mathbf{C}^u_\eta$	Covariance matrix of uth user's noise plus interference
$\mathrm{cov}(x, y)$	Covariance of x and y
$\mathrm{cov}(x, y \mid z)$	Covariance of x and y conditioned on z
$d_u(l)$	Interleaved and spreaded information bits of uth user
$d'_u(l)$	Spreaded information bits of uth user
$\mathbf{d}_{u,i}$	Unit vector for ith chip of uth user
$\mathcal{E}(L)$	Cost function of time-domain maximum likelihood channel estimator aiming to estimate L paths of the channel
$E\{x\}$	Expected value of x
$E\{x \mid y\}$	Expected value of x conditioned on y
$\mathbf{e}_n$	Time-domain error vector at the nth step
$\mathbf{E}_n$	Frequency-domain error vector at the nth step
$E_{u,r}$	Energy of uth user's received symbol
E_r	Energy of the received symbol in a single user link
E_s	Energy of the transmitted symbol in a single user link
$E_{T,r}$	Sum of all users' received symbols' energies
$E_{u,s}$	Energy of uth user's transmitted symbol
exp	Exponential function
$\mathrm{EXT}(s_u(i))$	Extrinsic information about uth user's ith chip
$f(x)$	Probability density function of Gaussian-mixture noise model
$\mathcal{F}_\epsilon$	Family of probability density functions
$f_{avg}(x)$	Probability density function of $\omega_{avg}(m)$
f_c	Carrier frequency

$f_I(x)$	Probability density function of shot noise
$f_{LF}(x)$	Least favorable probability density function
$f_{ma}(x)$	Probability density function of all disturbances, i.e. noise plus multiple access interference, at the output of the correlator in averaged template
$f_{ss}(x)$	Probability density function of $\omega_{ss}(m)$
$f_{ss,1}(x)$	Probability density function of $\omega_{ss,1}(m)$
$f_{ss,2}(x)$	Probability density function of $\omega_{ss,2}(m)$
$f_{ss,2}(x)$	Probability density function of $\omega_{ss,2}(m)$
$\mathbf{f}_{u,i}$	Minimum mean square estimator for ith chip of uth user
$f_{\omega_{ma,1}}(x)$	Probability density function of $\omega_{ma,1}(m)$
$f_{\omega_{ma,2}}(x)$	Probability density function of $\omega_{ma,2}(m)$
$f_{\omega_{ma,3}}(x)$	Probability density function of $\omega_{ma,3}(m)$
$\mathbf{g}$	Column vector collecting samples of the aggregate channel response
$\mathbf{G}$	Column vector collecting fast Fourier transforms of aggregate channel response samples
$g(x;\mu,\sigma^2)$	Gaussian probability density function with mean μ and variance σ^2
$g_u(j)$	Chip-level spreading sequence of uth user
$\hat{\mathbf{g}}$	Robust time-domain aggregate channel response estimate
$\hat{\mathbf{g}}_n$	Robust time-domain aggregate channel response estimate at nth step
$\hat{\mathbf{g}}_{td,m}$	Time-domain linear aggregate channel response estimate
$\hat{\mathbf{G}}_n(m)$	Robust frequency-domain aggregate channel response estimate at nth step
$\hat{\mathbf{G}}_{fd,m}(l)$	Frequency-domain linear aggregate channel response estimate
$h(t)$	Channel response for single user links
$H(l)$	Fast Fourier transform of samples of the channel response
$h(mT)$	mth sample of the channel response
$\hat{\mathbf{h}}$	Time-domain robust channel estimate
$\mathbf{h}$	Channel column vector collecting path gains to be estimated
$\tilde{\mathbf{h}}$	Channel column vector

$\hat{\mathbf{h}}_n$	Time-domain robust channel estimate at the nth step
$\mathbf{H}$	Channel matrix
H_0	The hypothesis denoting the case that -1 was transmitted
H_1	The hypothesis denoting the case that $+1$ was transmitted
$\mathbf{H}_u$	Channel matrix of uth user
$h^u(t)$	Channel response of the uth user
h_l	lth path gain of the channel for single user links
h_l^u	lth path gain of the uth user
$\hat{\mathbf{h}}_{td}$	Time-domain liner channel estimate
$\mathbf{I}$	Identity matrix
$\Im(x)$	Imaginary part of x
$J(\hat{\mathbf{G}}_n(m))$	Cost function of frequency-domain recursive channel estimator
$J(\hat{\mathbf{h}}_n)$	Cost function of time-domain recursive channel estimator
$\mathcal{J}_i^u$	Possible time-delays for uth user given that ith chip is a data chip
$\mathcal{J}_i^{u^c}$	Possible time-delays for uth user given that ith chip is not a data chip
k	Trimming parameter
$\mathbf{K}_h^n$	Covariance matrix of robust time-domain channel estimate at the nth step
$\mathbf{K}_{h,td}$	Covariance matrix of time-domain linear channel estimate
$\tilde{L}$	Maximum number of paths for single user links
$L_{\max}$	Maximum path number
L_u	Path number of uth user's channel
lim	Limit operator
log	Natural logarithm
m_u	Time-delay of uth user in frame-level
$\hat{m}_u$	Estimate of frame-level time-delay of uth user
max	Maximum function
min	Minimum function
$\mathbf{n}$	Noise vector for additive white Gaussian noise

$n(t)$	Additive white Gaussian noise
$\mathcal{N}(x, \sigma^2)$	Gaussian random variable with mean x and variance σ^2
N	Number of samples taken per data part of the received symbol
N_0	Variance of background noise
N'	Number of samples taken per cyclic prefix
N_c	Number of chips
N_f	Number of frames
$\tilde{n}_f$	Energy partition ratio in a single user link
$\hat{n}_{f,avg}$	Frame-offset estimate obtained via averaged template
$\hat{n}_{f,ss}$	Frame-offset estimate obtained via successive sampling
$\hat{\tilde{n}}_{f,avg}$	Estimate of the energy partition ratio obtained via averaged template in a single user link
$\hat{\tilde{n}}_{f,ss}$	Estimate of the energy partition ratio obtained via successive sampling in a single user link
N_G	Number of guard frames
N_p	Number of bits per packet
N_t	Number of training symbols
N_u	Number of users
$n_{u,f}$	Time-delay of the first path of uth user's channel in frame-level
$\tilde{n}_{u,f}$	Energy partition ratio of uth user
NMSE($\hat{n}_{f,ss}$)	Normalized mean square error of $\hat{n}_{f,ss}$
NMSE($\hat{\mathbf{G}}$)	Normalized mean square error of $\hat{\mathbf{G}}$
$\mathcal{O}(x)$	On the order of x
$\mathbf{P}$	Matrix whose columns are formed by $\mathbf{p}_i$s corresponding to the paths to be estimated
$\tilde{\mathbf{P}}$	Matrix whose columns are formed by all $\mathbf{p}_i$s
$p(t)$	Pulse waveform
$P^m_{e,fd}$	Probability of error of frequency-domain matched filter
$P^r_{e,fd}$	Probability of error of frequency-domain robust detector
$P^m_{e,td}$	Probability of error of time-domain matched filter
$P^r_{e,td}$	Probability of error of time-domain robust detector

$p_r(t)$	Received symbol waveform in a single user link
$\mathbf{p}_i$	Column vector for the samples of transmitted symbol shifted by ith path
$P_s(l)$	Fast Fourier transform of samples of transmitted symbol's waveform
$p_s(mT)$	mth sample of transmitted symbol waveform
$p_s(t)$	Transmitted symbol waveform in a single user link
$p_{u,r}(t)$	uth user's received symbol waveform
$p_{u,s}(t)$	uth user's transmitted symbol waveform
$r(t)$	Received signal
$q(x)$	Robust frequency-domain recursive estimator's clipping function
$Q(x)$	Q function
$\mathbf{R}$	Channel projection matrix
$\mathbf{r}$	Column vector of chip-matched filter
$\bar{r}(t)$	Averaged received signal
$r_{avg}(m)$	Correlator output in averaged template
$R_B(t-u)$	Autocorrelation function of $w_B(t)$
$\mathbf{r}^d$	Column vector of chip-matched filter for the data-sequence
$R_I(t-u)$	Autocorrelation function of $w_I(t)$
$R_n(t)$	Autocorrelation of $n(t)$
$r_s(t)$	Signal part of $r(t)$
$r_{ss}(m)$	Correlator output in successive sampling
$R_{ss}(\tau)$	Autocorrelation function of $\omega_{ss}(m)$
$\mathbf{r}^t$	Column vector of chip-matched filter for the training sequence
$\Re(x)$	Real part of x
$s(t)$	Transmitted signal
$\mathbf{s}$	Chip vector
$\tilde{\mathbf{s}}$	Mean of the chip vector
$\mathcal{S}_{i,l}^u$	The chips corresponding to the same information bit with ith chip of uth user
$\mathbf{s}_t^u$	Training chip vector of uth user

$\mathbf{s}_u$	Chip vector of uth user
$s_u(i)$	ith chip of uth user
$\tilde{s}_u(i)$	Mean of uth user's ith chip
$\hat{\mathbf{s}}_u$	Estimate of uth user's chip vector
$\hat{s}_u(i)$	Estimate of uth user's ith chip
$s_u(t)$	Transmitted signal of uth user
sgn()	Signum function
T	Sampling period
T_c	Chip duration
T_f	Frame duration
$T_{fd,m}(l)$	Output of frequency-domain matched filter
$T_{fd,r}(m)$	Decision statistic of frequency-domain robust decision rule
T_p	Pulse duration
T_s	Symbol duration
$T_{td,m}$	Output of time-domain matched filter
$T_{td,r}(m)$	Decision statistic of robust time-domain decision rule
Tr	Trace operator
var(x)	Variance of x
var($x \mid y$)	Variance of x conditioned on y
W	Bandwidth of the front-end filter
$w(t)$	Background noise modelled by a Gaussian-mixture
$\bar{w}(t)$	Averaged noise
$w_B(t)$	Thermal noise
$w_I(t)$	Shot noise
$\mathbf{w}_j$	Column vector for samples of Gaussian-mixture noise taken during jth received symbol
$\mathbf{W}_j$	Column vector collecting fast Fourier transforms of noise samples
$W_j(l)$	Fast Fourier transform of noise samples
$w_j(mT)$	mth sample of Gaussian-mixture noise taken during jth received symbol
$y(t)$	Received signal for single user links

$y(j(T_s + N_G T_f) + mT)$	Samples of the received signal
$\mathbf{y}$	Column vector for samples of received symbol
$\mathbf{y}_j$	Column vector for samples of jth received symbol
$\mathbf{Y}_j$	Column vector collecting fast Fourier transforms of received waveform's samples
$Y_j(l)$	Fast Fourier transform of received waveform's samples
$y_j(m)$	mth sample of jth received symbol
$z_n(m)$	Normalizing factor of robust frequency-domain recursive estimator
α	Step size of the modified residuals algorithm
α_1	Constant
α_2	Constant
α_l^u	Output of uth user data-aided synchronization block given that time-delay is l
β	Constant
γ	Expected value of the noise at the output frequency-domain clipping function
$\delta(t)$	Dirac delta function
δ_{ij}	Kronecker's delta function
$\mathbf{\Delta}_\mu^u$	Diagonal matrix whose diagonal entries are mean of uth user's minimum mean square error filter output
$\Delta\hat{\mathbf{G}}_n$	Robust frequency-domain aggregate channel estimate error at nth step
$\Delta\hat{\mathbf{G}}_{fd,m}(l)$	Frequency-domain linear aggregate channel estimate error
$\Delta\hat{\mathbf{h}}_n$	Robust time-domain channel estimate error at nth step
ϵ	Relative frequency of outliers
$\eta_u(i)$	Noise plus interference at the output of minimum mean square error filter for uth user's ith chip
$\boldsymbol{\eta}_u(i)$	Column vector of noise plus interference
θ_u	Time-delay of the first path of uth user's channel in pulse-level
$\Theta_{u,l}$	Cross-correlation between uth and lth user's received waveform

ϑ	Random timing-uncertainty due to time-hopping codes and pulse-level time-delay
κ	Relative variance of impulsive component with respect to nominal noise variance
λ	Forgetting factor
$\bar{\lambda}(n)$	Sum of forgetting factor's geometric series
$\mathbf{\Lambda}_l^u$	uth user's time-shift matrix given that time-delay is l
μ_{avg}	Mean of the correlator output in averaged template
$\hat{\mu}_{avg}$	Estimate of the mean of the correlator output obtained via averaged template
$\hat{\mu}_{avg}^{\ell}$	Estimate of the mean of the correlator output at the ℓth step of estimation via averaged template
μ_{ss}	Mean of the correlator output in successive sampling
$\hat{\mu}_{ss}$	Estimate of the mean of the correlator output obtained via successive sampling
$\hat{\mu}_{ss}^{\ell}$	Estimate of the mean of the correlator output at the ℓth step of estimation via successive sampling
$\mu_u(i)$	Mean of minimum mean square error filter output for uth user's ith chip
$\boldsymbol{\mu}_{\alpha}^{u}$	Mean vector of uth user's data-aided synchronization block's output
$\mu_{td,m}$	Mean of output of time-domain matched filter
$\mu_{td,r}$	Mean of robust time-domain decision rule
$\mu_{fd,m}(l)$	Mean of output of frequency-domain matched filter
$\mu_{fd,r}$	Mean of robust frequency-domain decision rule
ν_{asy}^2	Asymptotic variance of $M-$estimates
ν_{avg}^2	Asymptotic variance of $\hat{\mu}_{avg}$
$\nu(x)$	Arbitrary symmetric probability density function
$\nu_{fd,r}^2$	Variance of robust frequency-domain decision rule
$\nu_{fd,m}^2(l)$	Variance of output of frequency-domain matched filter
$\nu_u^2(i)$	Variance of uth user's ith chip's estimate obtained via minimum mean square error filter
ν_{ss}^2	Asymptotic variance of $\hat{\mu}_{ss}$

$\nu^2_{td,r}$	Variance of robust time-domain decision rule
$\nu^2_{td,m}$	Variance of output of time-domain matched filter
$\xi_1(m)$	First part of $\omega_{mui}(m)$
$\xi_2(m)$	Second part of $\omega_{mui}(m)$
Π_u	Interleaver function
Π_u^{-1}	Deinterleaver function
$\rho(x)$	$M-$estimator for the least favorable probability density function
$\rho_{avg}(x)$	Cost function of averaged template
$\rho_{ma}(x)$	Cost function of averaged template under multiple access interference
$\rho_{ss}(x)$	Cost function of successive sampling
σ^2_{avg}	Variance of the nominal noise at the output of the correlator for averaged template
σ^2	Variance of the background noise
σ^2_{ma}	Variance of $\omega_{ma}(m)$
σ^2_{mui}	Variance of $\omega_{mui}(m)$
σ^2_{ss}	Variance of the nominal noise at the output of the correlator for successive sampling
τ_l	Time-delay of lth path for single user links
τ^u_l	Time-delay of lth path of uth user's channel
τ_{max}	Maximum delay spread of the channel
$\phi(x)$	Gaussian probability density function with zero mean and unit variance
χ	Random time-uncertainty
$\psi(x)$	Clipping function, i.e. derivative of $\rho(x)$
$\psi'(x)$	Derivative of $\psi(x)$
$\psi_{avg}(x)$	Derivative of $\rho_{avg}(x)$
$\psi_{ss}(x)$	Derivative of $\rho_{ss}(x)$
$\mathbf{\Omega}$	Diagonal matrix whose entries are the variance of the robust time-domain channel estimate
$\omega_{avg}(m)$	Noise at the correlator output in averaged template

$\omega_{ma}(m)$	Noise at the correlator output in averaged template in the presence of multiple access
$\omega_{ma,1}(m)$	First part of $\omega_{ma}(m)$
$\omega_{ma,2}(m)$	Second part of $\omega_{ma}(m)$
$\omega_{ma,3}(m)$	Third part of $\omega_{ma}(m)$
$\omega_{mui}(m)$	Multiuser interference at the correlator output in averaged template
$\omega_{ss}(m)$	Noise at the correlator output in successive sampling
$\omega_{ss,1}(m)$	First part of the noise at the correlator output in successive sampling
$\omega_{ss,2}(m)$	Second part of the noise at the correlator output in successive sampling
$\omega_{ss,3}(m)$	Third part of the noise at the correlator output in successive sampling

A1	Assumption one
A2	Assumption two
A3	Assumption three
APP	A *posteriori* probability
AWGN	Additive white Gaussian noise
BER	Bit error rate
BJCR	Bah-Jelinek-Cocke-Raviv algorithm
CDMA	Code division multiple access
CM1	Channel model one
CM4	Channel model four
CMSE	Conditional mean square error
CLT	Central limit theorem
CSI	Channel state information
DS	Direct sequence
EM	Expectation maximization algorithm
FCC	Federal Communications Commission
FD	Frequency-domain

FFT	Fast Fourier transform
GPS	Global positioning system
IF	Intermediate frequency
IFI	Interframe interference
i.i.d.	identically and independently distributed
ISI	Intersymbol interference
LAN	Local area networks
LLR	Log-likelihood ratio
LOS	Line-of-sight
LR	Likelihood ratio
LMS	Least mean squares
MAI	Multiple access interference
ML	Maximum-likelihood
MMSE	Minimum mean square error
MUI	Multiuser interference
MUSIC	Multiple signal classification
NLOS	Non-line-of-sight
NMSE	Normalized mean square error
OFDM	Orthogonal frequency division multiplexing
PAM	Pulse amplitude modulation
PAN	Personal area networks
PDF	Probability density function
PMF	Probability mass function
PPM	Pulse position modulation
PWAM	Pilot waveform assisted modulation
RLS	Recursive least squares
r.v.	random variable
SC-FDE	Single carrier frequency domain equalization
SIC	Soft interference cancellation
SINR	Signal-to-noise-interference ratio
SISO	Soft input soft output

SNR	Signal-to-noise ratio
SV	Saleh-Valenzuela
TD	Time-domain
TDMA	Time division multiple access
TH	Time hopping
TR	Transmitted reference
UWB	Ultra-wideband
WLAN	Wireless local area networks

1. INTRODUCTION

UWB technology is defined as any wireless transmission scheme that occupies a fractional bandwidth $B/f_c > 20\%$ where B is the transmission bandwidth and f_c is the carrier frequency, or more than 500MHz absolute bandwidth [1]. This large bandwidth is attained via ultra short pulses, typically on the order of nanoseconds which are free of sine-wave carriers enabling such systems to operate directly at baseband without any *intermediate frequency* (IF) processing. By using such ultra-short pulses, UWB systems occupying an enormous bandwidth come up with unique advantages such as [2]

- enhanced capability to penetrate through obstacles,
- ultra high precision at the centimeter level,
- potential for achieving very high data rates with an increased multiuser efficiency,
- potentially small size and processing power,
- low cost transceivers,
- resistance to jamming, i.e. high processing gain.

In spite of these advantages, use of UWB system was limited to military applications, especially for radar systems until April 2002 when U. S. *Federal Communications Commission* (FCC) released use of UWB systems over a bandwidth of 7.5GHz, from 3.1GHz to 10.6Ghz, operating at noise floor [3]. After U. S. FCC allowed deployment of UWB devices in April 2002, UWB has attracted a rapidly increasing interest from both academia and industry, and regulatory efforts has started in both Europe and Japan similar to U. S. FCC's First Report and Order. As a reflection of this interest, an annual conference on solely dedicated to UWB technology started to be organized [4] and two issues of *IEEE Journal of Selected Areas in Communications* [5, 6] are dedicated to UWB. Moreover, both *IEEE Transactions on Microwave Theory and Techniques*[7] and *Eurasip Journal on Applied Signal Processing* [8] dedicated their one issue to UWB. Also, survey papers about UWB are published [1, 2].

Despite this renewed interest, the history of UWB can be traced to a century ago, to the invention of radio by Guglielmo Marconi because of the fact that radio communications use an enormous bandwidth at its early stages due to spark gap transmitters. However, modern UWB technology has been around since 1960s by the invention of impulse radars [9]. Starting with this invention, UWB systems are rather employed for military applications because of the facts that its fine resolution capabilities enable very accurate localization and imaging and that its robustness to jamming enables secure communication. Within the academic context, UWB investigations was pioneered by Prof. Scholtz and his group [10] since 1990s, whose focus was on low-rate applications of UWB.

Combining with recent developments in high-speed switching and narrowband pulse generation technology, U. S. FCC's release prompted very academic and industrial institutions to have a fresh look on UWB. These efforts lead a spread of UWB from military applications to consumer electronics with the hope of that UWB may resolve many long-existing problems in short-range wireless networks. These problems include high-speed, short-range networking in support of a variety of potential low-cost, low-power multimedia transport applications in various indoor environments and peer-to-peer communication of mobile wireless devices such as laptops for which the existing systems such as IEEE 802.11 *local area networks* (LANs) and Bluetooth *personal area networks* (PANs) fail. Therefore, UWB is now believed to be a stronger alternative for short-range wireless applications than IEEE 802.11 LANs and Bluetooth PANs.

In this introductory chapter, a general overview of UWB systems will be presented from a physical layer viewpoint. In Section 1.1, application areas of UWB systems will be explained. Section 1.2 will discuss the physical layer problems that should be solved in order to take the advantage of UWB systems where the primary focus will be along the direction of the problems addressed throughout the thesis. In Section 1.4, scope of the thesis will be drawn by clarifying the problems addressed in this thesis. Section 1.5 will conclude this introductory chapter with the outline of the rest of the thesis.

1.1. Applications

UWB finds itself wide and diverse application areas such as wireless networks, sensor networks, imaging systems and vehicular radar systems. Although, our focus on this thesis will be on the physical layer problems of UWB systems employed for wireless communication, its wide application areas will be briefly summarized in this section as follows [1, 2]:

- **Wireless networks:** Wireless networks, especially PANs, require connectivity of various types of electronic devices, reliable and fast file exchange between them, and cable replacement. UWB seems to fulfill these requirements because of its high data rate, low-complexity and power efficiency.
- **Sensor networks:** Sensor networks are more stringent in terms of power efficiency than wireless networks because of the difficulty in recharging batteries. Since UWB systems' duty cycle is very low and their receiver structures are rather simple, their power saving capability can be better than many existing structures such as Bluetooth implying its candidacy for sensor networks.
- **Imaging systems:** Since duration of UWB pulses is on the order of nanoseconds, their wavelength is smaller than the dimension of many targets. This leads to a pronounced sensitivity of UWB pulses to the scattering environment which results in a better resolution and identification of the targets. As a consequence, UWB systems are adopted to medical, ocean and through-wall imaging devices.
- **Vehicular radar systems:** The pronounced sensitivity to the scattering environment makes UWB systems also a promising candidate for vehicular radar systems to improve the resolution of conventional proximity and motion sensors. Therefore, UWB systems are expected to have applications in automotive industry via collision avoidance and/or road assistance and in home security via proximity detectors.

1.2. UWB Communications at the Physical Layer

In this section, physical layer problems of UWB systems will be outlined which stimulated research topics considered in this thesis. To take full advantage of UWB, low-complexity and power-efficient receivers should be designed. However, major impediments against this goal are acquisition of UWB signals within nanosecond accuracy and highly pronounced multipath diversity of a typical UWB channel.

1.2.1. Timing Acquisition and Synchronization

Timing acquisition and synchronization are the first two tasks to be performed at the receiver for demodulation. Timing acquisition refers to reduction of timing uncertainty into frame level and synchronization refers to localization of the received signal at the pulse level. Although these two inherently related tasks are generally combined and performed by a single unit for narrowband systems, for UWB case, individual treatments of these two tasks can yield more efficient solutions because of

- ultra short pulses,
- low-duty cycle,
- long spreading codes,
- low power constraints.

Ultra short pulses aim to achieve high-data rates via using all spectrum assigned to UWB. Low-duty cycle and long-spreading codes are necessary for efficient multiple access strategies. The low power constraints is an official regulation [3] for UWB systems aiming them to overlay with already existing services at its huge bandwidth such as the *global positioning system* (GPS) and IEEE 802.11 *wireless local area networks* (WLANs). The first three result in a large search space to be tracked for acquisition of received signal, i.e. long acquisition times, or in other words, slow acquisition. Moreover, combining with the last one, the acquisition probabilities of traditional techniques such as phase locked loops and early-late gate synchronizers fail due to difficulties re-

lated with sufficient energy capture [11].

Motivated by these observations, an exhaustive research effort has been devoted to this topic. First category of these researches aims to improve traditional acquisition techniques via proposing alternative search algorithms or search space reduction techniques for the ultra-wide search space of the timing uncertainty [12, 13, 14, 15, 16, 17]. The other category instead of trying to extend existing solutions, basically relies on estimation theoretic approaches [18, 19, 20, 21, 22]. Although the latter approach is more appropriate for timing acquisition, a new challenge appears as to acquire a reliable statistic without any channel knowledge. Since prior to synchronization, channel is unknown to receiver and the channel models proposed for UWB do not allow analytical tools [23], most estimation-based methods rely on noncoherent reception techniques to alleviate channel-related complications.

Therefore, the most practical way of achieving a rapid and reliable timing seems to be a combination of these two approaches [24]. Timing acquisition can be better implemented via estimation based approaches and synchronization task better suits search techniques based on threshold-detection. For a comprehensive survey of timing acquisition and synchronization for UWB signals, reader can refer to [25].

1.2.2. Channel Estimation

Although channel estimation is also critical in the context of any other wideband systems such as *code-division multiple access* (CDMA) and there exits many well-established channel estimation algorithms for these systems, two major issues prevent direct adoption of these algorithms to UWB. First is that required sampling rates become at the orders of GHzs and that rates cannot be reached any technology today. Second is that number of parameters to be estimated can be as large as 400 for a typical UWB indoor channel resulting in unaffordable complexity. These two impediments are due to ultra-short duration of the pulses employed for UWB because of

- that as time-duration gets shorter, the signal occupies a wider bandwidth resulting in an increase of required sampling rates,
- that as pulse gets narrower, channel resolvability increases, i.e. more and more paths are resolved increasing the number of parameters to be estimated.

Keeping these in mind, two different research branches have grown up for channel estimation. First one collects the *maximum likelihood* (ML) or ML-like estimation techniques where most of the existing literature has tried to get adjusted according to UWB meeting its specific requirements and the second category collects the methods relying on only first and second order statistics of the channel, i.e. a way from semi-noncoherent to noncoherent demodulation.

The earlier works in the first branch started with adoption of classical ML criterion to channel estimation in TD [26, 27, 28, 29] and later on the interest moved to FD techniques such as *orthogonal frequency division multiplexing* (OFDM) [30, 31, 32] and *single carrier frequency domain equalization* (SC-FDE) [33, 34, 35, 36] due to their lower complexities. As a consequence of these efforts, two proposals are manifested one of which suggests a time-frequency interleaved OFDM [37] and the other suggests multiband OFDM [38]. But how the classical drawbacks of OFDM such as peak-to-average power ratio and need for channel coding will be alleviated remains to be an open problem.

Also a serious attention has been paid to the second category to which *pilot waveform assisted modulation* (PWAM) and TR systems belong [39, 40, 41, 42, 43]. Both TR and PWAM obtain an estimate of aggregate channel response's analog waveform via averaging. However, these methods suffer from noise enhancement during demodulation because of using noisy templates. Moreover, their implementation for channels subject to ISI and *multiple access interference* (MAI) seems to be problematic. Noncoherent and differential receivers also attracted so much interest to bypass the channel estimation task [44, 45]. Yet, the problems such as how to handle noise enhancement, MUI and ISI still exist. Therefore, it is more realistic for UWB systems to stand at

some midpoint to simplify channel estimation task partially by giving up a fraction of data rate.

1.3. Scope of the Thesis

In this section, we will explain the problems addressed in this thesis. The problems will be announced with their background and the methodologies used in the proposed solutions will be outlined.

1.3.1. Timing Acquisition under Non-Gaussian Noise

Although timing acquisition methods, taking the aforementioned difficulties into account, are proposed, noise characteristic of the indoor environments, where UWB devices will be commonly deployed, is overlooked and is simply assumed to be AWGN. However, as stated in [46], indoor environments are subject to noise produced by photocopiers, printers, elevators, etc. in the office, which is of impulsive (non-Gaussian) in nature. Since the linear estimators designed to operate under AWGN suffer from a performance deterioration when they are subject to impulsive noise described by a heavier tailed *probability density function* (PDF), alternative robust acquisition methods should be in the order. Therefore, one of the problems to be considered in this thesis is decided to be timing acquisition of UWB signals under non-Gaussian noise.

For this problem, we applied the robust signal processing techniques combining them with TR methodology. The former are the robust procedures designed in minimax sense such that if some parameters in the system model are not known exactly, but rather they are known to lie in a certain family, the optimum receiver corresponding to the worst case in this family is adopted. Therefore, if the family capturing the uncertainty is wide, the resulting robust method can become overconservative and can lead a significant performance loss in nominal, highly expected, situation. But if the uncertainty is tolerable, in addition to substantial performance gains obtained for the deviations from the nominal case, there does not exist any significant performance loss for the nominal case. For a detailed treatment of this subject, reader can refer

to [47]. The latter, use of TR methodology, is decided to bypass channel estimation and to work with low-sampling rates. Therefore, proposed receivers work with samples at taken symbol rate without any channel knowledge and they are operational for both *time-hopping* (TH) and *direct-sequence* (DS) UWB. Moreover, proposed robust receivers are also extended to multiuser environment by treating MUI as a Gaussian r.v.

1.3.2. Multiuser Synchronization under ISI

Although the impact of low-duty cycle, ultra short duration pulses and low power constraints on the synchronization is a well-studied topic [12, 13, 14, 15, 16, 17, 18, 19, 20, 21, 22] , most of the existing works are limited to single user links or just they are adopted to multiuser environment by assuming MUI as white Gaussian noise with a few exceptions [48, 49]. Moreover, the effect of ISI on synchronization is not also considered in most of the works in spite of the extreme delay spread of the UWB channels. In the light of these issues, multiuser synchronization for UWB systems under ISI channels seems to be a meaningful research topic to investigate.

To be able to cope with both ISI and MAI, a chip-level interleaved UWB system with iterative equalization is used. The use of chip-level interleaving first proposed in [50] as alternative to coded CDMA because of its lower complexity and similar performance to the latter in ISI channels. Later, it was extended for UWB in [51] combining it with low rate codes. In chip-level interleaved systems, the original information bits are interleaved through the packet before modulation allowing iterative algorithms. Since the spreading can be viewed as a channel code in its simplest form, i.e. a repetition code, the resulting turbo equalization receivers are less complex than the existing methods [52, 53, 54].

Although, very high performance gains can be obtained through use of iterative algorithms, this performance gains are critically dependent on the reliability of the previous blocks' estimates such as synchronization. Most of the work in the literature, which dealt with iterative synchronization, mainly aim to improve the initial estimates

by incorporating soft information obtained via iterative algorithms [55, 56, 57, 58, 59]. Yet, this is different from what we propose: SISO synchronization algorithms, one blind and one data-aided, which work on the APPs of the chips and directly output soft information of the time-delays. The heart of this algorithm is use of TH codes to assist synchronization such that given the time-delay, TH codes uniquely determine the position of the pulses in the received signal. Moreover, in data-aided algorithm, a training sequence is used to initialize the probabilities of all possible time-delays rather than to obtain an initial hard estimate which is the most common approach. Furthermore, channel decoder is redesigned to work with the soft information provided by the synchronization algorithms.

1.3.3. Channel Estimation under Non-Gaussian Noise

The high sampling rates and computational complexity forbids use of many existing channel estimation algorithms for UWB. However, especially FD channel estimation algorithms attract so much attention since they can relax the computational complexity [33, 34, 35, 36]. But in these works, a well-detailed comparison of TD and FD processing is not outlined and the effect of channel estimator's performance on the probability of error is not studied. Moreover, in all of these works, noise is assumed to be AWGN although indoor environments generally do not obey this assumption. Therefore, a work filling these gaps in the literature appeared as the last part of this thesis.

The recursive channel estimation in both TD and FD can be accomplished via *recursive least squares* (RLS) or *least mean squares* (LMS) algorithms. However, since quadratic cost functions of this estimators are very sensitive to outliers (impulsive noise), they should be robustified. The robust channel estimation in TD is accomplished via an ad hoc robust estimator which makes use of one of the penalty functions given in [60] and the robust channel estimation in FD is accomplished via the robust recursive algorithm derived in [61]. The convergence analysis of this estimators are conducted to clarify differences between TD and FD channel estimation.

The primary work considering robust detection in minimax sense is due to [62] where two hypotheses are described by two sets of distributions without any overlap. However, resulting robust detection rule is not well-suited for detection processes using many observations rather than a single one because of its time-varying nonlinearity [63]. Therefore, robust detectors are designed according to method proposed in [64] for the sake of simplicity. The detectors' probability of error performance is investigated through taking the channel estimation errors into account to represent the overall performance of the receiver.

1.4. Outline of the Thesis

In Chapter 2, we present two robust acquisition methods with both theoretical and numerical performance evaluations. Moreover, the methods are extended to multiuser environment. In Chapter 3, we propose two multiuser synchronization algorithms under ISI channels one of which is blind and the other is data-aided. The numerical performance evaluations of these algorithms are also presented in Chapter 3. In Chapter 4, robust channel estimation and detection algorithms are presented for both TD and FD. Theoretical convergence analysis of the recursive channel estimators are conducted and the detectors' performance are evaluated both theoretically and via simulations taking the channel estimation errors into account. Finally, Chapter 5 concludes this thesis by a brief overview of possible future research directions.

2. ROBUST UWB SIGNAL ACQUISITION

Despite its advantages, UWB also introduces unique signal processing challenges, especially for timing synchronization and channel estimation [2]. Because the system performance deteriorates noticeably with noncoherent demodulation and even minor misalignments may result in the lack of sufficient energy capture, which renders symbol detection impossible [65], low-complexity timing synchronization mechanisms are needed.

The general solution to the synchronization of UWB signals is to divide the task into two parts: timing acquisition and fine synchronization. The former aims the reduction of timing uncertainty to the order of a pulse duration while the latter refers to fine tuning within pulse duration accuracy [25]. Two major issues that make UWB synchronization more challenging than traditional spread spectrum systems are the low-power constraint and the low duty cycle with very short duration pulses. The former is due to the rules and regulations imposed by the U.S. Federal Communications Commission [3] and it serves the aim of preventing UWB from interfering with legacy systems. The latter is necessary to spread the UWB signals and to allow for more efficient multiple-accessing.

The low-power constraint makes sufficient energy capture in the samples harder for an estimation-based approach. To that end, template selection for optimum detection plays a key role at the receiver [18]. The optimum template is the channel output waveform without noise, which can be generated with the knowledge of the channel impulse response at the receiver. In addition to the unavailability of the *channel state information* (CSI) during synchronization, it seems almost impossible to acquire the impulse response of a UWB channel because the number of paths for 85% energy capture varies typically between approximately 20 to 120 [23]. Moreover, the channel statistics may not be reliable enough to obtain useful information which disallows prior assumptions.

The low duty cycle with very short pulses makes detection-based synchronization systems difficult to implement in UWB. To allow multiple access and to remove the spectral lines resulting from the pulse repetition pattern present in the transmitted UWB signal [25], long spreading codes are used, which makes the search space large. Unlike narrowband systems, synchronization via linear search techniques with phase-locked loops or early-late gate synchronizers is not viable. In [12] and [13], alternative techniques such as bit reversal search and look-and-jump by K bins, are employed, but they fail to yield an acceptable solution in terms of the mean acquisition times.

The impact of low duty cycle and low power constraints on synchronization performance in UWB systems has been investigated in [12, 13, 14, 15, 16, 17, 18, 19, 20, 21, 22], with the assumption that the ambient noise is AWGN. However, as reported in [46], the indoor environments, where the UWB devices are envisioned to be deployed, are subject to interference produced by photocopiers, printers, elevators, etc. in the office. Such interference exhibits bursts of high-amplitude emissions, whose rate of occurrence depends on the device usage frequency, and will hereafter be referred to as impulsive noise. A proper probabilistic model that accounts for man-made interference and ambient noise simultaneously has to be of non-Gaussian form, characterized by heavy tails for the impulsive outliers.

Conventional synchronization methods suffer from a performance drop in case of non-Gaussian disturbance just like the detectors designed solely to counteract Gaussian noise. In this paper, we focus on the synchronization of signal within frame-level accuracy, i.e. timing acquisition for which estimation-theoretic approaches seem to be the strongest candidate. Taking into account the impulsive noise phenomenon, a robust UWB acquisition system is proposed to combat occasional deviations in the noise PDF from the nominal Gaussian assumption. The main approach is to combine minimax design for non-Gaussian noise with the TR methodology. In TR systems, each symbol consists of a modulated part (data) and an unmodulated part that serves as a template for the demodulation of the former. Because half of the signal is reserved for the unmodulated non-data part and also because noisy signals are used as the

template, the associated *bit error rate* (BER) performance is poor [39]. On the other hand, such a system suits the timing task well, as stated in [19], where an analog system under AWGN is proposed. Here, as in [19], instead of allocating half of the transmitted symbols to the templates (unmodulated signal), we use short training sequences which force the received samples to be related with the delay parameters. Then, these delay parameters are determined through the M-estimation procedure, which is a minimax design when the uncertainty about the system stems from the PDFs. In M-estimation, the worst case performance of the system at the neighborhood of the PDF is found, and at that point the overall performance of the system is optimized [60].

In this chapter, two data-aided robust acquisition algorithms are presented using the robust estimation techniques mentioned above. One of them uses the received symbol waveform as template and the other uses averaged version of the received symbols as template to decrease the level of noise enhancement which mainly occurs due to cross noise terms. The robust signal acquisition procedures work with samples taken at symbol rate with/without TH codes or DS spreading and do not require any CSI. Moreover, their superior performance over linear methods, i.e. that designed to be optimum under AWGN, is shown both theoretically and via simulations. Furthermore, proposed receivers are extended to multiuser environments via assuming the MUI to obey a Gaussian distribution.

This chapter is organized as follows: Section 2.1 outlines the signal and noise model. Section 2.2 describes the proposed robust acquisition procedures. Section 2.3 carries out an asymptotic performance analysis. Section 2.4 extends the robust acquisition procedure to multiuser environments. Section 2.5 presents performance evaluation via simulations, and Section 2.6 makes some concluding remarks.

2.1. Signal and Noise Model

In an impulse radio UWB communication system, every symbol is transmitted over a duration of T_s in which N_f frames, each with a duration of T_f, are sent, i.e.,

$T_s = N_f T_f$. In each frame, a pulse, $p(t)$, with a duration of T_p is transmitted. Typically, the pulse duration is much shorter than the frame duration, i.e., $T_p \ll T_f$, which leads to the low-duty cycle characteristic of UWB. For multiple access and channel separation, usually TH or DS codes are employed. With TH codes, the pulse is hopped by an amount of $c_u(n)T_c$ where $c_u(n)$ is the TH code corresponding to uth user's transmitted pulse in the nth frame of the symbol and T_c is the duration of the bins to which the pulses are allowed to hop. The allowable range for TH codes is $[0, N_c)$ where $N_c = T_f/T_c$. Although the general tendency for data modulation is towards *pulse position modulation* (PPM) because of its easier implementation [2], binary *pulse amplitude modulation* (PAM) will be considered. The transmitted signal for uth user is given by

$$s_u(t) = \sum_{n=0}^{\infty} b_u(n) p_{u,s}(t - nT_s) \tag{2.1}$$

where $b_u(n) \in \{+1, -1\}$ represents the PAM symbols and $p_{u,s}(t - nT_s)$ is the transmitted symbol waveform of the uth user given by

$$p_{u,s}(t) = \sqrt{E}_{u,s} \sum_{n=0}^{N_f - 1} p(t - nT_f - c_u(n)T_c) \tag{2.2}$$

where $E_{u,s}$ is the energy of the transmitted symbol of the uth user. The quasi-static channel is modelled as

$$h^u(t) = \sum_{l=1}^{L_u} h_l^u \delta(t - \tau_l^u) \tag{2.3}$$

where superscript u stands for uth user and L_u is the number of paths of the uth user's channel. $\delta(t)$ denotes the Dirac delta function. h_l^u and τ_l^u denote the path gain and the time-delay of lth multipath component of the uth user's channel response. The frame duration is set to satisfy $\mid \tau_{L_u}^u - \tau_1^u \mid + T_p < T_f$ and $c_u(N_f) = 0$ to avoid ISI. However, it should be noted that *interframe interference* (IFI) is allowed by these restrictions.

In this part of the thesis, the estimation of the first path's delay, τ_1^u, will be

considered while it is restricted to lie in one symbol duration, T_s. The time-delay of the first path can be expressed as $\tau_1^u = n_{u,f}T_f + \theta_u$ where $n_{u,f} = \lfloor \tau_1^u / T_f \rfloor$ and $\theta_u = \tau_1^u - n_{u,f}T_f$ represent the time-delay at frame-level and pulse-level, respectively. ($\lfloor\ \rfloor$ denotes the integer floor operation.) The delay of the other paths can be written as $\tau_l^u = \tau_{l,1}^u + \tau_1^u$ for $l = 1, \ldots, L_u$ where $\tau_{l,1}^u$ represents the relative time-delay of the lth path with respect to first one. The goal is to estimate $n_{u,f}$ from the received signal which can be written as

$$\begin{aligned} r(t) &= \sum_{u=1}^{N_u} \sum_{l=1}^{L_u} h_l^u s_u(t - \tau_{l,1}^u - \tau_1^u) + w(t) \\ &= \sum_{u=1}^{N_u} \sum_{n=0}^{\infty} b_u(n) p_{u,r}(t - nT_s - \tau_1^u) + w(t) \end{aligned} \tag{2.4}$$

where $p_{u,r}(t) = \sum_{l=1}^{L_u} h_l^u p_{u,s}(t - \tau_{l,1}^u)$ is the received symbol waveform and N_u denotes number of users. In (2.4), $w(t)$ is impulsive noise modeled as a two-term Gaussian mixture, which is a more realistic model for UWB systems whose main application will be in indoor environments. As shown in [46], the indoor noise is typically impulsive in nature due to the interference emanating from other man-made devices. The two-term Gaussian mixture is an approximation to the more general Middleton's Class A noise model, which consists of an infinite sum of Gaussian PDFs with identical means and increasing variances [66], and it adequately describes the Class A model when the impulsive interference constitutes about 0.1-1% of the total disturbance (noise plus interference) [67]. The two-term Gaussian mixture noise can be expressed as

$$f(x) = (1 - \epsilon) g(x; 0, \sigma^2) + \epsilon g(x; 0, \kappa\sigma^2) \tag{2.5}$$

where $g(x; \mu, \sigma^2)$ is the Gaussian PDF with mean μ and variance σ^2. In the mixture, the first term accounts for the nominal noise with higher prior probability, while the second term represents the impulsive noise with its heavier tails. Here, κ is the impulsive part's relative variance with respect to the nominal noise variance, and ϵ is the relative frequency of the outliers.

Notation Convention: Until Section 2.4, the subscript and the superscript, u, denoting the number of the user will be dropped for notational simplicity. (e.g. $b(m)$ denotes the information bit of a user in a single user link)

2.2. Robust Acquisition for UWB

The key issues for the estimation-based synchronization of an UWB system are template selection and sampling rate [25]. Templates play a critical role because for a typical UWB system, combined with low-power transmission, the multipath effect makes it difficult to capture an estimate of the transmitted symbol with sufficiently high energy. The possible lack of prior information about the channel impulse response calls for alternative approaches for template selection. In [18], the received symbol and the averaged received symbols are proposed as templates for transmission without and with TH, respectively. In [19], similar to [18], the received symbols and an averaged form of the received symbols are proposed as templates. Both approaches originate from the TR methodology [39], where for each data symbol, an unmodulated reference symbol is sent for demodulation.

2.2.1. Successive Sampling

Here, as in [18, 19], instead of allocating half of the symbol duration to a template (reference) signal, with the aid of a training sequence, successive symbols will be used as template. When ISI is absent, each symbol-length waveform at the receiver consists of two successively transmitted symbols [19]. By using each received symbol-length waveform as a template for the next one, the mean of the samples is directly governed by the frame-level delay, and therefore, the estimate of the mean of the training sequence can be employed as a tool for timing acquisition.

As a first step, the received symbol-length waveform is correlated with the pre-

vious one, yielding

$$r_{ss}(m) = \int_0^{T_s} r\left(t + mT_s\right) r\big(t + (m+1)T_s\big) dt, \tag{2.6}$$

which results in [18]

$$r_{ss}(m) = b(m)C_g\big[b(m-1)\tilde{n}_f + b(m+1)(N_f - \tilde{n}_f)\big] + \omega_{ss}(m) \tag{2.7}$$

where C_g is the energy of the received frame and $\tilde{n}_f = n_f + \chi$ with χ being the random uncertainty induced by the TH codes and/or the pulse-level uncertainty [18]. Here, $\chi \in [0, 1)$ so that the integer floor of $\tilde{n}_f$ is equal to n_f, frame-offset time delay. In (2.7), $\omega_{ss}(m)$ is the noise sample which consists of three parts, one noise-noise term and two signal-noise terms. The overall PDF of the noise is given by

$$\begin{aligned} f_{ss}(\omega) &= (1-\epsilon)^3 g\big(x; 0, \sigma^2(2E_r + 4T_s W\sigma^2)\big) \\ &+ 2\epsilon(1-\epsilon)^2 g\big(x; 0, \sigma^2((1+\kappa)E_r + 4T_s W\sigma^2)\big) \\ &+ \epsilon(1-\epsilon)^2 g\big(x; 0, \sigma^2(2E_r + 4\kappa^2 T_s W\sigma^2)\big) \\ &+ 2\epsilon^2(1-\epsilon) g\big(x; 0, \sigma^2((1+\kappa)E_r + 4\kappa^2 T_s W\sigma^2)\big) \\ &+ \epsilon^2(1-\epsilon) g\big(x; 0, \sigma^2(2\kappa E_r + 4T_s W\sigma^2)\big) \\ &+ \epsilon^3 g\big(x; 0, \sigma^2(2\kappa E_r + 4\kappa^2 T_s W\sigma^2)\big) \end{aligned} \tag{2.8}$$

where $E_r = N_f C_g$ is the energy of received symbol and W is the bandwidth of the front-end-filter at the receiver, which is typically given by $W \approx 1/T_p$. The derivation of (2.8) is given in Appendix A.

The primary goal is to estimate $\tilde{n}_f$ whose integer floor will give us the estimated frame-offset, $\hat{n}_{f,ss}$. To develop an understanding of the training sequence's structure required for estimation of $\tilde{n}_f$, first the following observations will be considered.

1. if $b(m-1) = b(m+1)$, (2.7) reduces to $r_{ss}(m) = b(m)b(m+1)N_f C_g + \omega_{ss}(m)$ from which C_g can be estimated,

2. if $b(m-1) = -b(m+1)$, (2.7) reduces to $r_{ss}(m) = b(m)b(m+1)C_g(N_f - 2\tilde{n}_f) + \omega_{ss}(m)$ from which $\tilde{n}_f$ can be estimated.

Therefore, by using a training sequence of length N_t, whose first $N_t/2$ elements are identically $+1$, and remaining half is $\{+1, +1, -1, -1, \ldots, +1, +1, -1, -1\}$, one can obtain the necessary equations for estimation of C_g and $\tilde{n}_f$.

Robust estimation procedures are generally designed in a minimax sense such as the M-estimates by Huber [60], which was originally developed for location parameter estimation. In Huber's solution, the maximal asymptotic variance of the estimator is minimized by finding the least favorable PDF within a certain family of the distributions, which turns out to possess the minimum Fisher information. This minimax procedure is completed by determining the ML estimator of the least favorable PDF.

For the so-called ϵ-contaminated Gaussian mixture model in (2.5), the PDF family can be described by the set

$$\mathcal{F}_\epsilon = \{(1-\epsilon)g(x; 0, \sigma^2) + \epsilon v(x); v(x) \text{ is a symmetric PDF}\}, \tag{2.9}$$

for which the least favorable PDF of such a family is the one which obeys the Gaussian distribution at the center and then decays with exponential tails [60] such that

$$f_{LF}(x) = \begin{cases} \frac{1-\epsilon}{\sqrt{2\pi}\sigma} \exp\left\{-\frac{x^2}{2\sigma^2}\right\} & \text{for } |x| \le k\sigma^2, \\ \\ \frac{1-\epsilon}{\sqrt{2\pi}\sigma} \exp\left\{\frac{k^2\sigma^2}{2} - k|x|\right\} & \text{for } |x| > k\sigma^2, \end{cases} \tag{2.10}$$

where k, σ and ϵ are related through

$$\frac{\phi(k\sigma)}{k\sigma} - Q(k\sigma) = \frac{\epsilon}{2(1-\epsilon)} \tag{2.11}$$

and $\phi(u) = (1/\sqrt{2\pi}) \exp(-u^2/2)$, $Q(u) = (1/\sqrt{2\pi}) \int_u^\infty \exp(-t^2/2)dt$. The M-estimate is then the ML estimate with respect to this least favorable PDF such that it can be

obtained through minimizing a cost function of the form, $\rho(x) = -\log f_{LF}(x)$.

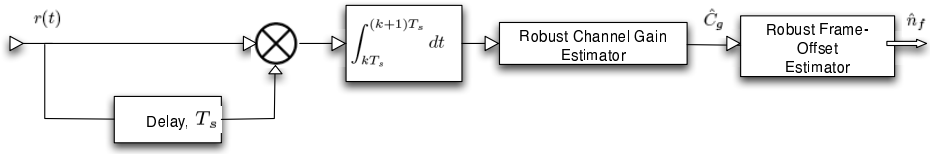

Figure 2.1. Block diagram for successive sampling.

Huber's solution corresponds to a situation where the nominal PDF is Gaussian and in the neighborhood of the nominal PDF, there exist symmetric contaminations, as in (2.9). If we consider the noise PDF in (2.8), there exists a dominating Gaussian term with a priori probability of $(1-\epsilon)^3$ and five more Gaussians with lower prior probabilities. Because the contaminations are symmetric and dominating PDF is Gaussian, Huber's solution to ϵ-contaminated Gaussian models can be adopted here, as well. To that end, one needs to define the nominal situation and the corresponding PDF. We define the nominal case as the one in which both of the two successively received symbols face just thermal noise, in which case the contamination consists of all terms where either one or both of the received successive symbols face outliers. Therefore, the least favorable PDF can be found by replacing σ^2 with $\sigma^2(2E_r + 4T_sW\sigma^2)$ and ϵ with $1-(1-\epsilon)^3$ in (2.10). The cost function for the successive sampling can be written as

$$\rho_{ss}(x) = \begin{cases} \frac{x^2}{2\sigma_{ss}^2} & \text{for } |x| \leq k\sigma_{ss}^2, \\ \\ \frac{k^2\sigma_{ss}^2}{2} - k|x| & \text{for } |x| > k\sigma_{ss}^2 \end{cases} \tag{2.12}$$

where $\sigma_{ss}^2 \triangleq \sigma^2(2E_r + 4T_sW\sigma^2)$ and k can be found by solving

$$\frac{1-(1-\epsilon)^3}{2(1-\epsilon)^3} = \frac{\phi\big(k\sigma_{ss}\big)}{k\sigma_{ss}} - Q\big(k\sigma_{ss}\big). \tag{2.13}$$

Using the cost function in (2.12), the estimates for the means of the two parts of the

training sequence can be found as

$$\hat{C}_{g,ss} = \arg\min_{C_{g,ss}} \sum_{m=0}^{N_t/2-1} \rho_{ss}\big(r_{ss}(m) - b(m)b(m+1)N_f C_{g,ss}\big), \tag{2.14}$$

$$\hat{\mu}_{ss} = \arg\min_{\mu_{ss}} \sum_{m=N_t/2}^{N_t} \rho_{ss}\big(r_{ss}(m) - b(m)b(m+1)\hat{C}_{g,ss}\mu_{ss}\big) \tag{2.15}$$

where μ_{ss} and $\hat{\mu}_{ss}$ are defined by $\mu_{ss} \triangleq (N_f - 2\tilde{n}_f)$ and $\hat{\mu}_{ss} \triangleq (\widehat{N_f - 2\tilde{n}_f})$. The closed form solutions to this equations do not exist, but they can be computed iteratively via modified residuals method [60]. Assuming that $\hat{C}^{\ell}_{g,ss}$ and $\hat{\mu}^{\ell}_{ss}$ are the estimates of $\hat{C}_g$ and $\hat{\mu}_{ss}$ at the ℓth step, respectively, recursive solutions of (2.14) and (2.15) are given by

$$\hat{C}^{\ell+1}_{g,ss} = \hat{C}^{\ell}_{g,ss} + \alpha \sum_{m=0}^{N_t/2-1} b(m)b(m+1)N_f \psi_{ss}\big(r_{ss}(m) - b(m)b(m+1)N_f \hat{C}^{\ell}_{g,ss}\big) \tag{2.16}$$

$$\hat{\mu}^{\ell+1}_{ss} = \hat{\mu}^{\ell}_{ss} + \alpha \sum_{m=N_t/2}^{N_t} b(m)b(m+1)\hat{C}_{g,ss}\psi_{ss}\big(r_{ss}(m) - b(m)b(m+1)\hat{C}_{g,ss}\hat{\mu}^{\ell}_{ss}\big) \tag{2.17}$$

where α is the step-size, taken about 0.1, and $\psi_{ss}(x)$ is the derivative of ρ_{ss} given in (2.12). At first iteration, all estimates are set to zero initially, and convergence is typically established in less than ten iteration. Once the final channel gain estimate $\hat{C}_{g,ss}$ is obtained through iterative use of (2.16), it is employed in (2.17) for the estimation of $\mu_{\rm ss}$ whose final value at the end of the iterations will be denoted by $\hat{\mu}_{\rm ss}$. Then, $\tilde{n}_f$ is determined, whose integer floor gives the estimate of the frame-offset as

$$\hat{n}_{f,ss} = \lfloor \hat{\tilde{n}}_{f,ss} \rfloor = \left\lfloor \frac{N_f - \hat{\mu}_{ss}}{2} \right\rfloor \tag{2.18}$$

where $\hat{\tilde{n}}_{f,ss}$ denotes the value of $\tilde{n}_f$ calculated using $\hat{\mu}_{ss}$ and $\hat{n}_{f,ss}$ represent the estimate of the frame-offset obtained via successive sampling. The overall algorithm is summarized in Table 2.1 and the block diagram of the acquisition unit is given in Figure 2.1.

Table 2.1. Robust UWB Acquisition via Successive Sampling

1. Take correlation of two successive received symbols to obtain (2.7).
2. Estimation of C_g:
i. Collect data samples for the first half of the training sequence.
ii. Solve (2.16) iteratively.
3. Estimation of $\tilde{n}_f$:
i. Collect data samples for the second half of the training sequence.
ii. Solve (2.17) iteratively.
The integer floor of $\hat{\tilde{n}}_{f,ss}$ gives $\hat{n}_{f,ss}$.

2.2.2. Averaged Template

In TR systems, or in autocorrelation-based receivers, one significant issue is the double noise (noise-noise) terms which result in an increase of noise variance as in our case. It is possible to decrease the noise level of the samples by employing a template that is obtained by averaging over the training sequence. Suppose that during the first half of the training sequence, the received symbols are averaged to obtain a template as follows

$$\bar{r}(t) = \frac{2}{N_t} \sum_{i=0}^{N_t/2-1} r(t+iT_s) = p_r(t+T_s-\tau_1) + p_r(t-\tau_1) + \bar{w}(t) \qquad (2.19)$$

where $\bar{w}(t)$ is the averaged noise over $N_t/2$ symbol-length waveforms whose PDF is given by

$$f_{\bar{w}}(x) = (1-\epsilon)g\left(x; 0, \frac{2\sigma^2}{N_t}\right) + (1-\epsilon)g\left(x; 0, \frac{2\kappa\sigma^2}{N_t}\right). \qquad (2.20)$$

Through averaging, the noise variance of the template is reduced by $N_t/2$ according to (2.20), which is crucial for suppressing the double noise terms. Using the template in

(2.19), samples are obtained as

$$r_{avg}(m) = \int_0^{T_s} r(t + mT_s)\bar{r}(t)dt,\ m = 0, 1, \ldots, N_t - 1, \tag{2.21}$$

which results in [18]

$$r_{avg}(m) = C_g\Big(b(m-1)\tilde{n}_f + b(m)(N_f - \tilde{n}_f)\Big) + \omega_{avg}(m) \tag{2.22}$$

where $\omega_{avg}(m)$ is the sequence of noise samples having a PDF of

$$\begin{aligned} f_{avg}(x) &= (1-\epsilon)^3 g\left(x; 0, \sigma^2\left(E_r + 4T_s W\frac{\sigma^2}{N_t}\right)\right) \\ &+ \epsilon(1-\epsilon)^2 g\left(x; 0, \sigma^2\left(E_r + 4\kappa^2 T_s W\frac{\sigma^2}{N_t}\right)\right) \\ &+ \epsilon(1-\epsilon)^2 g\left(x; 0, \sigma^2\left(2E_r\frac{\kappa}{N_t} + 4T_s W\frac{\sigma^2}{N_t}\right)\right) \\ &+ \epsilon^2(1-\epsilon) g\left(x; 0, \sigma^2\left(2E_r\frac{\kappa}{N_t} + 4\kappa^2 T_s W\frac{\sigma^2}{N_t}\right)\right) \\ &+ \epsilon(1-\epsilon) g\left(x; 0, \sigma^2\left(\kappa E_r + 4T_s W\frac{\sigma^2}{N_t}\right)\right) \\ &+ \epsilon^2 g\left(x; 0, \sigma^2\left(\kappa E_r + 4\kappa^2 T_s W\frac{\sigma^2}{N_t}\right)\right) \end{aligned} \tag{2.23}$$

whose derivation is given in Appendix A.

The samples in (2.22) differs from those (2.7) and a new training sequence should be designed for estimation $\tilde{n}_f$. Similar to successive sampling without averaging, here we observe that

1. if $b(m) = b(m-1)$, (2.22) reduces to $r_{avg}(m) = b(m)C_g N_f + \omega_{avg}(m)$ from which C_g can be estimated,
2. if $b(m) = -b(m-1)$, (2.22) reduces to $r_{avg}(m) = C_g b(m)(N_f - 2\tilde{n}_f) + \omega_{avg}(m)$ from which $\tilde{n}_f$ can be estimated.

In this case, a training sequence whose first half consists of only +1's and the

remaining half having a structure of $\{+1, -1, +1, -1, \ldots, -1, +1\}$ enables us to estimate C_g and $\tilde{n}_f$ separately. In addition, the template can be obtained by averaging the received symbols of the first half of the training sequence.

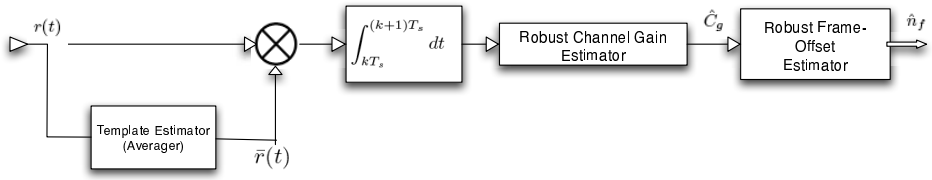

Figure 2.2. Block diagram for averaged template.

For the implementation of the robust estimation procedure, the nominal situation is defined to be in effect when neither the averaged template nor the sampled symbol contains outliers. Thus, the term with the *a priori* probability of $(1-\epsilon)^3$ is the nominal PDF, and the rest represent the contamination with impulsive components. In this case, the least favorable PDF can be found by replacing σ^2 with $\sigma^2(E_r + 2T_sW\sigma^2/N_t)$ and ϵ with $1-(1-\epsilon)^3$ in (2.10). The cost function for averaged template can then be written as

$$\rho_{avg}(x) = \begin{cases} \frac{x^2}{2k\sigma_{avg}^2} & \text{for } |x| \le k\sigma_{avg}^2, \\ \\ \frac{k^2\sigma_{avg}^2}{2} - k|x| & \text{for } |x| > k\sigma_{avg}^2, \end{cases} \tag{2.24}$$

where $\sigma_{avg}^2 \triangleq \sigma^2(E_r + 4T_sW\sigma^2/N_t)$ and k can be found from

$$\frac{1-(1-\epsilon)^3}{2(1-\epsilon)^3} = \frac{\phi\left(k\sigma_{avg}\right)}{k\sigma_{avg}} - Q\left(k\sigma_{avg}\right). \tag{2.25}$$

Therefore, using (2.25), the estimated values for the means of the two parts of the training sequence are given by

$$\hat{C}_{g,avg} = \arg\min_{C_g} \sum_{m=0}^{N_t/2-1} \rho_{avg}\Big(r(m) - N_f C_g\Big) \tag{2.26}$$

$$\hat{\mu}_{avg} = \arg\min_{\mu_{avg}} \sum_{m=N_t/2}^{N_t-1} \rho_{avg}\Big(r(m) - b(m)\hat{C}_{g,avg}\mu_{avg}\Big) \tag{2.27}$$

where $\mu_{avg} = \mu_{ss} = (N_f - 2\tilde{n}_f)$ and $\hat{\mu}_{avg} \triangleq \widehat{(N_f - 2\tilde{n}_f)}$. Since the closed form solutions do not exist, they should be solved iteratively via the modified residuals method in [60] as

$$\hat{C}_{g,avg}^{\ell+1} = \hat{C}_{g,avg}^{\ell} + \alpha \sum_{m=0}^{N_t/2-1} b(m) N_f \psi_{avg}\big(r(m) - b(m) N_f \hat{C}_{g,avg}^{\ell}\big) \tag{2.28}$$

$$\hat{\mu}_{avg}^{\ell+1} = \hat{\mu}_{avg}^{\ell} + \alpha \sum_{m=N_t/2}^{N_t-1} b(m) \hat{C}_{g,avg} \psi_{avg}\big(r(m) - b(m) \hat{C}_{g,avg} \hat{\mu}_{avg}^{\ell}\big) \tag{2.29}$$

where $\psi_{avg}(x)$ is the derivative of ρ_{avg} given in (2.25) and $\hat{C}_{g,avg}^{\ell+1}, \hat{\mu}_{avg}^{\ell+1}$ denote the estimates of $C_{g,avg}$ and μ_{avg} at the ℓth step. As with successive sampling, α is the step size around 0.1, and all initial estimates are set to zero. The iterative use of (2.28) produces the final channel gain estimate, $\hat{C}_{g,\text{avg}}$, which is then employed in (2.29) for determining μ_{avg}, whose final value at the end of the iterations will be denoted by $\hat{\mu}_{\text{avg}}$. Finally, $\tilde{n}_{f,\text{avg}}$ is calculated using $\hat{\mu}_{\text{avg}}$, and its integer floor gives the estimate of the frame-offset as

$$\hat{n}_{f,avg} = \lfloor \hat{\tilde{n}}_{f,avg} \rfloor = \left\lfloor \frac{N_f - \hat{\mu}_{avg}}{2} \right\rfloor \tag{2.30}$$

where $\hat{\tilde{n}}_{f,avg}$ denotes the value of $\tilde{n}_f$ calculated using $\hat{\mu}_{avg}$ and $\hat{n}_{f,avg}$ represent the estimate of the frame-offset obtained via averaged template. The overall algorithm is summarized in Table 2.2 and the block diagram of the proposed receiver is given in Figure 2.2. In the next section, asymptotic performance analysis of these estimators will be carried out.

2.3. Asymptotic Performance Analysis

The M-estimates are asymptotically consistent and normal-distributed. The asymptotic variance of the robust mean estimator using the PDF in (2.10) is given by

Table 2.2. Robust UWB Acquisition with Averaged Template

1. Average the first half of the training sequence to obtain (2.19), averaged template.
2. Sample the received symbols with averaged template, (2.19), to obtain (2.22).
3. Estimation of C_g:
i. Take the sample values for the first part of the training sequence.
ii. Solve iteratively (2.28).
4. Estimation of $\tilde{n}_f$.
i.Take the sample values for the second part of the training sequence.
ii. Solve iteratively (2.29).
The integer floor of $\hat{\tilde{n}}_{f,avg}$ gives $\hat{n}_{f,avg}$.

$$\nu_{asy}^2 = \frac{E\left[\psi^2(x)\right]}{\left(E\left[\psi'(x)\right]\right)^2} = \frac{\int \psi^2(x) f_{LF}(x)dx}{\left[\int \psi'(x) f_{LF}(x)dx\right]^2} \tag{2.31}$$

where ν_{asy}^2 denotes the asymptotic variance and $\psi'(x)$ is the derivative of $\psi(x)$ which itself is the derivative of the cost function, i.e. $\rho(x)$. To calculate the asymptotic variance of the successive sampling and the averaged template, $\psi(x)$ and $f_{LF}(x)$ in (2.31) should be replaced with (2.8)-(2.12) (2.23)-(2.25), respectively. Denoting the asymptotic variances for the successive sampling and averaged template as ν_{ss}^2 and ν_{avg}^2, respectively, the estimation errors obey a normal PDF such as

$$\sqrt{\frac{N_t}{2}} C_g(\mu_{ss} - \hat{\mu}_{ss}) \sim \mathcal{N}(0, \nu_{ss}^2) \tag{2.32}$$

$$\sqrt{\frac{N_t}{2}} C_g(\mu_{avg} - \hat{\mu}_{avg}) \sim \mathcal{N}(0, \nu_{avg}^2) \tag{2.33}$$

where $\mathcal{N}(0, \sigma^2)$ denotes a Gaussian random variable with zero mean and variance σ^2. Moreover, since M-estimates can be viewed as a generalization of the ML-estimates, the

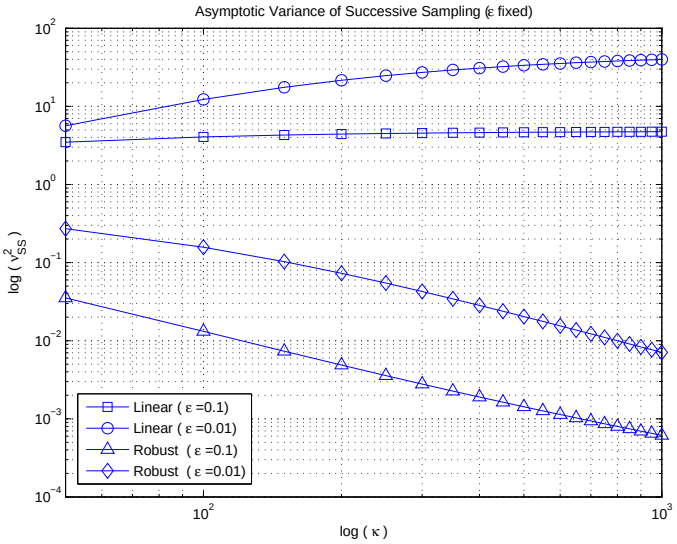

Figure 2.3. Asymptotic variance of the successive sampling when ϵ is fixed and $(1-\epsilon)+\epsilon\kappa)\sigma^2 = (0.1)^2$.

asymptotic variance of the linear estimator designed to be optimum under AWGN but operating under an impulsive noise can be calculated via (2.31) by setting $\psi(x) = x$. Since the noise PDFs, i.e. (2.8) and (2.23), are complicated, the asymptotic variances of the estimators, ν_{ss}^2 and ν_{avg}^2, are calculated numerically and plotted in Figures 2.3-2.4. From these two figures, it can be concluded when ϵ and the total noise variance, i.e. $((1-\epsilon)+\epsilon\kappa)\sigma^2 = (0.1)^2$, are fixed, the variance of the robust estimators are monotonically decreasing in κ in contrary to linear estimators whose asymptotic variance is almost invariant to changes in κ. This was also observed and stated in [68] for robust multiuser detectors in non-Gaussian channel.

Now, assuming that ν_{ss}^2 and ν_{avg}^2 are at hand, the *probability mass functions* (PMFs) of the robust estimators will be derived to calculate *normalized mean square error* (NMSE). To that end, first the conditional probability of frame offset's estimate obtained via successive sampling will be considered which is given by

$$\begin{aligned}\Pr\{\hat{n}_{f,ss} = x \mid \tilde{n}_f\} &= \Pr\left\{x \le \frac{N_f - \hat{\mu}_{ss}}{2} < x+1 \middle| \tilde{n}_f\right\} \\ &= Q\left(\frac{N_f - 2x - 2 - \mu_{ss}}{\nu_{ss}/\left(C_g\sqrt{N_t/2}\right)}\right) - Q\left(\frac{N_f - 2x - \mu_{ss}}{\nu_{ss}/\left(C_g\sqrt{N_t/2}\right)}\right) \quad (2.34)\end{aligned}$$

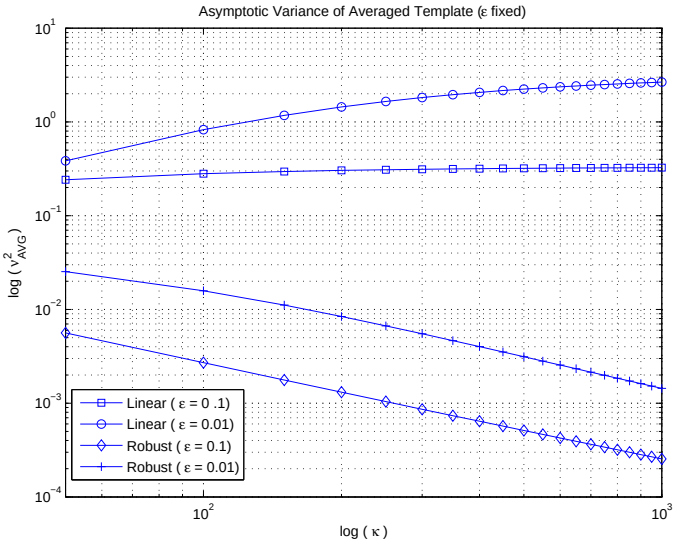

Figure 2.4. Asymptotic variance of the averaged template when ϵ is fixed and $((1-\epsilon)+\epsilon\kappa)\sigma^2 = (0.1)^2$.

Using the fact that $\mu_{ss} = N_f - 2\tilde{n}_f$, (2.34) can be alternatively expressed as

$$\Pr\{\hat{n}_{f,ss} = x \mid \tilde{n}_f\} = Q\left(\frac{2\tilde{n}_f - 2x - 2}{\nu_{ss}/\left(C_g\sqrt{N_t/2}\right)}\right) - Q\left(\frac{2\tilde{n}_f - 2x}{\nu_{ss}/\left(C_g\sqrt{N_t/2}\right)}\right) \tag{2.35}$$

where $\tilde{n}_f$ can be decomposed as $\tilde{n}_f = n_f + \vartheta$ with ϑ being the random time-uncertainty induced by the TH codes and/or pulse-level uncertainty, θ, which is assumed to be uniformly distributed in $[0, 1)$. To alleviate the dependency of (2.35) on ϑ, expectation

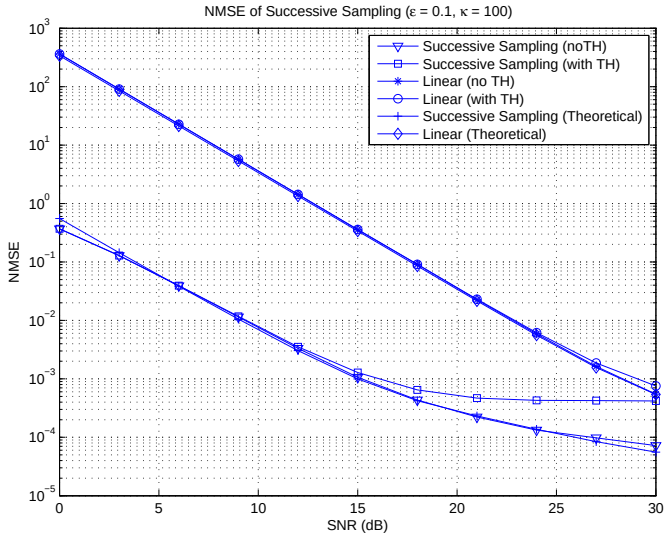

Figure 2.5. Simulation results for the NMSE of the successive sampling based robust acquisition and the corresponding linear acquisition for $\epsilon = 0.1$, $\kappa = 100$.

of (2.35) should be taken over ϑ resulting in

$$\begin{aligned}
\Pr(\hat{n}_{f,ss} = x \mid n_f) &= \int_0^1 \Pr(\hat{n}_f = x \mid \tilde{n}_f) d\vartheta = \int_0^1 \Pr(\hat{n}_f = x \mid n_f, \vartheta) d\vartheta \\
&= 2(n_f - x) Q\left(\frac{2n_f - 2x}{\nu_{ss} / \left(C_g \sqrt{N_t/2} \right)} \right) \\
&- (n_f - x - 1) Q\left(\frac{2n_f - 2x - 2}{\nu_{ss} / \left(C_g \sqrt{N_t/2} \right)} \right) \\
&- (n_f - x + 1) Q\left(\frac{2n_f - 2x + 2}{\nu_{ss} / \left(C_g \sqrt{N_t/2} \right)} \right) \\
&+ \frac{\nu_{ss}}{2 C_g \sqrt{\pi N_t}} \left[\exp\left\{ -N_t C_g \left(\frac{n_f - x - 1}{\nu_{ss}} \right)^2 \right\} \right. \\
&+ \exp\left\{ -N_t C_g \left(\frac{n_f - x + 1}{\nu_{ss}} \right)^2 \right\} \\
&- \left. 2 \exp\left\{ -N_t C_g \left(\frac{n_f - x}{\nu_{ss}} \right)^2 \right\} \right]
\end{aligned} \tag{2.36}$$

which is the PMF of the frame-offset estimate conditioned on the actual value of n_f.

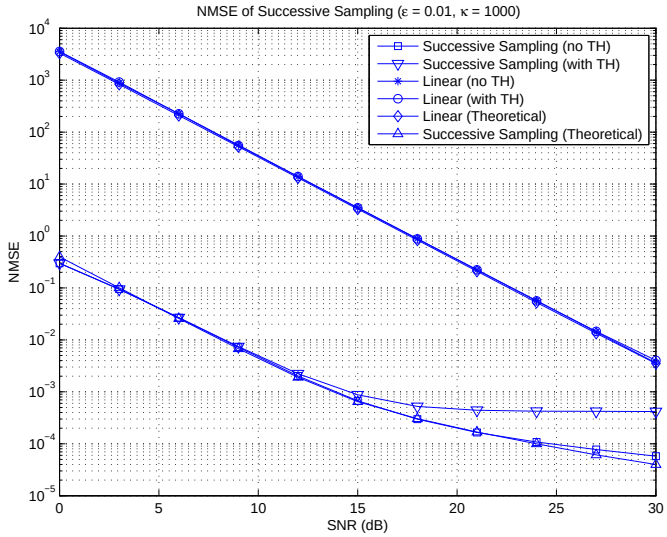

Figure 2.6. Simulation results for the NMSE of the successive sampling based robust acquisition and the corresponding linear acquisition for $\epsilon = 0.01$, $\kappa = 1000$.

Therefore, NMSE of $\hat{n}_{f,ss}$ can be calculated as follows

$$\begin{aligned} \text{NMSE}(\hat{n}_{f,ss}) &\triangleq E\left\{\left(\frac{\hat{n}_{f,ss}-n_f}{N_f}\right)^2\right\} \\ &= \frac{1}{N_f^2}\sum_{x=0}^{N_f-1}\Pr(n_f=x)E\left\{(\hat{n}_{f,ss}-n_f)^2 \mid n_f=x\right\} \end{aligned} \tag{2.37}$$

where $E\left\{(\hat{n}_{f,ss}-n_f)^2 \mid n_f=x\right\}$ is the *conditional mean square error* (CMSE). Assuming n_f to be uniform over $[0, N_f-1]$, (2.37) can be expressed as

$$\text{NMSE}(\hat{n}_{f,ss}) = \frac{1}{N_f^3}\sum_{x=0}^{N_f-1}\sum_{y=-\infty}^{\infty}\Pr(\hat{n}_{f,ss}=y \mid n_f=x)\,(y-x)^2 \tag{2.38}$$

where $\Pr(\hat{n}_{f,ss}=y \mid n_f=x)$ is given in (2.36). Since the NMSE of the frame-offset estimate obtained via averaged template can be calculated with the same procedure described, its derivation is omitted. In the next section, the robust timing acquisition will be investigated under MAI.

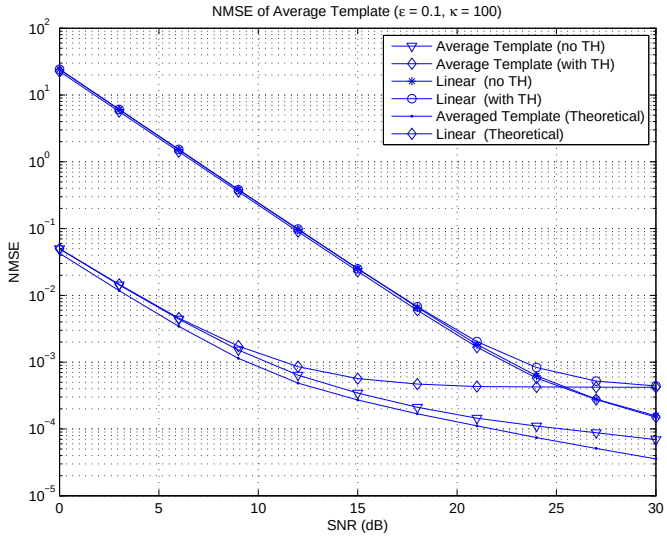

Figure 2.7. Simulation results for the NMSE of the averaged template based robust acquisition and the corresponding linear acquisition for $\epsilon = 0.1$, $\kappa = 100$.

2.4. Multiuser Environment

So far, a point-to-point link was considered and it was assumed that user separation is accomplished via channelization [19]. In this section, the performance of the proposed algorithms are explored when asynchronous users which are assumed to transmit *independent and identically distributed* (i.i.d) data symbols interfere with the desired user. The goal is to achieve timing acquisition with only one user in the presence of both impulsive noise and multiuser interference. The averaged template method with the associated training sequence, i.e. first half consisting of $+1$'s and the remaining half having a structure of $\{-1, +1, \ldots, -1, +1\}$, is adopted for the multiuser environment because of its better performance as attested by the asymptotic variance comparison in the previous section. In the presence of MUI, the averaged template becomes

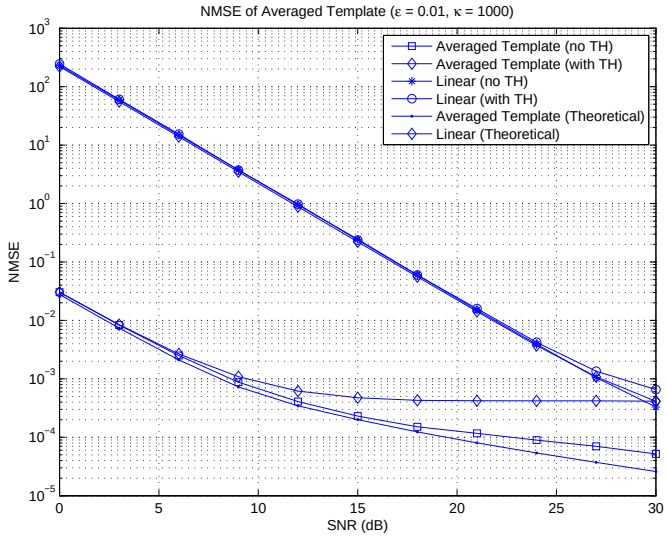

Figure 2.8. Simulation results for the NMSE of the averaged template based robust acquisition and the corresponding linear acquisition for $\epsilon = 0.01$, $\kappa = 1000$.

$$\begin{aligned} \bar{r}(t) &= \frac{2}{N_t} \sum_{i=0}^{N_t/2-1} r(t + iT_s) \\ &= \frac{2}{N_t} \sum_{u=1}^{N_u} \sum_{i=0}^{N_t/2-1} [b_u(i-1)p_{u,r}(t + T_s - \tau_1^u) + b_u(i)p_{u,r}(t - \tau_1^u)] + \bar{w}(t) \end{aligned} \quad (2.39)$$

where $\bar{w}(t)$ is the averaged noise whose PDF is given in (2.20). The received samples are formed via

$$r(m) = \int_0^{T_s} r(t + mT_s)\bar{r}(t)dt \quad (2.40)$$

which is explicitly given by

$$r(m) = C_{d,g}\big(b_d(m-1)\tilde{n}_{d,f} + b_d(m)(N_f - \tilde{n}_{d,f})\big) + \omega_{mui}(m) + \omega_{ma}(m) \quad (2.41)$$

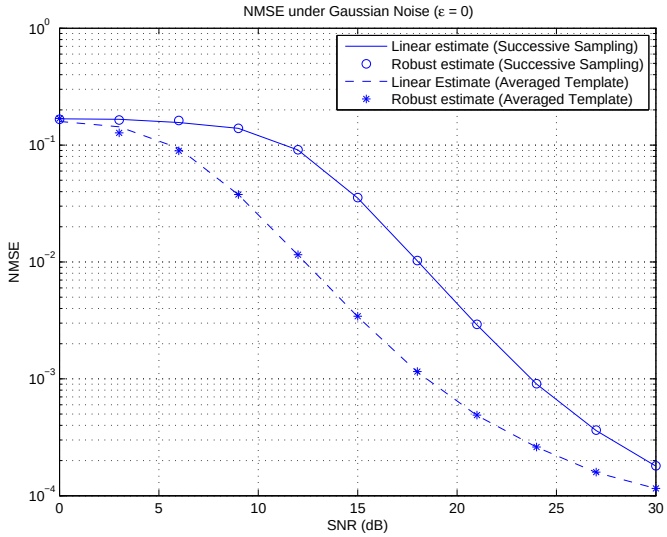

Figure 2.9. NMSE performance of all receivers under Gaussian noise.

where subscript, d, denotes desired user, $\omega_{mui}(m)$ and $\omega_{ma}(m)$ denote the MUI and noise term, respectively. The variance of the MUI is given by

$$\sigma^2_{mui} \approx \frac{2}{N_t} \sum_{\substack{u=1 \\ u \neq d}}^{N_u} E^2_{u,r} \tag{2.42}$$

whose derivation is given in Appendix B. MUI term can be approximated by a Gaussian distribution using CLT for sufficiently large N_u. Therefore, the overall PDF of all disturbances, noise plus MUI, is given by

$$\begin{aligned} f_{ma}(z) &= (1-\epsilon)^3 g\left(z; 0, \sigma^2\left(E_{d,r} + 4T_s W\frac{\sigma^2}{N_t}\right) + \sigma^2_{mui}\right) \\ &+ \epsilon(1-\epsilon)^2 g\left(0, \sigma^2\left(E_{d,r} + 4\kappa^2 T_s W\frac{\sigma^2}{N_t}\right) + \sigma^2_{mui}\right) \\ &+ \epsilon(1-\epsilon)^2 g\left(z; 0, \sigma^2\left(2\kappa\frac{E_{T,r}}{N_t} + 4T_s W\frac{\sigma^2}{N_t}\right) + \sigma^2_{mui}\right) \\ &+ \epsilon^2 g\left(z; 0, \sigma^2\left(\kappa E_{d,r} + 4\kappa^2 T_s W\frac{\sigma^2}{N_t}\right) + \sigma^2_{mui}\right) \\ &+ \epsilon(1-\epsilon) g\left(z; 0, \sigma^2\left(\kappa E_{d,r} + 4T_s W\frac{\sigma^2}{N_t}\right) + \sigma^2_{mui}\right) \\ &+ \epsilon^2(1-\epsilon) g\left(z; 0, \sigma^2\left(2\kappa\frac{E_{T,r}}{N_t} + 4\kappa^2 T_s W\frac{\sigma^2}{N_t}\right) + \sigma^2_{mui}\right) \end{aligned} \tag{2.43}$$

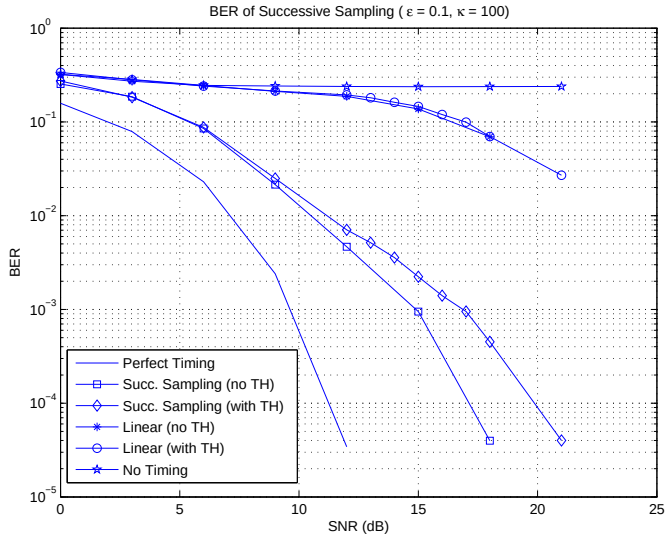

Figure 2.10. BER of successive sampling-based robust acquisition and corresponding linear acquisition under $\epsilon = 0.1$, $\kappa = 100$.

where $E_{T,r} = \sum_{u=1}^{N_u} E_{u,r}$ is the sum of all users' received energies. The derivation of (2.43) is also in given in Appendix B. Note that the MUI introduces an additional term to the variance of the noise PDF given in (2.23), thereby resulting in (2.43), which is independent of *signal-to-noise ratio* (SNR) which is defined as the ratio of symbol energy to the variance of the background noise. The MUI induces a noise floor which cannot be lowered by increasing the transmitted power.

The nominal part of (2.43) is the first term with a priori probability $(1-\epsilon)^3$ and all other terms are treated as interference-contaminated. In this case, the least favorable PDF can be found by setting σ^2 to $\sigma^2\left(E_{d,r} + 4T_sW\sigma^2/N_t\right) + \sigma^2_{\text{mui}}$, and ϵ to $1-(1-\epsilon)^3$ in (2.10). The cost function for multiuser environment is thus given by

$$\rho_{ma}(x) = \begin{cases} \frac{x^2}{\sigma^2_{ma}} & \text{for } |x| \le k\sigma^2_{ma} \\ \\ \frac{k^2\sigma^2_{ma}}{2} - k|x| & \text{for } |x| > k\sigma^2_{ma} \end{cases} \tag{2.44}$$

where $\sigma^2_{ma} \triangleq \sigma^2\left(E_{d,r} + 4T_sW\sigma^2/N_t\right) + \sigma^2_{mui}$ and k can be found by solving

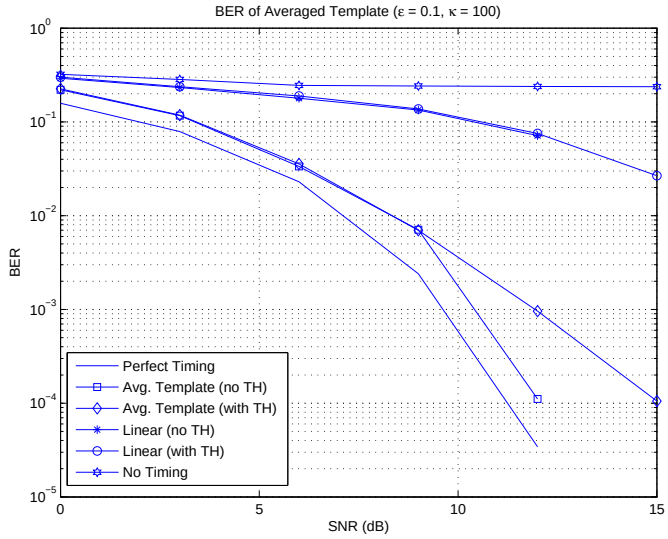

Figure 2.11. BER of averaged template-based robust acquisition and corresponding linear acquisition under $\epsilon = 0.1$, $\kappa = 100$.

$$\frac{\phi\left(k\sigma_{ma}\right)}{k\sigma_{ma}} - Q\left(k\sigma_{ma}\right) = \frac{1-(1-\epsilon)^3}{2(1-\epsilon)^3}. \tag{2.45}$$

The estimation of $C_{d,g}$ and $\tilde{n}_{d,f}$ can be carried over as indicated in (2.26)-(2.28) and (2.27)-(2.29) using first and second halves of the training sequence.

2.5. Simulation Results

In this section, we test the performance of the robust estimator introduced in Section 2.2 and Section 2.4. The pulse is selected as the second derivative of the Gaussian function with duration $T_p = 1$ ns. The *channel model four* (CM4) is implemented [23]. The frame duration is selected to be 40 ns. Each symbol consists of $N_f = 30$ frames resulting in $T_s = 1200$ ns. The chip duration is chosen as $T_c = 1$ ns, and the TH codes are randomly generated from a uniformly distributed set of $\{0, 1, \ldots, N_f - 1\}$. The tracking level uncertainty in time-delay, i.e. θ, is randomly generated from a uniform distribution on $[0, T_f)$. The linear acquisition system that is considered as the competitor here is the Gaussian-optimal ML solution as developed in [18]. The total

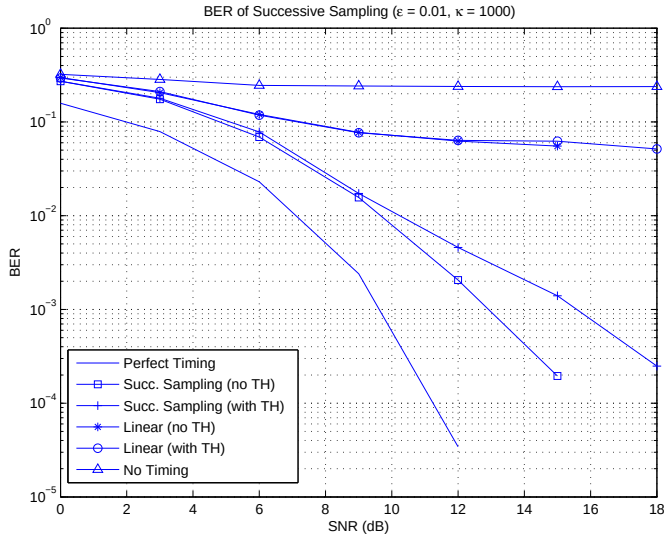

Figure 2.12. BER of successive sampling-based robust acquisition and corresponding linear acquisition under $\epsilon = 0.01$, $\kappa = 1000$.

number of training symbols is thirty, where the first half is used to estimate channel gain and second half is used to estimate the timing delay. In all simulations, the SNR $\triangleq E_s/((1-\epsilon)\sigma^2 + \epsilon\kappa\sigma^2)$, where $(1-\epsilon)\sigma^2 + \epsilon\kappa\sigma^2$ is the total noise variance at the input of the receiver and it is fixed. The NMSE is calculated through sample averaging. Although $n_f \in \{0, \ldots, N_f - 1\}$, the estimated frame-offsets $\hat{n}_f$ often go out of that range in simulations with linear acquisition. In such cases, instead of discarding the out-of-range frame-offset estimates, we incorporated them to reflect the system's performance more realistically, with NMSE values exceeding unity by a large margin at low SNR.

Figures 2.5-2.8 demonstrate that robust acquisition methods outperform the conventional Gaussian-optimal linear system significantly. For the SNR range of 0-20 dB, the performance of Gaussian-optimal acquisition is unacceptable, justifying the design of robust procedures. Specifically, to attain NMSE $= 1 \times 10^{-3}$ when $\epsilon = 0.1$ and $\kappa = 100$, linear acquisition requires 12 dB higher SNR compared to the robust scheme with averaged template. The same margin grows to 17 dB for $\epsilon = 0.01$ and $\kappa = 1000$, i.e. when the interference intensifies. We are concerned with the estimation of only frame-level time-offset and the random pulse-level uncertainty results in error floors in all cases. The error floor is higher when TH codes are employed because they induce

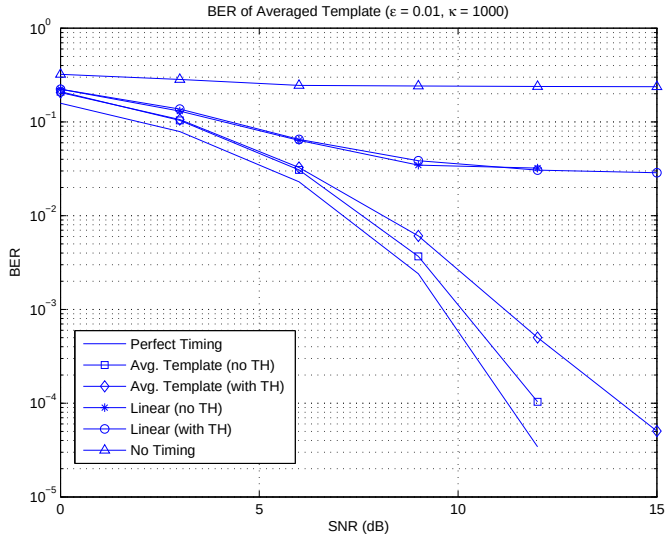

Figure 2.13. BER of averaged template-based robust acquisition and corresponding linear acquisition under $\epsilon = 0.01$, $\kappa = 1000$.

IFI that results in an additional timing uncertainty in $\hat{n}_f$ as stated in [18]. From the figures, it is clear that average-templated based robust acquisition outperforms successive sampling alone due to better noise suppression. The theoretical NMSEs are also plotted for both robust and linear methods without TH in Figures 2.5-2.8 showing good agreement with simulation results. In Figure 2.9, receivers' performances are presented for the case of AWGN only. Robust methods do not incur any noticeable performance loss in the nominal case.

To observe the impact of timing mismatch in an impulsive environment, BER graphs are plotted assuming that the receiver has perfect knowledge of the channel and impulsive noise occurs only during transmission of the training sequence. In the BER simulations, 30 training symbols are followed by 1000 data symbols. The performance gains obtained by the robust methods become clearer with Figures 2.10-2.13. The Gaussian-optimal ML estimators cannot track the UWB signal in impulsive noise, whereas the robust methods can within an acceptable range of SNR. Moreover, when the averaged template is employed, its performance moves within 1 dB of perfect timing when no TH is employed. In these figures, the effect of IFI induced by the TH codes can again be observed considering the performance gaps between no-TH and TH cases.

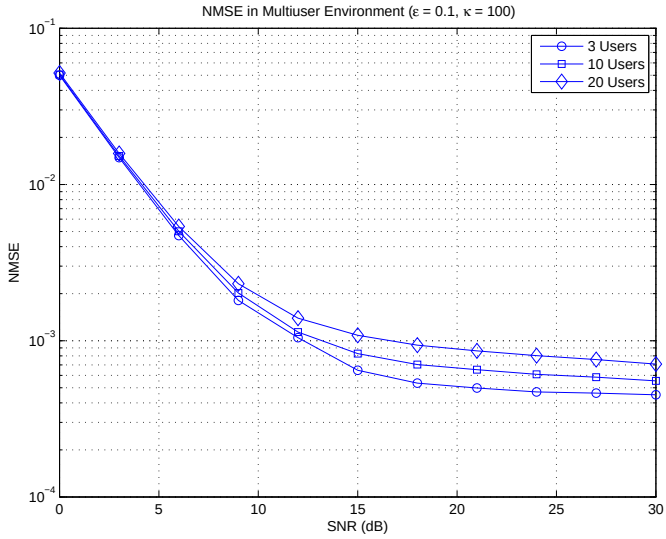

Figure 2.14. Simulation results for the NMSE of the robust acquisition designed for multiuser environment and corresponding linear acquisition under $\epsilon = 0.1$, $\kappa = 100$.

Lastly, we tested the averaged template's performance in a multiuser environment where $3, 10, 20$ users transmit at 10 dB below the desired user. Figures 2.14 depicts the rise in the NMSE error floor due to MUI. In Figure 2.15, BER performances are shown. When three users are present, the system can reach 1×10^{-5} bit errors but when we increase the number of users, i.e. MUI, there exists an error floor in BER graphs. Moreover this error floor increases with the number of users. In our algorithm only thing to combat with MUI is to use longer training sequences to average the template which will decrease the MUI and error floors caused by the later.

2.6. Discussions

In this chapter, we presented UWB timing acquisition schemes that combine TR methodology with robust estimation techniques for operation in the presence of interference modeled as impulsive noise. For a single user link, successive sampling- and averaged template-based robust acquisition methods are proposed. The former one suffers from noise enhancement because of noisy signal correlations, while the latter provides improvement through averaging. Both of these robust methods offer substantial performance gains over their linear counterparts, i.e., ML estimators designed

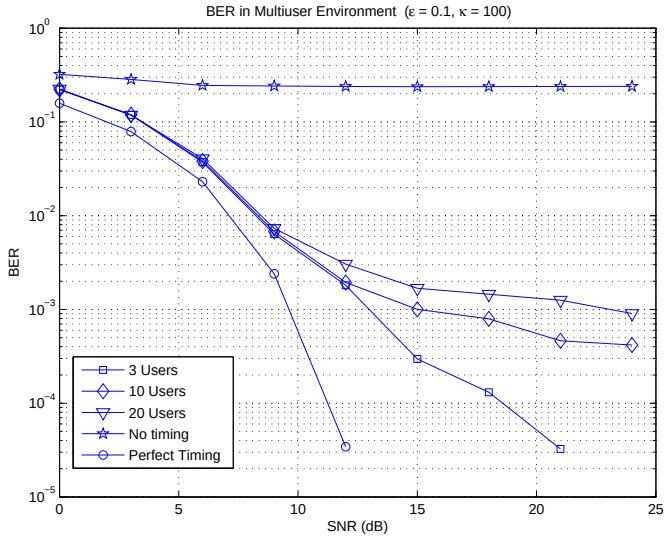

Figure 2.15. BER of the robust acquisition designed for multiuser environment and corresponding linear acquisition under $\epsilon = 0.1$, $\kappa = 100$.

under the Gaussian noise assumption, which is not appropriate for indoor environments.

The averaged template-based robust acquisition is extended to multiuser environments where the MUI is treated as a Gaussian random variable by invoking CLT. Although the performance of the multiuser receiver is satisfactory for moderate number of users, the specific correlation structure of MUI is not exploited here for further suppression. Synchronization methods employing MUI suppression in ISI channels will be explored in the future.

3. ITERATIVE MULTIUSER SYNCHRONIZATION OF UWB SIGNALS UNDER ISI

Although there is a vast literature on synchronization and timing acquisition of UWB signals [25] (and references therein), most of the existing works consider single user scenarios in ISI free channels. Because of the fact that in UWB systems equipped with TH codes, a different chip position is assigned to each user in each frame, TH-UWB systems can be viewed as using *time-division multiple access* (TDMA). However, the multipath channel with extreme delay spread [23] spoils the orthogonality of users' transmitted waveforms resulting in MAI in addition to ISI. Therefore, in addition to the inherent difficulties associated with synchronization of UWB signals such as low-duty cycle with very short duration pulses and low-power constraints, presence of ISI and MAI should be also considered in the design of synchronization algorithms for UWB signals. To the best our knowledge, there is a limited amount of work directly aims synchronization in the presence of MAI and ISI for TH-UWB systems [48, 49]. [48] proposes a blind synchronization scheme for multiuser TR UWB systems using subspace techniques, specifically a *multiple signal classification* MUSIC-like search to estimate the delay of the packet. The proposed receiver in [48] is for uplink which estimates time delays of all users. In contrast to [48], in [49] a downlink synchronization scheme is proposed that basically depends on the periodic transmission of non-zero mean symbols, allowing for template signal and time delay estimation in the presence of MAI and ISI. Moreover, in [49], it is claimed that the proposed estimator owns the asymptotic optimality in the maximum signal-to-interference-plus-noise (SINR) ratio.

In this chapter, we consider the synchronization of UWB multiple access signals in the presence of ISI for uplink scenarios, and estimate time delays of all users. However, in order to cope with ISI and MAI, we use a chip-level interleaved UWB system in which the chips corresponding to the same information bit are distributed in the packet according to the interleaver that comes before modulation. The general idea in using an interleaver after spreading the information bits and before modulating this spreaded

sequence is allow the chips corresponding to the same information bit to be as less correlated as possible. Chip-level interleaving was originally proposed in [50] as an alternative to channel-coded CDMA systems for ISI and MAI mitigation and extended to UWB systems in [51]. Since in both TH and DS spreading, many pulses are sent for each bit, iterative equalization methods proposed for coded systems can be applied to chip-level interleaved systems treating these many pulses as a repetition code. In chip-level interleaved systems, equalization and decoding of interleaved chips are the two blocks of the iterative algorithm yielding substantial performance gains through exchanging soft information.

The performance of the iterative algorithms depends on the performance of the other blocks in the receiver such as synchronization and channel estimation. To achieve good performances, the preceding blocks of the receiver are generally embedded in the iterative part of the receiver. In the context of synchronization, the tendency is to use soft information provided by the iterative algorithm to enhance the reliability of the estimates which is generally accomplished via *expectation-maximization* (EM) algorithm [55, 56, 57, 58, 59]. At each iteration, using soft values, the estimate of synchronization parameter, which correspond to the carrier phase in these works, is updated. Approaching the problem from a different point of view, [69] seems to be a benchmark work where the effect of the timing jitter on turbo equalization is investigated and a joint timing-equalization method is proposed which effectively redesigns the channel output trellis according to possible timing jitters on which a *Bahl-Jelinek-Cocke-Raviv* (BCJR)-like algorithm [70] jointly decides about the timing jitter and symbols.

The work in this chapter is different from these works in two aspects: **1:** The synchronization methods proposed here are for multiple access channels contrary to [55, 56, 57, 58, 59], where the single user links are considered. **2:** The algorithms presented in this chapter directly produces APPs of the possible time delays; i.e. synchronization unit is a SISO block, unlike other algorithms which eventually provide a hard estimate to the subsequent blocks in each iteration [55, 56, 57, 58, 59]. All the algorithms mentioned above, designed to work for phase synchronization (an exception is [69]),

are incompliant with UWB systems which are generally designed to operate at base-band in a carrierless fashion.

The block diagram of the proposed receiver is given in Figure 3.1, where the synchronization unit can work either blindly or in a data-aided manner. The *minimum mean squared error* (MMSE) *soft interference cancellation* (SIC) block is reminiscent of the algorithms presented in [52, 53, 54] with slight differences. Since the location of the pulses in the received packet cannot be determined due to unknown time delays, the MMSE SIC block produces the APP of each chip treating them as independent random variables with domain {-1,0,1}. The synchronization unit using the APPs provided by the MMSE SIC block produces the APPs of time delays with the aid of TH codes. For data-aided synchronization, training sequence is used for faster convergence of APPs of time-delays. In general, training sequences are used to obtain hard estimates of the parameters contrary to what we propose here, which uses training sequences to obtain APPs of the time delays. Although the decoder for chip-interleaved systems is rather simple [50, 51], due to unknown time delays, it becomes more involved in order to take the APPs of time delays into account. It produces extrinsic information for each chip at each iteration and it computes the APPs of the information bits at the last iteration.

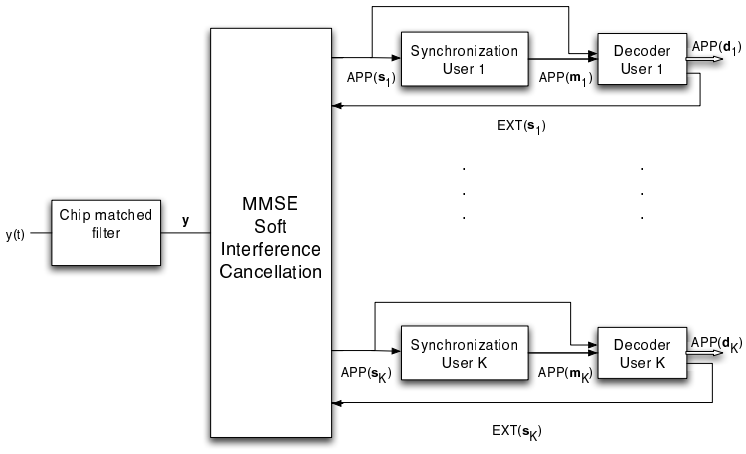

Figure 3.1. The block diagram of the proposed receivers.

This chapter is organized as follows: Section 3.1 explains the signal model of the chip-level interleaved UWB system, Section 3.2 outlines the blind synchronization method, Section 3.3 outlines the data-aided synchronization method and Section 3.4

describes the decoder. The simulation results are presented in Section 3.5 and Section 3.6 contains the discussions.

Notation Convention: Throughout Chapter 3, $x \doteq y$ means that x and y differ by a multiplicative constant.

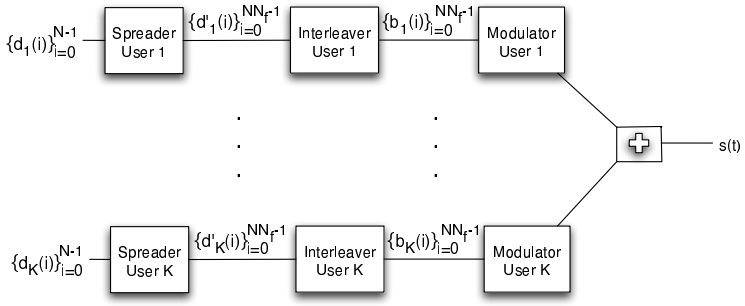

Figure 3.2. The block diagram of the transmitter.

3.1. Signal Model

In this paper, we consider a chip-level interleaved TH-UWB system for which the block diagram of the transmitter is given in Figure 3.2. The original information bits, $\{b_u(l)\}_{l=0}^{N_p-1}$, is first spread to $\{d'_u(l)\}_{l=0}^{N_pN_f-1}$ by using the TH code, $\{c_u(i)\}_{i=0}^{N_pN_f-1}$, then interleaved to $\{d_u(l)\}_{l=0}^{N_pN_f-1}$ by using the interleaver which is denoted by Π_u. The transmitted signal is given by

$$s(t) = \sum_{u=1}^{N_u} \sum_{j=0}^{N_pN_f} d_u\left(\left\lfloor \frac{j}{N_f} \right\rfloor\right) p\big(t - c_u(j)T_c\big) \tag{3.1}$$

where $c_u(j) \in \{\lfloor j/N_c \rfloor N_c, \ldots, \lfloor j/N_c \rfloor N_c + N_c - 1\}$ denote the position of chips in the packet in contrary to previous chapter where TH codes denote position of chips in each frame. An alternative spreading sequence, $\{g_u(j)\}_{j=0}^{N_pN_fN_c}$, can be defined as

$$g_u(j) = \begin{cases} d_u\left(\left\lfloor \frac{j}{N_fN_c} \right\rfloor\right) & \text{if } j = c_u\left(\left\lfloor \frac{j}{N_c} \right\rfloor\right), \\ \\ 0 & \text{otherwise} \end{cases} \tag{3.2}$$

where $g_u(j) = 0$ if no pulse is sent during jth chip and $g_u(j) = +1$ (resp. -1) if a pulse for information bit, $d_u(\lfloor j/N_f N_c \rfloor) = +1$ (resp. -1), is sent during jth chip. Therefore, transmitted signal in (3.1) can be written as

$$s(t) = \sum_{u=1}^{N_u} \sum_{j=0}^{N_p N_f N_c} g_u(j) p(t - jT_c) \tag{3.3}$$

where $g_u(j)$ can be viewed as chip-level spreading sequence of the uth user. The channel is modelled by

$$h_u(t) = \sum_{\ell=0}^{L_u - 1} h_\ell^u \delta\big(t - (\ell + m_u)T_c\big) \tag{3.4}$$

where the path delays are assumed to be integer multiples of the chip duration, T_c. Although this assumption results in a loss of the generality, the corresponding multipath channel model is quite common [72], especially if the channel resolvability is restricted to the pulse duration [71], T_c, as in our case. The variable m_u in (3.4) denotes the the delay of the first path, which is also assumed to be an integer that lies in $[0, N_f N_c - 1)$; i.e. time delay of the first path is assumed to be bounded by a symbol duration. As it will be clear when the receiver structures are explained, this restriction does not lead to a loss of generality, and it keeps simulation times to reasonable lengths. Furthermore, as indicated in [25], two-step synchronization methods can be employed for UWB systems, in which case algorithms presented in this paper constitute the fine synchronization stage of the signals from the acquisition stage where the timing uncertainty is reduced to the order of the pulse duration.

The received signal is formed by the receiver by observing the channel output over a duration of $(N_p + 1)N_f T_f$, where the additional symbol duration for each packet is necessary because of unknown time delays. Therefore, the received signal is given by

$$r(t) = \sum_{u=1}^{N_u} \sum_{j=0}^{(N_p+1)N_f N_c - 1} \sum_{\ell=0}^{L_u - 1} h_\ell^u g_u(j) p\Big(t - jT_c - \big(\ell + m_u T_c\big)\Big) + n(t) \tag{3.5}$$

where $n(t)$ is AWGN with zero mean and autocorrelation of $R_n(\tau) = \sigma^2\delta(\tau)$. The continuous time received signal, $r(t)$, is passed through a chip-matched filter and sampled at the multiples of T_c yielding

$$\mathbf{r} = \mathbf{H}\mathbf{s} + \mathbf{n} \tag{3.6}$$

where $\mathbf{r}$ is $((N_p+1)N_fN_c) \times 1$ column vector collecting chip-matched filter's output and first $\min_{u\in\{1,\ldots,N_u\}} m_u$ and last $N_fN_c - \max_{u\in\{1,\ldots,N_u\}} m_u$ entries consist of noise samples only. $\mathbf{H}$ is $((N_p+1)N_fN_c + L_{max} - 1) \times (N_u(N_p+1)N_fN_c)$ channel matrix consisting of N_u subchannel matrices as $\mathbf{H} = [\mathbf{H}_1 \ldots \mathbf{H}_{N_u}]$ where $\mathbf{H}_u$ is the channel matrix of the uth user and is given by

$$\mathbf{H}_u = \begin{bmatrix} h^u_0 & 0 & & \ldots & 0 \\ \vdots & h^u_0 & 0 & \ldots & 0 \\ h^u_{L_{\max}-1} & \vdots & & & \\ 0 & h^u_{L_{\max}-1} & & & 0 \\ & & & & \\ & & & & h^u_0 \\ \vdots & & & & \vdots \\ 0 & \ldots & & 0 & h^u_{L_{\max}-1} \end{bmatrix}$$

which is lower-triangular Toeplitz and $L_{\max} = \max_{u\in\{1,\ldots,N_u\}} L_u$ is the maximum path number among the users' channels and each user's channel response is extended to $L_{\max}$ paths by assuming that $h^u_\ell = 0, L_u - 1 < \ell < L_{\max}$. $\mathbf{s}$ in (3.6) is a $N_u(N_p+1)N_fN_c \times 1$ column matrix given by $\left[\mathbf{s}_1^T \ldots \mathbf{s}_{N_u}^T\right]^T$ and $\mathbf{s}_u$ is given by

$$\mathbf{s}_u = \left[\mathbf{0}^T_{m_u} g_u(0) \ldots g_u(N_pN_fN_c - 1)\mathbf{0}^T_{N_fN_c - m_u}\right]^T \tag{3.7}$$

where $\mathbf{0}_k$ denotes a $k \times 1$ column vector whose entries are identically 0. Moreover, $\mathbf{n}$ in (3.6) is the column vector consisting of noise samples which is Gaussian-distributed with zero-mean and a covariance of $\sigma^2\mathbf{I}$ where $\mathbf{I}$ denotes the identity matrix.

3.2. MMSE Soft Interference Cancellation

The MMSE SIC block is reminiscent of the iterative (turbo) equalization methods originally proposed in [52] and further developed in [53] for joint equalization and decoding, and also of the iterative algorithm presented in [54] for joint MAI plus ISI suppression and decoding. In these works, the equalization of modulated signals and the decoding of the channel code constitute two consecutive parts of the iterative algorithm. By exchanging their soft information which they extract from the independent pieces of the received vector (due to interleaver), substantial performance gains are obtained. However, since in TH-UWB multiple number of pulses are sent for each information bit, i.e. a repetition code is used, iterative equalization methods [53, 54] can be adopted to TH-UWB systems without using any further channel coding except this inherent repetition code in TH-UWB [51].

While we follow the general procedure described by the linear estimation methods of [53] and [54] for interference cancellation, the MMSE SIC block employed in this paper has slight differences which originate from both the UWB signal model and the unknown time delays. Because timing of the each user is unknown, our block cannot have any information about the locations of chips in the observed vector during which a pulse is sent. Moreover, in the absence of any prior information on $\{m_u\}_{u=1}^{K}$, the TH codes, which indicate relative positions of the chips in each frame, cannot be used, either. Therefore, instead of producing APPs of each data chip (during which a pulse is sent) indicating whether a +1 or -1 was sent, for each chip in the observed vector, $\mathbf{r}$, this block should generate APPs of each chips indicating whether a -1 or 0 or +1 was sent. Then, these APPs are feed into the synchronization block. While producing the APPs of the chips, this block ignores the information provided by the TH and repetition code by treating chip values as independent random variables. To produce reliable APPs, first this block uses an MMSE estimator to suppress both MAI and ISI. The MMSE estimator for the uth user's ith chip is of the form

$$\hat{s}_u(i) = \mathbf{f}_{u,i}^T \mathbf{r} + a \tag{3.8}$$

where $\mathbf{f}_{u,i}$ and a are chosen to minimize

$$\{\mathbf{f}_{u,i}, a\} = \arg\min_{\mathbf{f}_{u,i},a} E\left\{\mid s_u(i) - \hat{s}_u(i) \mid^2\right\} \tag{3.9}$$

where $s_u(i)$ denotes the ith element of $\mathbf{s}_u(i)$. The solution of (3.9) is given by [53]

$$\mathbf{f}_{u,i} = \left[\mathbf{H}\mathbf{C}_s\mathbf{H}^T + \sigma^2\mathbf{I}\right]^{-1}\mathbf{H}\mathbf{d}_{u,i}\nu_u^2(i) \tag{3.10}$$

$$a = \tilde{s}_u(i) - \mathbf{f}_{u,i}^T\mathbf{H}\tilde{\mathbf{s}} \tag{3.11}$$

where $\mathbf{d}_{u,i}$ is the $N_u(N_p+1)N_fN_c \times 1$ column vector whose entries are identically zero except $\mathbf{d}_{u,i}\left((u-1)(N_p+1)N_fN_c+i\right)=1$. $\tilde{s}_u(i)$ in (3.11) is the expected value of $s_u(i)$ which is given by

$$\tilde{s}_u(i) = \mathrm{EXT}\left(s_u(i)=+1\right) - \mathrm{EXT}\left(s_u(i)=-1\right) \tag{3.12}$$

where $\left\{\mathrm{EXT}\left(s_u(i)\right)\right\}_{i=0}^{(N_p+1)N_fN_c-1}$ are the extrinsic information about uth user's chips supplied to the MMSE SIC block by the uth user's decoder. Note that since chips values can take $\{-1,0,+1\}$, $\sum_{s_u(i)=-1}^{s_u(i)=+1}\mathrm{EXT}\left(s_u(i)\right)=1$. The $\tilde{\mathbf{s}}$ in (3.11) is the $N_u(N_p+1)N_fN_c \times 1$ column vector consisting of the mean values of the chips whose $\big((u-1)(N_p+1)N_fN_c+i\big)$th entry is denoted by $\tilde{s}_u(i)$. $\nu_u^2(i)$ in (3.10) is the variance of $s_u(i)$ which is given by

$$\nu_u^2(i) = \mathrm{EXT}\left(s_u(i)=+1\right) + \mathrm{EXT}\left(s_u(i)=-1\right) - \tilde{s}_u^2(i). \tag{3.13}$$

$\mathbf{C}_s$ in (3.10) is the covariance matrix of the $\mathbf{s}$ which is diagonal and $\big((u-1)(N_p+1)N_fN_c+i\big)$th diagonal element is $\nu_u^2(i)$. Therefore, using (3.10) and (3.11), the MMSE estimator of $s_u(i)$ can be expressed as

$$\hat{s}_u(i) = \mathbf{f}_{u,i}^T(\mathbf{r} - \mathbf{H}\tilde{\mathbf{s}}) + \tilde{s}_u(i) \tag{3.14}$$

where soft interference cancellation is performed first, followed by residual interfer-

ence (MAI plus ISI) and noise suppression by $\mathbf{f}_{u,i}$. Since our aim is to produce extrinsic information about the chip $s_u(i)$, we should alleviate dependency of $\hat{s}_u(i)$ on $\{\mathrm{EXT}\,(s_u(i))\}_{i=0}^{(N_p+1)N_fN_c-1}$ provided by the decoder in order to avoid any possible positive feedback between the receiver blocks. Therefore, mean and the variance of $s_u(i)$ in (3.10)-(3.11) should be replaced with the mean and variance values calculated according to uniform distribution which results in $\tilde{s}_u(i) = 0$ and $\nu_u^2(i) = 2/3$ because of the fact that each chip can take from $\{-1, 0, 1\}$. The MMSE estimator is given by

$$\begin{aligned} \hat{s}_u(i) &= \mathbf{d}_{u,i}^T\mathbf{H}^T\left[\mathbf{H}\mathbf{C}_s\mathbf{H}^T + \sigma^2\mathbf{I} + \left(\frac{2}{3} - \nu_u^2(i)\right)\mathbf{H}\mathbf{d}_{u,i}\left(\mathbf{H}\mathbf{d}_{u,i}\right)^T\right]^{-1} \\ &\times \left[\mathbf{r} - \mathbf{H}\big(\tilde{\mathbf{s}} - \mathbf{d}_{u,i}\tilde{s}_u(i)\big)\right] \end{aligned} \tag{3.15}$$

and by defining $\mathbf{C} \triangleq \mathbf{H}\mathbf{C}_s\mathbf{H}^T$ and employing matrix inversion lemma, we have

$$\left[\mathbf{C} + \left(\frac{2}{3} - \nu_u^2(i)\right)\mathbf{H}\mathbf{d}_{u,i}\left(\mathbf{H}\mathbf{d}_{u,i}\right)^T\right]^{-1} = \mathbf{C}^{-1} - \frac{\mathbf{C}^{-1}\mathbf{H}\mathbf{d}_{u,i}\left(\mathbf{H}\mathbf{d}_{u,i}\right)^T\mathbf{C}^{-1}}{\frac{1}{\frac{2}{3}-\nu_u^2(i)} + \left(\mathbf{H}\mathbf{d}_{u,i}\right)^T\mathbf{H}\mathbf{d}_{u,i}} \tag{3.16}$$

By equation (3.16), a single matrix inversion is carried out and modified according to the chip to be estimated for all users instead of calculating the matrix inverse in (3.15) for every chip of each user. Furthermore, the calculation of the matrix inverse in the right hand side of (3.16), i.e. $\mathbf{C}^{-1}$, can be managed in $\mathcal{O}(M^2)$ computations where M is the size of the matrix. This algorithm, presented in [54], exploits the diagonal structure of $\mathbf{C}_s$ and recursively calculates the matrix inverse. Now, the soft information from the output of the MMSE estimator will be generated. First, the output of the MMSE estimator can be rewritten as

$$\hat{s}_u(i) = \mu_u(i)s_u(i) + \eta_u(i) \tag{3.17}$$

where $\mu_u(i)$ is the mean of the MMSE estimator and $\eta_u(i)$ is the residual interference term plus noise which is well modelled by Gaussian distribution [73]. The expected

value of the MMSE estimator is given by [54]

$$\mu_u(i) = E\left\{\hat{s}_u(i)s_u(i)\right\} = \left(\mathbf{Hd}_{u,i}\right)^T \left[\mathbf{C}^{-1} - \frac{\mathbf{C}^{-1}\mathbf{Hd}_{u,i}\left(\mathbf{Hd}_{u,i}\right)^T\mathbf{C}^{-1}}{\frac{1}{\frac{2}{3}-\nu_u^2(i)} + \left(\mathbf{Hd}_{u,i}\right)^T\mathbf{Hd}_{u,i}}\right]\mathbf{Hd}_{u,i}. \quad (3.18)$$

The mean of $\eta_u(i)$ is zero, i.e. $E\{\eta_u(i) = 0\}$, and the variance is given by [54]

$$E\big\{\eta_u^2(i)\big\} = E\big\{\hat{s}_u^2(i)\big\} - \mu_u^2(i) = \mu_u(i) - \mu_u^2(i). \quad (3.19)$$

Therefore, APPs of chip values conditioned on the MMSE estimator outputs are given by

$$\mathrm{APP}(s_u(i) = -1) \doteq \exp\left(-\frac{\big(\hat{s}_u(i) + \mu_u(i)\big)^2}{2\mu_u(i)\big(1-\mu_u(i)\big)}\right), \quad (3.20)$$

$$\mathrm{APP}(s_u(i) = 0) \doteq \exp\left(-\frac{\hat{s}_u^2(i)}{2\mu_u(i)\big(1-\mu_u(i)\big)}\right), \quad (3.21)$$

$$\mathrm{APP}(s_u(i) = 1) \doteq \exp\left(-\frac{\big(\hat{s}_u(i) - \mu_u(i)\big)^2}{2\mu_u(i)\big(1-\mu_u(i)\big)}\right) \quad (3.22)$$

which are provided to the synchronization block of each user after normalization. In the next two sections, we will explain the blind and data-aided synchronization methods, respectively.

3.3. Blind Synchronization

The blind synchronization algorithm is presented in this section. In the blind synchronization method proposed here, using the APPs provided by the MMSE SIC block and the structure of TH codes, the APPs of time-delays will be generated which is essential for decoding of the information bits. Given time-delay, only N_pN_f of the total chips, namely of $(N_p+1)N_fN_c$ chips, in the received vector, $\mathbf{r}$, can take non-zero values. The exact positions of the chips in the received vector that can take non-zero values are governed by the TH code and they are unique given the time-delay. Therefore, the

APP of the time-delay of the uth user can be written as

$$\begin{aligned}\mathrm{APP}^b(m_u = l) &= \Pr\left\{m_u = l \mid \{c_u(i)\}_{i=0}^{N_pN_f-1}, \{s_u(j)\}_{j=0}^{(N_p+1)N_fN_c-1}\right\} \\ &= \frac{\Pr\left\{\{s_u(j)\}_{j=0}^{(N_p+1)N_fN_c-1} \mid m_u = l, \{c_u(i)\}_{i=0}^{N_pN_f-1}\right\}\Pr\{m_u = l\}}{\Pr\left\{\{s_u(j)\}_{j=0}^{(N_p+1)N_fN_c-1} \mid \{c_u(i)\}_{i=0}^{N_pN_f-1}\right\}}\end{aligned} \tag{3.23}$$

where unconditional probabilities of the time-delay, $\Pr\{m_u = l\}$, are assumed to be equal and the probabilities of the chip values can be viewed as independent of the TH code. It should be noted that unless the time-delay is known, the TH code cannot provide any information about the location of the data chips (in which a pulse is sent) and null chips (in which no pulse is sent) justifying the mutual independence of $\{s_u(j)\}_{j=0}^{(N_p+1)N_fN_c-1}$ and $\{c_u(i)\}_{i=0}^{N_pN_f-1}$. Therefore, (3.23) can be written as

$$\begin{aligned}\mathrm{APP}^b(m_u = l) &\doteq \Pr\left\{\{s_u(j)\}_{j=0}^{(N_p+1)N_fN_c-1} \mid m_u = l, \{c_u(i)\}_{i=0}^{N_pN_f-1}\right\} \\ &= \prod_{i=0}^{N_pN_f-1} \Pr\left\{s_u\big(l + c_u(i)\big) = +1 \text{ or } s_u\big(l + c_u(i)\big) = -1\right\} \\ &\times \prod_{j=0, j\notin\{c_u(i)+l, i=0,\ldots,N_pN_f-1\}}^{(N_p+1)N_fN_c-1} \Pr\left\{s_u(j) = 0\right\} \\ &= \prod_{i=0}^{N_pN_f-1} \Big[1 - \Pr\left\{s_u\left(l + c_u(i)\right) = 0\right\}\Big] \\ &\times \prod_{j=0, j\notin\{c_u(i)+l, i=0,\ldots,N_pN_f-1\}}^{(N_p+1)N_fN_c-1} \Pr\left\{s_u(j) = 0\right\}\end{aligned} \tag{3.24}$$

where in the second equality, we use the fact that given time-delay and TH code, a chip in the receiver value can take either 0 or $\{-1, +1\}$. It is also assumed that chips are independent, i.e. we did not the use the information of the repetition code and the interleaver, use of which are postponed to the decoding stage. Using the APPs of the

chips provided by the MMSE SIC block, namely (3.20)-(3.22), (3.25) can be written as

$$\begin{aligned} \mathrm{APP}^b(m_u = l) \;&\doteq\; \prod_{i=0}^{N_p N_f - 1} \Big[1 - \mathrm{APP}\big\{s_u\left(l + c_u(i)\right) = 0\big\}\Big] \\ &\times \prod_{j=0, j\notin\{c_u(i)+l, i=0,\ldots,N_p N_f-1\}}^{(N_p+1)N_f N_c - 1} \mathrm{APP}\big\{s_u\left(j\right) = 0\big\} \end{aligned} \tag{3.25}$$

which is computed for all-possible delays, $l = 0, \ldots, N_f N_c - 1$, and after normalization, is sent to the decoder which produces the extrinsic information for chips and the APPs of the information bits using the APPs of the time-delays, chips and the structure of the repetition code with interleaver.

3.4. Data-Aided Synchronization

In data-aided synchronization, a training sequence is sent for each user at the beginning of its packet both to improve upon the blind synchronization performance and to provide faster convergence of the APPs of the time delays. Suppose that N_t training symbols, i.e. $N_t N_f$ training frames, are transmitted for each packet as a preamble. The receiver first works on the training sequence whose received vector is denoted by $\mathbf{r}^t$ that consists of first $(N_t{+}1)N_f N_c$ entries of $\mathbf{r}$ where additional one symbol observation, i.e. $N_f N_c$, is necessary due to unknown time delay. After completion of training sequence processing, receiver starts to work for data sequence which is denoted $\mathbf{r}^d$. While the receiver is working on data sequence, the APPs of time delays are also obtained blindly, and combined with the APPs obtained from the training sequence. Since acquiring APPs of time delays blindly is explained in the previous section, we focus on obtaining APPs from $\mathbf{r}^t$ using the knowledge of the training sequence and the MMSE SIC block outputs.

The position of the training sequence in $\{\mathbf{s}_u\}_{u=1}^K$, and the received vector, $\mathbf{r}^t$, cannot be located in the absence of any prior information about time delays of the users, and the use of the training sequence in the MMSE SIC block may become problematic. Moreover, initialization of MMSE SIC block with hard estimate of the

time delays, which can be obtained through use of training sequences, may result in performance losses. Therefore, through data-aided synchronization, MMSE SIC block is decided to be kept same to produce the APPs of all chips given by (3.20)-(3.22) ignoring the knowledge of the training sequence.

The synchronization block should use training sequence in conjunction with the APPs provided by the MMSE SIC block to produce soft information about time delays. It should be noted that training sequences are generally used to obtain hard estimates of the parameters contrary to what we propose here, where training sequences are employed to obtain APPs of the time delays. The output of the MMSE SIC block for uth user's training sequence can be expressed in matrix form as

$$\hat{\mathbf{s}}_u = \mathbf{\Delta}_\mu^u \mathbf{\Lambda}_l^u \mathbf{s}_t^u + \boldsymbol{\eta}_u \tag{3.26}$$

where $\hat{\mathbf{s}}_u$ is an $(N_t+1)N_fN_c \times 1$ column vector whose entries are the MMSE estimates of the chips of the uth user's training sequence, $\mathbf{\Delta}_\mu^u$ is an $(N_t+1)N_fN_c \times (N_t+1)N_fN_c$ diagonal matrix whose jth diagonal entry is the mean value of the MMSE estimate of the jth chip of the uth user's training sequence, $\mathbf{\Lambda}_l^u$ is an $(N_t+1)N_fN_c \times N_tN_fN_c$ matrix whose first l and last $N_fN_c - l$ rows are all zero rows and the remaining part is given by given by an $N_tN_fN_c \times N_tN_fN_c$ identity matrix and $\mathbf{s}_t^u$ is an $N_tN_fN_c \times 1$ column vector consisting of the training sequence of the uth user. The effect of the time-delay on the received signal is governed by $\mathbf{\Lambda}_l^u$. $\boldsymbol{\eta}_u$ is the column vector consisting of the noise plus residual interference terms at the output of the MMSE SIC block. Note that it has been shown in Section 3.2 that the mean of $\boldsymbol{\eta}_u$ is zero. Moreover, since the variance of each term in $\boldsymbol{\eta}_u$ is calculated at the MMSE SIC block to produce APPs, at data-aided synchronization block, there is no need to recalculate. Furthermore, as in MMSE SIC block, $\boldsymbol{\eta}_u$ is assumed to be Gaussian and its covariance matrix will be denoted by $E\left\{\boldsymbol{\eta}_u \boldsymbol{\eta}_u^T\right\} = \mathbf{C}_\eta^u$ which is assumed to be diagonal to simplify calculations. Validation of this assumption is given by the performance results presented in Section 3.6.

Since the system works with soft values (APPs) of time-delay, the goal is to

produce APPs of time-delay using the signal model in (3.26), the training sequence $\mathbf{s}_t^u$, the mean matrix $\boldsymbol{\Delta}_\mu^u$, and the covariance matrix $\mathbf{C}_\eta^u$ of $\boldsymbol{\eta}_u$. Examination of ML-estimator of the time-delay provides the necessary insight to derive soft-values. The ML estimate is

$$\begin{aligned}
\hat{m}_u &\doteq \arg\max_l \exp\left\{-\frac{1}{2}\left(\hat{\mathbf{s}}_u - \boldsymbol{\Delta}_\mu^u \boldsymbol{\Lambda}_l^u \mathbf{s}_t^u\right)^T \mathbf{C}_\eta^{u^{-1}} \left(\hat{\mathbf{s}}_u - \boldsymbol{\Delta}_\mu^u \boldsymbol{\Lambda}_l^u \mathbf{s}_t^u\right)\right\} \\
&\doteq \arg\max_l \left\{\left(\boldsymbol{\Lambda}_l^u \mathbf{s}_t^u\right)^T \left(\boldsymbol{\Delta}_\mu^u\right)^T \mathbf{C}_\eta^{u^{-1}} \hat{\mathbf{s}}_u - \frac{1}{2}\left(\boldsymbol{\Delta}_\mu^u \boldsymbol{\Lambda}_l^u \mathbf{s}_t^u\right)^T \mathbf{C}_\eta^{u^{-1}} \left(\boldsymbol{\Delta}_\mu^u \boldsymbol{\Lambda}_l^u \mathbf{s}_t^u\right)\right\} \quad (3.27) \\
&\approx \arg\max_l \left(\boldsymbol{\Lambda}_l^u \mathbf{s}_t^u\right)^T \left(\boldsymbol{\Delta}_\mu^u\right)^T \mathbf{C}_\eta^{u^{-1}} \hat{\mathbf{s}}_u \quad (3.28)
\end{aligned}$$

where the second terms in (3.27) is negligible with respect to first one. Therefore, ML estimator chooses the maximum of the following r.v.s

$$\alpha_l^u = \left(\boldsymbol{\Lambda}_l^u \mathbf{s}_t^u\right)^T \left(\boldsymbol{\Delta}_\mu^u\right)^T \mathbf{C}_\eta^{u^{-1}} \hat{\mathbf{s}}_u \quad (3.29)$$

whose mean, variance and covariance conditioned on the actual delay, m_u, are respectively given by

$$\begin{aligned}
E\left\{\alpha_l^u \mid m_u\right\} &= \left(\boldsymbol{\Lambda}_l^u \mathbf{s}_t^u\right)^T \left(\boldsymbol{\Delta}_\mu^u\right)^T \mathbf{C}_\eta^{u^{-1}} \left(\boldsymbol{\Delta}_\mu^u\right) \left(\boldsymbol{\Lambda}_{m_u}^u \mathbf{s}_t^u\right) \quad (3.30) \\
\mathrm{var}\{\alpha_l^u \mid m_u\} = \mathrm{var}\{\alpha_l^u\} &= \left(\boldsymbol{\Lambda}_l^u \mathbf{s}_t^u\right)^T \left(\boldsymbol{\Delta}_\mu^u\right)^T \mathbf{C}_\eta^{u^{-1}} \left(\boldsymbol{\Delta}_\mu^u\right) \left(\boldsymbol{\Lambda}_l^u \mathbf{s}_t^u\right) \quad (3.31) \\
\mathrm{cov}\{\alpha_l^u, \alpha_k^u \mid m_u\} &= \left(\boldsymbol{\Lambda}_l^u \mathbf{s}_t^u\right)^T \left(\boldsymbol{\Delta}_\mu^u\right)^T \mathbf{C}_\eta^{u^{-1}} \left(\boldsymbol{\Delta}_\mu^u\right) \left(\boldsymbol{\Lambda}_k^u \mathbf{s}_t^u\right). \quad (3.32)
\end{aligned}$$

In classical ML set up, hard estimate is produced by choosing the maximum of $\{\alpha_i^u\}_{i=0}^{N_f N_c - 1}$. But to represent the estimate with its reliability, that is to produce soft information, not hard estimates, the probabilities of each possible situation should be sent. Then, the APPs of time-delay, m_u, conditioned on the r.v.s, $\{\alpha_i^u\}_{i=0}^{N_f N_c - 1}$ should be generated as follows

$$\begin{aligned}
\mathrm{APP}^t(m_u = l) &\triangleq \Pr\left\{m_u = l \mid \{\alpha_i^u\}_{i=0}^{N_f N_c - 1}\right\} \\
&\doteq \Pr\left(\{\alpha_i^u\}_{i=0}^{N_f N_c - 1} \mid m_u = l\right) \Pr\left\{m_u = l\right\} \quad (3.33)
\end{aligned}$$

where $\Pr\left(\{\alpha_i^u\}_{i=0}^{N_f N_c-1} \mid m_u = l\right)$ is the conditional distribution of $\{\alpha_i^u\}_{i=0}^{N_f N_c-1}$ which is assumed to be Gaussian with moments given in (3.30)-(3.32). By defining the mean vector and the covariance matrix of $\{\alpha_i\}_{i=0}^{N_f N_c-1}$ to be $\boldsymbol{\mu}_\alpha^u$ and $\mathbf{C}_\alpha^u$, respectively, and assuming $\Pr\{m_u = l\}$ to have a uniform distribution, (3.33) becomes

$$\mathrm{APP}^t(m_u = l) \doteq \exp\left\{-\frac{1}{2}\left(\boldsymbol{\alpha}^u - \boldsymbol{\mu}_\alpha^u\right)^T \mathbf{C}_\alpha^u \left(\boldsymbol{\alpha}^u - \boldsymbol{\mu}_\alpha^u\right)\right\} \tag{3.34}$$

where $\boldsymbol{\alpha}^u$ is the column vector representation of $\{\alpha_i^u\}_{i=0}^{N_f N_c-1}$. It should be noted that as for data sequences, all the blocks of the receiver except for synchronization unit assume training sequence to be an unknown data sequence. Therefore, receiver performs iterations on the training sequence where at each iteration, the APPs of the time-delays, (3.34), formed through the training sequence, are updated.

Once the APPs of the time-delays are obtained from the training sequence, the receiver starts to work on data part of the received vector, $\mathbf{r}^d$, from which APPs of the time-delays can be obtained blindly as described in the previous section. Therefore, the two APPs obtained by data part of the packet and the training sequence should be combined. The probability of time-delays conditioned on both training and data sequences can be written as

$$\begin{aligned}\mathrm{APP}(m_u = l) &\triangleq \Pr\left\{m_u = l \mid \mathbf{r}^d, \mathbf{r}^t\right\} \doteq \Pr\left(\mathbf{r}^d, \mathbf{r}^t \mid m_u = l\right) \Pr\{m_u = l\} \\ &\doteq \Pr\left(\mathbf{r}^d, \mathbf{r}^t \mid m_u = l\right). \end{aligned} \tag{3.35}$$

Using independence of $\mathbf{r}^d$ and $\mathbf{r}^t$, (3.35) can be written as

$$\begin{aligned}\mathrm{APP}(m_u = l) &\doteq \Pr\left(\mathbf{r}^d \mid m_u = l\right) \Pr\left(\mathbf{r}^t \mid m_u = l\right) \\ &\approx \mathrm{APP}^t(m_u = l)\mathrm{APP}^b(m_u = l). \end{aligned} \tag{3.36}$$

The APPs in (3.36) are sent to decoder which will produce extrinsic information about chip values and the information bit probabilities using the knowledge of the interleaver and the repetition code.

3.5. Decoder

The decoder produces the extrinsic information about chip values and the information bit probabilities. In generation of these probabilities, the decoder employs the knowledge of the interleaver structure, the repetition code and the soft information about chip values provided by the MMSE SIC block in addition to the APPs of the time delay given by (3.25) if the system works in a blind mode and by (3.36) if the system works in a data-aided manner. As the MMSE SIC block, the decoder also ignores the knowledge of the training sequence if the receiver works in a data-aided manner.

The main objectives in this block are to generate extrinsic information about chip values which are provided to the MMSE SIC block, and to calculate the information bit probabilities at the last iteration of the packet to provide decision statistics. The extrinsic information about chip values is

$$\mathrm{EXT}(s_u(i)) \triangleq \Pr\left\{ s_u(i) \mid \{s_u(n)\}_{n=0,n\neq i}^{(N_p+1)N_fN_c-1}, \Pi_u, \{c_u(j)\}_{j=0}^{N_pN_f-1} \right\} \tag{3.37}$$

which is the conditional probability of ith chip of the uth user, that is $s_u(i)$, conditioned on the other chips and the TH code of the uth user, and the interleaver function, Π_u. (3.37) can be written as

$$\begin{aligned} \mathrm{EXT}(s_u(i)) &= \sum_{l=0}^{N_fN_c-1} \Pr\{m_u = l\} \\ &\times \Pr\left\{ s_u(i) \mid \{s_u(n)\}_{n=0,n\neq i}^{(N_p+1)N_fN_c-1}, \Pi_u, \{c_u(j)\}_{j=0}^{N_pN_f-1}, m_u = l \right\} \end{aligned} \tag{3.38}$$

using the probability distribution of the time-delay. The cases $\{s_u(i) = +1 \text{ or } s_u(i) = -1\}$ and $s_u = 0$ will be treated separately. For the conditional probability

$$\Pr\left\{ s_u(i) = +1 \mid \{s_u(n)\}_{n=0,n\neq i}^{(N_p+1)N_fN_c-1}, \Pi_u, \{c_u(j)\}_{j=0}^{N_pN_f-1}, m_u = l \right\} \tag{3.39}$$

to be non-zero,

$$i = l + c_u\left(\left\lfloor \frac{i-l}{N_c} \right\rfloor\right) \tag{3.40}$$

should be satisfied where $l \in \{0, \ldots, N_f N_c - 1\}$. The reasoning of the condition (3.40) is that if time-delay is zero, i.e. $m_u = 0$, the positions of the data chips in $\mathbf{r}$ is given by $\{c_u(j)\}_{j=0}^{N_p N_f N_c - 1}$ but if time-delay is not zero, each data chip's position shifts according to the time-delay, $m_u = l$. Therefore, for a chip position, say ith chip, in the received vector to belong a data chip, its original location should be $c_u(j)$ in the transmitted signal but shifted to this position in the received signal due to time-delay which implies $c_u(j) + l = i$, i.e. $c_u(j) = i - l$. Since j in $c_u(j)$ is the number of frame into where $i - l$ falls, $j = \lfloor (i-l)/N_c \rfloor$ yielding (3.40). Moreover, the range of l is given by $\{0, \ldots, N_f N_c - 1\}$ because of the fact that time-delay is restricted to one symbol duration which also implies that there exists only N_f possible values of l satisfying (3.40). Denoting the set of l values that satisfy (3.40) as $\mathcal{J}_i^u$, for $s_u(i) = +1$, (3.38) can be written as

$$\mathrm{EXT}\big(s_u(i) = +1\big) = \sum_{l \in \mathcal{J}_i^u} \Pr\{m_u = l\} \Pr\left\{ s_u(i) = +1 \mid \left\{ s_u(n), n \in \mathcal{S}_{i,l}^u \right\}, m_u = l \right\} \tag{3.41}$$

where $\mathcal{S}_{i,l}^u$ is the index of the chips in the received vector, that correspond to the same information bit given that time-delay, $m_u = l$, which is explicitly given by

$$\mathcal{S}_{i,l}^u = \left\{ \Pi_u\left(c_u(j)\right) \neq i : j \in \left\{ \left\lfloor \frac{\Pi_u^{-1}(i-l)}{N_f N_c} \right\rfloor N_f, \ldots, \left(\left\lfloor \frac{\Pi_u^{-1}(i-l)}{N_f N_c} \right\rfloor + 1 \right) N_f - 1 \right\} \right\} \tag{3.42}$$

which contains the $N_f - 1$ chip positions. The conditional probability in (3.41) is

$$\begin{aligned}
&\Pr\left\{s_u(i) = +1 \mid \left\{s_u(n), n \in \mathcal{S}_{i,l}^u\right\}, m_u = l\right\} \\
&= \frac{\Pr\left\{\left\{s_u(n), n \in \mathcal{S}_{i,l}^u\right\}, s_u(i) = +1, m_u = l\right\}}{\Pr\left\{\left\{s_u(n), n \in \mathcal{S}_{i,l}^u\right\}, m_u = l\right\}} \\
&\approx \prod_{n \in \mathcal{S}_{i,l}^u} \frac{\Pr\left\{s_u(n), s_u(i) = +1 \mid m_u = l\right\}}{\Pr\left\{s_u(n) \mid m_u = l\right\}} \\
&= \prod_{n \in \mathcal{S}_{i,l}^u} \frac{\Pr\left\{s_u(n) = +1, s_u(i) = +1 \mid m_u = l\right\}}{\sum_{s_u(i)=-1}^{+1} \Pr\left\{s_u(n), s_u(i) \mid m_u = l\right\}}
\end{aligned} \tag{3.43}$$

where we assume that the chips in $\mathcal{S}_{i,l}^u$ are independent to simplify calculations and at the last step we use the fact that polarity of all chips in $\mathcal{S}_{i,l}^u$ are the same as that of $s_u(i)$. The denominator in (3.43) is given by

$$\begin{aligned}
\sum_{s_u(i)=-1}^{+1} \Pr\left\{s_u(n), s_j(i) \mid m_u = l\right\} &= \Pr\left\{s_u(n) = s_u(i) = +1 \mid m_u = l\right\} \\
+ \quad \Pr\left\{s_u(n) = s_u(i) = -1 \mid m_u = l\right\} &+ \Pr\left\{s_u(n) = s_u(i) = 0 \mid m_u = l\right\}
\end{aligned} \tag{3.44}$$

where $\Pr\left\{s_u(n) = 0, s_u(i) = 0 \mid m_u = l\right\}$ is zero because given $m_u \in \mathcal{J}_i^u$, $s_u(n)$ and $s_u(i)$ correspond to the chips during which pulses are transmitted which means that they can be either $+1$ or -1. Therefore, (3.43) can be written as

$$\begin{aligned}
&\Pr\left\{s_u(i) = +1 \mid \left\{s_u(n), n \in \mathcal{S}_{i,l}^u\right\}, m_u = l\right\} = \\
&\quad \prod_{n \in \mathcal{S}_{i,l}^u} \frac{\Pr\left\{s_u(n) = s_u(i) = +1 \mid m_u = l\right\}}{\Pr\left\{s_u(n) = s_u(i) = +1 \mid m_u = l\right\} + \Pr\left\{s_u(n) = s_u(i) = -1 \mid m_u = l\right\}} \\
&= \prod_{n \in \mathcal{S}_{i,l}^u} \frac{\mathrm{APP}\left\{s_u(n) = +1\right\}}{\mathrm{APP}\left\{s_u(n) = +1\right\} + \mathrm{APP}\left\{s_u(n) = -1\right\}}
\end{aligned} \tag{3.45}$$

where $\mathrm{APP}(s_u(n))$s are given by (3.20)-(3.22). Therefore, putting (3.45) into (3.41),

the extrinsic information for the cases $s_u(i) = \pm 1$ can be obtained as

$$\begin{aligned} \mathrm{EXT}(s_u(n) = \pm 1) &= \sum_{l \in \mathcal{J}_i^u} \Pr\{m_u = l\} \\ &\times \prod_{n \in \mathcal{S}_{i,l}^u} \frac{\mathrm{APP}\left\{s_u(n) = \pm 1\right\}}{\mathrm{APP}\left\{s_u(n) = +1\right\} + \mathrm{APP}\left\{s_u(n) = -1\right\}}. \end{aligned} \quad (3.46)$$

We will consider extrinsic information for $s_u(i) = 0$ next. To that end, first the probability

$$\Pr\left\{s_u(i) = 0 \mid \{s_u(n)\}_{n=0, n\neq i}^{(N_p+1)N_f N_c - 1}, \Pi_u, \{c_u(j)\}_{j=0}^{N_p N_f - 1}, m_u = l\right\} \quad (3.47)$$

is considered for which to be non-zero,

$$i \neq l + c_u\left(\left\lfloor \frac{i-l}{N_c} \right\rfloor\right) \quad (3.48)$$

should be satisfied which is nothing but the complement of (3.40) which states the possible values of the time-delay which result in the situation that a pulse is sent during ith chip position. Therefore, if (3.48) is satisfied, no pulse is transmitted during ith chip position in which case the probability in (3.47) becomes 1, or in other words,

$$\Pr\left\{s_u(i) = \pm 1 \mid \{s_u(n)\}_{n=0, n\neq i}^{(N_p+1)N_f N_c - 1}, \Pi_u, \{c_u(j)\}_{j=0}^{N_p N_f - 1}, m_u = l\right\} = 0. \quad (3.49)$$

Furthermore, if (3.48) is not satisfied, i.e. (3.40) is satisfied, the probability in (3.47) becomes 0, or in other words

$$\Pr\left\{s_u(i) \neq 0 \mid \{s_u(n)\}_{n=0, n\neq i}^{(N_p+1)N_f N_c - 1}, \Pi_u, \{c_u(j)\}_{j=0}^{N_p N_f - 1}, m_u = l\right\} = 1. \quad (3.50)$$

By defining the complement of $\mathcal{J}_i^u$ as $\mathcal{J}_i^{u^c}$ and using (3.38), the extrinsic information of $s_u(i) = 0$ can be written as

$$\mathrm{EXT}(s_u(i)=0)=\sum_{l\in\mathcal{J}_i^{u^c}}\Pr\{m_u=l\}. \tag{3.51}$$

Extrinsic information for each chip is calculated at each iteration via (3.46) and (3.51) and provided to the MMSE SIC block which uses this knowledge in MMSE filtering. At the last iteration, decoder also computes the information bit probabilities using the TH and repetition code, and the APPs of chips and the time-delay. The APPs of uth user's information bits, $\{b_u(i)\}_{i=0}^{N_p-1}$, are given by

$$\begin{aligned}\mathrm{APP}(b_u(i)) &\triangleq \Pr\left\{b_u(i)\mid \{s_u(n)\}_{n=0,n\neq i}^{(N_p+1)N_fN_c-1},\Pi_u,\{c_u(j)\}_{j=0}^{N_pN_fN_c-1}\right\}\\ &= \sum_{l=0}^{N_fN_c-1}\Pr\{m_u=l\}\Pr\left\{b_u(i)\mid \{s_u(n)\}_{n=0}^{(N_p+1)N_fN_c-1},\Pi_u,\{c_u(j)\}_{j=0}^{N_pN_fN_c-1},m_u=l\right\}\end{aligned} \tag{3.52}$$

where the conditional probability of bits depend on only N_f of $\{s_u(n)\}_{n=0}^{(N_p+1)N_fN_c-1}$ for a particular value of time-delay, $m_u=l$, because of the fact that for each information bit N_f pulses are sent. Defining the set of these N_f indexes as

$$\mathcal{B}_{i,l}^u=\left\{n: n=\Pi_u\left(c_u(j)\right)\ \text{where } j\in\{iN_f,\ldots,(i+1)N_f-1\}\right\}, \tag{3.53}$$

(3.52) can be expressed as

$$\mathrm{APP}\big(b_u(i)\big)=\sum_{l=0}^{N_fN_c-1}\Pr\{m_u=l\}\Pr\left\{b_u(i)\mid \{s_u(n)\}_{n\in\mathcal{B}_{i,l}^u},m_u=l\right\} \tag{3.54}$$

where the conditional probability can be written as

$$\begin{aligned}
\Pr\left\{b_u(i) \mid \{s_u(n)\}_{n\in\mathcal{B}^u_{i,l}}, m_u = l\right\} &= \frac{\Pr\left\{b_u(i), \{s_u(n)\}_{n\in\mathcal{B}^u_{i,l}} \mid m_u = l\right\}}{\Pr\left\{\{s_u(n)\}_{n\in\mathcal{B}^u_{i,l}} \mid m_u = l\right\}} \\
&\approx \prod_{n\in\mathcal{B}^u_{i,l}} \frac{\Pr\{b_u(i), s_u(n) \mid m_u = l\}}{\Pr\{s_u(n) \mid m_u = l\}} \\
&= \prod_{n\in\mathcal{B}^u_{i,l}} \frac{\Pr\{b_u(i), s_u(n) \mid m_u = l\}}{\sum_{\forall b_u(i)\in\{-1,+1\}} \Pr\{b_u(i), s_u(n) \mid m_u = l\}} \\
&= \prod_{n\in\mathcal{B}^u_{i,l}} \frac{\mathrm{APP}(s_u(n))}{\mathrm{APP}(s_u(n) = +1) + \mathrm{APP}(s_u(n) = -1)}
\end{aligned} \tag{3.55}$$

where we assume that chips are independent. Therefore, using (3.55), the APP of $b_u(i)$, i.e. (3.54), can be expressed as

$$\mathrm{APP}(b_u(i)) = \sum_{l=0}^{N_f N_c - 1} \Pr\{m_u = l\} \prod_{n\in\mathcal{B}^u_{i,l}} \frac{\mathrm{APP}(s_u(n))}{\mathrm{APP}(s_u(n) = +1) + \mathrm{APP}(s_u(n) = -1)} \tag{3.56}$$

which is computed for all information bits at the last iteration and decision is declared according to these values.

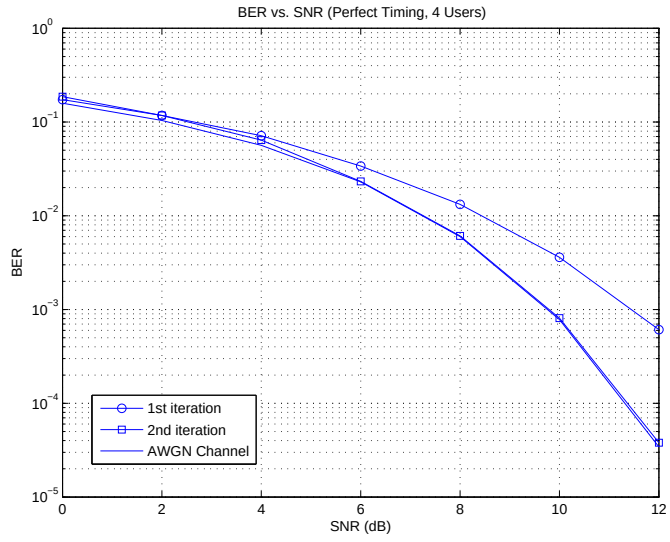

Figure 3.3. The bit-error-rate of the iterative equalization with perfect knowledge of time-delays in a four user link.

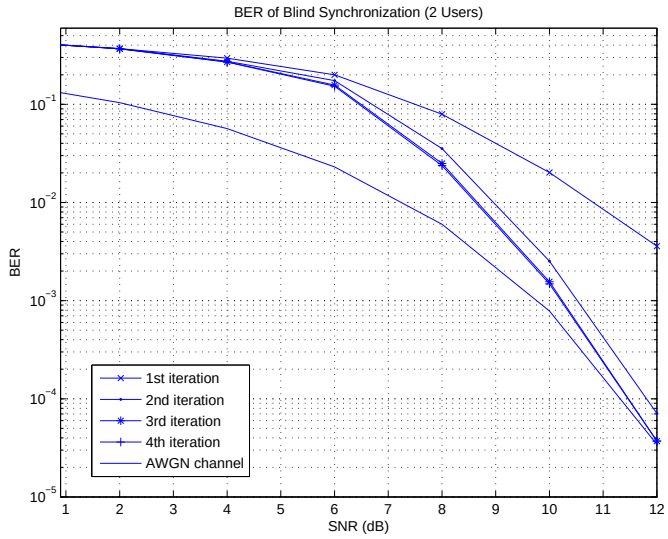

Figure 3.4. The bit-error-rate of blind synchronization in a two user link.

3.6. Simulation Results

In this section, simulation results of both blind and data-aided synchronization are presented. In all simulations, *channel model one* (CM1) [23] was used as the multipath channel whose delay spread is about 30 ns which leads to severe ISI and IFI. Each user's TH code is generated randomly as well as the mapping of the interleaver function, i.e. Π_u. In all graphs, AWGN channel represents the case where a single user transmits through an ISI free channel. Pulse and chip durations are set equal to 1 ns, i.e. $T_c = T_p = 1$ ns. The packet size is 100 information bits. The SNR is defined to be E_s/σ^2. But it should be noted that effective SNR, which is the ratio of received symbol energy to the noise variance, depends on the IFI, hence the channel spread.

First, the performance of the receiver with perfect knowledge of all users' time delays is considered. The number of users, K, is set to 4, the frame duration, T_f, is selected as 8 ns and each bit is sent via 5 pulses, i.e. $N_f = 5$. Figure 3.3 shows that the BER of the receiver with perfect knowledge of time delays converges to the single user bound in just two iterations. This graph and the single user bound (AWGN channel) are the benchmarks for performance evaluation of synchronization methods proposed in this chapter such that closeness of the BER of the proposed receivers to the single user bound and the number of iterations that take receivers to convergence this bound

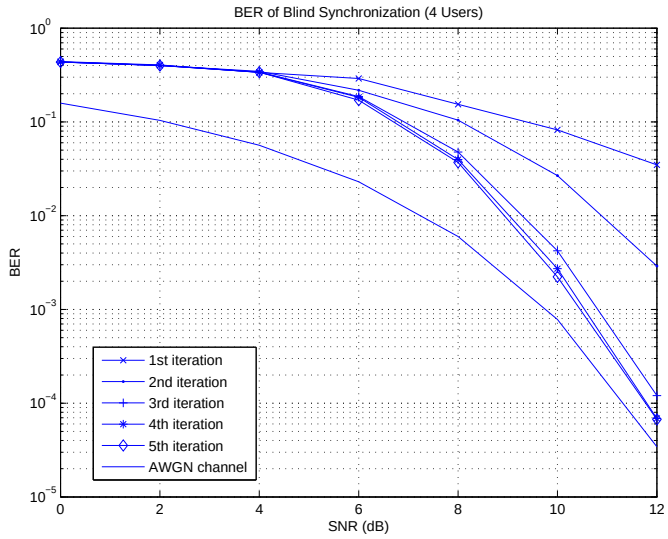

Figure 3.5. The bit-error-rate of blind synchronization in a four user link.

are of interest.

We consider blind synchronization method, next. The frame duration and number of frames are kept the same such as $T_f = 8$ ns and $N_f = 5$. The performance of the receiver is evaluated for a two-user link, the results are given in Figure 3.4, where it can be seen that blind synchronization catches up with the single user bound in just three iterations and at SNR values of 12 dB and higher. Although the number of users is doubled in Figure 3.5, the performance is still within $0.5 - 1$ dB of the single user link in four iterations and at SNR values such as $10 - 12$ dB. These two graphs indicate the convincing performance of the blind synchronization method proposed in this chapter.

Concentrating on the data-aided synchronization, the frame duration is shortened to 6 ns, i.e. $T_f = 6$ ns, and the number of pulses sent for each information bit is decreased to 4, i.e. $N_f = 4$. With these changes, ISI and IFI increase and the redundancy due to spreading decreases. First, a four-user link is simulated where only 10 training bits are sent for each packet. The result is given in Figure 3.6, where the BER with data-aided synchronization catches up with single-user bound in only three iterations and at 6 dB which is approximately same as the performance of receiver with perfect knowledge of the time delay. Then, we increase the number of users to six and the number of training bits to 20, whose result is given in Figure 3.7. It should

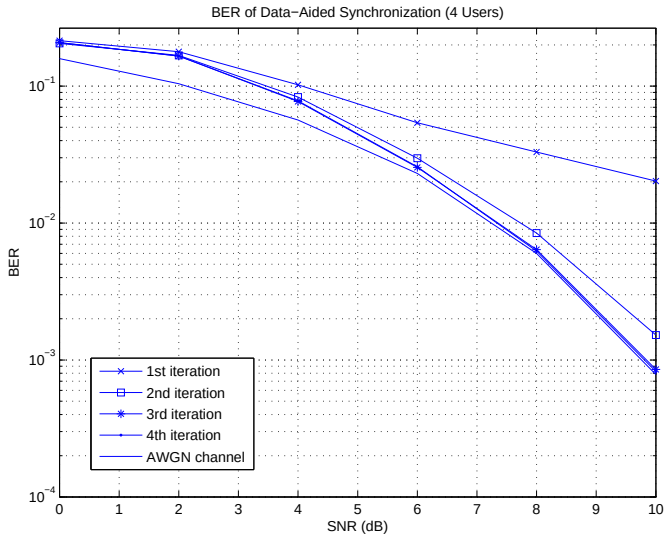

Figure 3.6. The bit-error-rate of data-aided synchronization in a four user link.

be noted that six users is the multiple access limit of this system that allows no collision between users. In such case, the performance of data-aided synchronization still catches up with single user bound in four iterations and at 8-10 dB SNR.

3.7. Discussions

In this chapter, two iterative synchronization methods are proposed for chip-level interleaved TH-UWB signals. They work directly on soft information provided by the MMSE SIC block and produce soft information about time delay, i.e. they are SISO. The adoptability of these synchronization methods to transmission links subject to ISI and MAI is accomplished by using a MMSE SIC block and a channel decoder and employing turbo equalization method. Although, these are two standard blocks of the iterative equalization, they should be modified to incorporate soft information of time delays. However, in contrary to the MMSE SIC block, whose adaptation is rather straightforward, the channel decoder is almost redesigned to work with soft information about time delay. It is shown that proposed receivers can catch the single user bound at moderate SNRs within a few iterations.

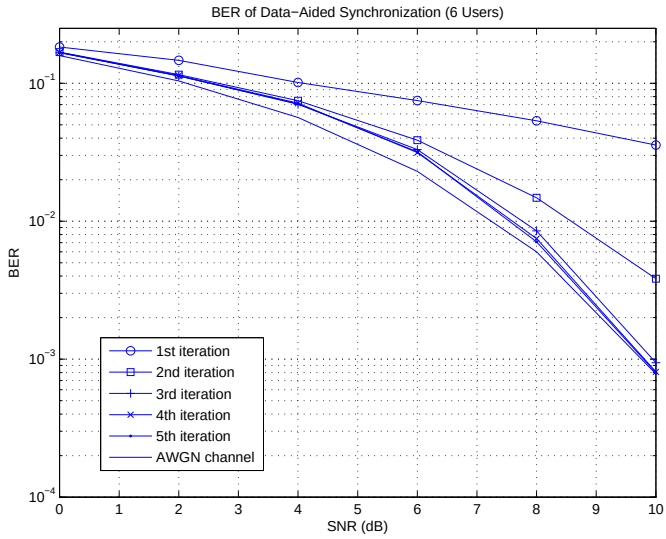

Figure 3.7. The bit-error-rate of data-aided synchronization in a six user link.

4. ROBUST CHANNEL ESTIMATION UNDER NON-GAUSSIAN NOISE

UWB communication faces severe frequency selectivity and requires high sampling rates, therefore it introduces unique signal processing challenges in the receiver design, especially in the areas of synchronization, channel estimation and signal detection [2]. For instance, sampling rates in UWB systems are on the order of 10 GHz, which makes the number of parameters to be estimated 24 for line-of-sight (LOS) and as large as 400 for *non-line-of-sight* (NLOS) indoor channels [23]. In addition to the severe ISI effect of the channels at high sampling rates, another phenomenon that must be considered in UWB system design is the noise, which is often overlooked and is simply assumed to be AWGN. However, as reported in [46], indoor environments where the UWB devices are envisioned to be deployed are subject to noise produced by electronic devices running concurrently, which is impulsive (non-Gaussian) in nature. Therefore, UWB systems designed to be optimum under Gaussian noise face severe performance losses when the actual noise distribution deviates from the assumed nominal Gaussian model [74]. For these reasons, in this chapter we consider the general channel estimation and detection problem for UWB systems under impulsive noise and present robust receiver algorithms.

The existing literature on UWB channel estimation and detection is usually limited to the scenarios where true noise is assumed to be Gaussian. For example, in [27], a two step estimation procedure is proposed where the first step consists of a time-delay search and the second step estimates the path gains. In this approach, the number of rays are assumed to be known at the receiver resulting in a performance loss otherwise. Another drawback, even in the Gaussian case, is computational load that is exponentially increasing with the number of rays. This prohibitive complexity is partially simplified in [26, 27, 28, 29] by assuming a resolvable channel where the paths are uncorrelated. However, this is not a fully justified assumption under realistic UWB indoor channel models such as the *Saleh-Valenzuela* (S-V) model [23] where the

multipath components arrive at the receiver in clusters with nonresolvable rays. Even with this assumption, the large number of multipath components in an UWB channel for sufficient energy capture still brings am unaffordable computational complexity to the detection and estimation. For this reason and inspired by the SC-FDE techniques proposed in [75, 76, 77, 78, 79], FD detection and estimation approaches have been proposed in [33, 34, 35, 36] for UWB systems over frequency selective channels. SC-FDE is originally designed as an alternative to OFDM because of its performance improvement in frequency selective channels without any need for channel coding. FD channel estimation and detection is feasible not only because it requires only the time-delay of the first path and nothing about number of paths, but also because it is computationally less demanding depending on the channel structure. Moreover, adaptive algorithms generally converge faster and are more stable in the FD [79]. However, like their TD counterparts FD detection and estimation algorithms mentioned above also consider AWGN as ambient noise and are bound to suffer from a performance loss when the noise is impulsive. Moreover, a detailed comparison of TD and FD channel estimation does not exist in the literature.

Receiver design under non-Gaussian noise has been considered mostly in the context of other spread-spectrum systems [68, 80] and recently for UWB systems [74]. A robust multiuser receiver is proposed in [54] for CDMA systems under non-Gaussian noise which makes use of robust estimation techniques, namely $M-$estimates, rather than robust detection principles to design a robust decorrelating multiuser receiver. In [80], robust detection rule originally derived in [62] is employed directly for the case that each hypothesis can be described by a set of PDFs without any overlap. In [62], the minimax detection rule for this case is found to be a *likelihood-ratio* (LR) of the distributions that have minimum Kullback-Leibler divergence. In [74], using the results of [62], an ad-hoc robust UWB detector is proposed which makes use of a clipping function to detect outliers and to eliminate the detrimental effects of the impulsive noise.

In this chapter, we consider the channel estimation and detection for impulse radio UWB systems under non-Gaussian noise and present robust TD and FD receiver architectures. Robust TD and FD channel estimation algorithms are presented with their theoretical convergence analysis to clarify differences between TD and FD processing. Because the quadratic cost function in the RLS estimator is very sensitive to the outliers, recursive estimators with new cost functions should be defined. For robust TD channel estimation, a robust ad-hoc recursive estimator is proposed in order not to deal with the complications related with the vector estimation from the non-Gaussian multivariate PDFs. For robust FD channel estimation, the robust recursive method described in [61] is used with another cost function. In addition to their theoretic performance analysis, simulation results are also presented.

Next, robust detection is considered for which instead of the primary work in [62], alternative approaches are followed because of difficulties associated with the method proposed in [62]. These difficulties arise when one tries to apply this rule to weak-signal conditions and detection processes using a vector of observation [63, 64]. Therefore, the method proposed in [64] to alleviate these difficulties is used for the sake of simplicity. This approach allows two hypotheses to be characterized by the same set of PDFs differing in their means only which brings out a computational relaxation. The resulting detectors' performances are evaluated both theoretically and via simulations taking the channel estimation error into account. Moreover, a detailed comparison of TD and FD processing is outlined.

In the light of all theoretical and numerical results, robust receivers are shown to outperform their linear counterparts. But also, inherent robustness of FD processing to channel statistics is observed as well as that FD processing seems to be a lower complexity solution than its TD counterpart, especially for the NLOS channels. Also it should be noted that our theoretical results cover the AWGN case such that by setting the impulsive part's ratio in the background noise zero, all the results can be modified to cover the case that noise is Gaussian.

The chapter is organized as follows: Section 4.1 describes signal model, Section 4.2 explains robust TD channel estimation and detection with their convergence and performance analysis, respectively. Section 4.3 presents robust FD channel estimation and detection with their convergence and performance analysis, respectively. Section 4.4 presents a comprehensive comparison of TD and FD processing. Section 4.5 presents numerical results and Section 4.6 concludes the chapter.

Notation conventions: The sign function is given by sgn(.), δ_{ij} represent the Kronecker delta. The hypothesis in the binary hypothesis test are given by H_1 and H_0 where H_1 corresponds to the case that +1 was transmitted and H_0 corresponds to the case that -1 was transmitted. Since a single user-link will be considered, the subscript or superscript u denoting the user index is dropped for all previously defined symbols.

4.1. Signal Model

In this chapter, a TH-UWB system will be considered for which transmitted signal is given by

$$\begin{aligned} s(t) &= \sqrt{E}_s \sum_{j=-\infty}^{\infty} \sum_{i=-N_G}^{N_f-1} b(j) p\big(t - iT_f - c(i)T_c - j(T_s + N_G T_f)\big) \\ &= \sum_{j=-\infty}^{\infty} b(j) p_s\big(t - j(T_s + N_G T_f)\big) \end{aligned} \tag{4.1}$$

where E_s is the symbol energy, $b(j) \in \{+1, -1\}$ are the PAM symbols, $c(j) \in \{0, N_f - 1\}$ is the TH code for jth frame and $p_s(t) = \sqrt{E}_s \sum_{i=-N_G}^{N_f-1} p\big(t - iT_f - c(i)T_c\big)$. N_G in (4.1) is the number of guard frames which serve as prefix for FD processing to make linear convolution of each symbol with channel look like circular convolution which is essential for *fast Fourier transform* (FFT)-based processing techniques. In order to guarantee that, $N_G T_f > \tau_{\max}$ should be satisfied where $\tau_{\max}$ is the maximum channel delay spread. It should be noted that N_G is set to 0 when TD processing is concerned.

The channel is modeled by

$$h(t) = \sum_{l=1}^{\tilde{L}} h_l \delta(t - \tau_l) \tag{4.2}$$

where $\tilde{L}$ is the number of paths, h_l, and τ_l are the channel gain and time-delay of the lth path. Throughout the paper, channel gains and associated time-delays will be treated as unknown deterministic quantities.

Background noise, $w(t)$, is modelled by the commonly used Gaussian mixture noise whose PDF is given by

$$f(x) = (1 - \varepsilon) g(x; 0, \sigma^2) + \varepsilon g(x; 0, \kappa\sigma^2). \tag{4.3}$$

As mentioned previously in Chapter 1, in the mixture model, first term accounts for nominal noise with higher prior probability of occurrence, while the second term is the impulsive part with heavier tails. κ is the impulsive part's relative variance with respect to nominal noise variance and ϵ is the relative frequency of outliers. Therefore, received signal is given by

$$y(t) = \left[\sum_{j=-\infty}^{\infty} b(j) p_s\big(t - j(T_s + N_G T_f)\big) \right] * h(t) + w(t) \tag{4.4}$$

where $*$ denotes the linear convolution and $w(t)$ is the noise which is modelled by a two-term Gaussian-mixture whose PDF is given by (4.3). After sampling, the mth sample of the jth symbol is given by

$$\begin{aligned} y_j(mT) &\triangleq y\big(j(T_s + N_G T_f) + mT\big), \qquad m = -N', \ldots, 0, \ldots, N-1 \\ &= b(j) p_s(mT) * h(mT) + w_j(mT), \quad m = -N', \ldots, 0, \ldots, N-1, \end{aligned} \tag{4.5}$$

where T is the sampling period. $w_j(mT)$ in (4.5) is the noise sample taken at $t = j\big(T_s + N_G T_f\big) + mT$, i.e. $w_j(mT) \triangleq w\left(j\big(T_s + N_G T_f\big) + mT\right)$. N' in (4.5) is the number of samples taken per guard interval, i.e. $N' = N_G T_f / T$, and N in (4.5) is the number of samples taken per data interval, i.e. $N = T_s/T$. Since number of guard frames, i.e. N_G, is zero in TD processing, the mth sample of the jth symbol is given by

$$y_j(mT) = b(j) \sum_{l=1}^{\tilde{L}} h_l p_s(mT - \tau_l) + w_j(mT),\ m = 0, \ldots, N-1 \tag{4.6}$$

whose equivalent matrix representation is given by

$$\mathbf{y}_j = b(j)\tilde{\mathbf{P}}\tilde{\mathbf{h}} + \mathbf{w}_j = b(j)\mathbf{g} + \mathbf{w}_j \tag{4.7}$$

where $\mathbf{y}_j$ is a $N \times 1$ column vector consisting of the samples of the received signal, i.e.

$$\mathbf{y}_j = \begin{bmatrix} y_j(0)\ y_j(T) \ldots y_j\big((N-1)T\big) \end{bmatrix}^T. \tag{4.8}$$

$\tilde{\mathbf{P}}$ in (4.6) is a $N \times \tilde{L}$ matrix whose ith column is given by

$$\mathbf{p}_i = \begin{bmatrix} p_s(-\tau_i) \ldots p_s\big((N-1)T - \tau_i\big) \end{bmatrix}^T \tag{4.9}$$

which collects the samples of the symbol waveform shifted by τ_i. $\tilde{\mathbf{h}}$ in (4.6) is a $\tilde{L} \times 1$ column vector which collects the channel gains, i.e. $\tilde{\mathbf{h}} = \big[h_1 \ldots h_{\tilde{L}}\big]^T$. $\mathbf{g}$ in (4.6) is an $N \times 1$ column vector which is the aggregate channel response capturing the transmitted symbol and multipath channel, i.e. $\mathbf{g} = \tilde{\mathbf{P}}\tilde{\mathbf{h}}$. $\mathbf{w}_j$ in (4.6) is an $N \times 1$ column vector consisting of the noise samples, i.e.

$$\mathbf{w}_j = \begin{bmatrix} w_j(0) \ldots w_j\big((N-1)T\big) \end{bmatrix}^T. \tag{4.10}$$

Now, the discrete signal model will be explained for the case $N_G \neq 0$, i.e. signal transmitted for FD processing. Due to cyclic prefix used for FD processing, the linear

convolution in (4.5) results a circular convolution of the data part of the transmitted signal with the channel response, which is explicitly given by

$$y_j(mT) = b(j)p_s(mT) \star h(mT) + w_j(mT), \quad m = 0, 1, \ldots, N-1, \tag{4.11}$$

where $\star$ denote the circular convolution. Therefore, FFT of the received signal is given by

$$Y_j(l) = b(j)P_s(l)H(l) + W_j(l), \quad l = 0, 1, \ldots, N-1, \tag{4.12}$$

where $Y_j(l), P_s(l), H(l)$ and $W_j(l)$ denote the FFT of the $y_j(mT), p_s(mT), h(mT)$ and $w_j(mT)$, respectively. It should be noted that since both $p_s(mT), h(mT)$ and $w_j(mT)$ are real-valued sequences, Hermitian symmetry results in $P_s(l) = P_s^*(N-l), H(l) = H^*(N-l)$ and $W_j(l) = W_j^*(N-l)$ where superscript $*$ complex conjugate operation. Therefore, received signal in FD can be rewritten as

$$\mathbf{Y}_j = b(j)\mathbf{G} + \mathbf{W}_j \tag{4.13}$$

where $\mathbf{Y}_j, \mathbf{G}$ and $\mathbf{W}_j$ are the $N \times 1$ column vectors collecting the first half of the received samples, aggregate channel response samples, i.e. $\mathbf{G}$, and the noise samples which are explicitly given by

$$\mathbf{Y} = \Big[\Re(Y_j(0)) \ldots \Re(Y_j(N/2))\ \Im(Y_j(0)) \ldots \Im(Y_j(N/2))\Big]^T \tag{4.14}$$

$$\mathbf{G} = \Big[\Re\big(P_s(0)H(0)\big) \ldots \Re\big(P_s(N/2)H(N/2)\big) \Im\big(P_s(0)H(0)\big) \ldots \Im\big(P_s(N/2)H(N/2)\big)\Big]^T \tag{4.15}$$

$$\mathbf{W}_j = \Big[\Re(W_j(0)) \ldots \Re(W_j(N/2))\ \Im(W_j(0)) \ldots \Im(W_j(N/2))\Big]^T, \tag{4.16}$$

where $\Re\{x\}$ and $\Im\{x\}$ denote the real and imaginary part of x, respectively. It should be noted that $\mathbf{W}_j$ consists of i.i.d noise samples which will enable us to estimate each element of the aggregate channel response i.e. $\mathbf{G}$, independently.

4.2. Robust TD Channel Estimation and Detection for UWB Systems

4.2.1. Robust TD Channel Estimation

In this section, robust TD channel estimator will be presented. Before directly starting to derive robust TD channel estimator, we will outline the TD ML channel estimation in AWGN. Assuming that delays of all multipath components are at hand, then ML approach tries to minimize [26]

$$\mathcal{E}(L) = \sum_{j=1}^{n} || \mathbf{y}_j - \mathbf{P}\boldsymbol{h} ||^2 \tag{4.17}$$

where $|| \mathbf{c} ||$ denotes the L-2 norm of the $\mathbf{c}$, L ($L \leq \tilde{L}$) is the number of multipath components to be estimated, $\mathbf{h}$ is the $L \times 1$ column vector collecting channel gains of the first L path of the channel, i.e. $\boldsymbol{h} = \begin{bmatrix} h_1 \dots h_L \end{bmatrix}^T$, and $\mathbf{P}$ is the $N \times L$ matrix whose ith column consists of samples of $p_s(t - \tau_i)$, i.e. $\mathbf{P} = \begin{bmatrix} \mathbf{p}_1 \dots \mathbf{p}_L \end{bmatrix}$. By defining the cost function of the estimator as (4.17), only first L paths of the total $\tilde{L}$ are aimed to be estimated using n symbols. Exponentially weighted least squares formulation yields a cost function of

$$J(\hat{\boldsymbol{h}}_n) = \sum_{j=1}^{n} \lambda^{n-j} || \mathbf{y}_j - \mathbf{P}\hat{\boldsymbol{h}}_n ||^2 \tag{4.18}$$

where λ is the forgetting factor. $\hat{\mathbf{h}}_n$ in (4.18) the estimated channel response at the nth iteration using n symbol observations. From (4.18), update equations can be obtained as

$$\hat{\boldsymbol{h}}_n = \hat{\boldsymbol{h}}_{n-1} + \frac{1-\lambda}{1-\lambda^n}\mathbf{R}\mathbf{e}_n \tag{4.19}$$

$$\mathbf{e}_n = \mathbf{y}_n - \hat{\mathbf{g}}_{n-1} = \mathbf{g} - \hat{\mathbf{g}}_{n-1} + \mathbf{w}_n = \Delta\hat{\mathbf{h}}_{n-1} + \mathbf{w}_n \tag{4.20}$$

where $\mathbf{e}_n$ is the composite error vector, i.e. channel estimation error plus noise. $\hat{\mathbf{g}}_{n-1}$ in (4.20) is the estimated aggregate channel response at the $(n-1)$th step which is

given by $\hat{\mathbf{g}}_{n-1} = \mathbf{P}\hat{\boldsymbol{h}}_{n-1}$. $\Delta\hat{\mathbf{h}}_{n-1}$ in (4.20) is given by $\Delta\hat{\mathbf{h}}_{n-1} = \mathbf{g} - \hat{\mathbf{g}}_{n-1}$ which is the channel estimation error. $\mathbf{R}$ in (4.19) is given by $\mathbf{R} = (\mathbf{P}^T\mathbf{P})^{-1}\mathbf{P}^T$ which can be precomputed and stored since it is invariant during estimation due to the assumption that time-delays are at hand.

Now, we will seek a robust form of (4.19). The vulnerability of this estimator to the impulsive noise stems from that error is directly projected on the estimate. This is a direct consequence of the quadratic cost function in (4.18). Therefore, to obtain an estimator that is robust to impulses, the quadratic cost function should be replaced with one of the penalty functions proposed in [60] which generally do not work on only squared error to be able to suppress the impulses. However, use of these penalty functions becomes somewhat complicated due to vector estimation in (4.18). Therefore, to suppress the outliers we propose the following estimator

$$\hat{\boldsymbol{h}}_n = \hat{\boldsymbol{h}}_{n-1} + \frac{1-\lambda}{1-\lambda^n}\sigma^2\mathbf{R}\psi(\mathbf{e}_n) \tag{4.21}$$

where ψ is the clipping function that is given by

$$\psi(x) = \begin{cases} \frac{x}{\sigma^2} & \text{for } |x| < k\sigma^2, \\ \\ k\,\mathrm{sgn}(x) & \text{for } |x| > k\sigma^2, \end{cases} \tag{4.22}$$

where k is the trimming parameter that should be adjusted according to impulsiveness of the noise, i.e. according to ϵ and κ. The clipping function works on each entry of the error vector independently and decides whether each sample of the error vector contains an outlier or not. If an outlier is detected, it is clipped, otherwise it is directly projected on channel estimate.

4.2.2. Convergence Analysis of the Robust TD Channel Estimator

In this section, we will investigate the mean and covariance convergence properties of the robust TD channel estimator given by (4.21). Before starting, an assumption will be introduced which is used throughout this section:

A1: For sufficiently large n, the channel estimation error of the mth sample, i.e., $\Delta\hat{\mathbf{h}}_{n-1}(m)$, is small compared to $\mathbf{w}_n(m)$ for $\forall m \in \{0, 1, \ldots, N-1\}$.

This assumption means that the noise value determines the region of clipping function, $\psi(.)$, where $\mathbf{e}_n(m)$ falls into, either linear or constant part. The rationale behind this assumption is that the composite error usually fall in the constant part of clipping function when noise comes from the impulsive part in (4.3). In other case, i.e. if the noise does not come through the impulsive part, since composite error is clipped at every step, the channel estimation error is not expected to have extremely large values that can result in the change of region where error fall into.

4.2.2.1. Convergence of the Mean. In this section, we will analyze the convergence of the mean of the robust TD channel estimator given by (4.21). The recursive relationship for the expected value of the channel estimate is given by

$$E\{\hat{\mathbf{h}}_n\} = E\{\hat{\mathbf{h}}_{n-1}\} + \frac{1-\lambda}{1-\lambda^n}\sigma^2 \mathbf{R} E\{\psi(\mathbf{e}_n)\} \tag{4.23}$$

where the expectation is over both noise and the channel estimation error. The output of the clipping function can be written as

$$\psi(\mathbf{e}_n(m)) = \begin{cases} \frac{\mathbf{e}_n(m)}{\sigma^2} & \text{if } \mid \mathbf{w}_n(m) \mid \leq k\sigma^2 \\ k \ \text{sgn}\left(\mathbf{w}_n(m)\right) & \text{if } \mid \mathbf{w}_n(m) \mid > k\sigma^2 \end{cases} \tag{4.24}$$

using (4.20) and (**A1**). Therefore, expected value of the clipping function's output conditioned on the estimated path gains can be calculated as

$$\begin{aligned} E\left\{\psi(\mathbf{e}_n(m)) \mid \hat{\mathbf{h}}_{n-1}\right\} &= \int_{-k\sigma^2}^{k\sigma^2} \frac{\mathbf{e}_n(m)}{\sigma^2} f(w)dw = \frac{2\beta}{\sigma^2}\Delta\hat{\mathbf{h}}_{n-1}(m) \\ &= \frac{2\beta}{\sigma^2}\left(\mathbf{g}(m) - \hat{\mathbf{g}}_{n-1}(m)\right) \end{aligned} \tag{4.25}$$

where β is given by

$$\beta = 0.5 - (1-\epsilon)Q(k\sigma) - \epsilon Q\left(\frac{k\sigma}{\sqrt{\kappa}}\right). \tag{4.26}$$

Putting (4.25) into (4.23), the recursive relationship for the mean of the estimated channel gains becomes

$$\begin{aligned} E\left\{\hat{\mathbf{h}}_n\right\} &= E\left\{\hat{\mathbf{h}}_{n-1}\right\} + 2\beta\frac{1-\lambda}{1-\lambda^n}\mathbf{R}\left(\mathbf{g} - E\{\hat{\mathbf{g}}_{n-1}\}\right) \\ &= \left(1 - 2\beta\frac{1-\lambda}{1-\lambda^n}\right) E\left\{\hat{\mathbf{h}}_{n-1}\right\} + 2\beta\frac{1-\lambda}{1-\lambda^n}\mathbf{R}\tilde{\mathbf{P}}\tilde{\mathbf{h}} \end{aligned} \tag{4.27}$$

from which the asymptotic mean of the channel gains' estimate can be derived as

$$\lim_{n\to\infty} E\left\{\hat{\mathbf{h}}_n\right\} = \mathbf{R}\tilde{\mathbf{P}}\tilde{\mathbf{h}} = \mathbf{h} + \sum_{i=L+1}^{\tilde{L}} h_i \mathbf{R}\mathbf{p}_i \tag{4.28}$$

which becomes equal to $\mathbf{h}$ if the channel is resolvable, i.e. $\mathbf{p}_i^T\mathbf{p}_j = ||\ \mathbf{p}_i\ ||^2\ \delta_{ij}$, or in other words if the paths are uncorrelated. Otherwise estimated channel gains include correlations from other paths resulting in a bias. Therefore, if all paths are not aimed to be estimated and the channel is correlated, TD channel estimator is biased, otherwise it is asymptotically unbiased.

4.2.2.2. Convergence of the Variance. In this section, we will investigate the convergence of the variance of the robust TD channel estimator. The recursive relationship

for the second moment of the estimated channel gains is given by

$$\begin{aligned} E\{\hat{\mathbf{h}}_n\hat{\mathbf{h}}_n^T\} &= E\{\hat{\mathbf{h}}_{n-1}\hat{\mathbf{h}}_{n-1}^T\} + 2\frac{1-\lambda}{1-\lambda^n}\sigma^2\mathbf{R}E\{\psi(\mathbf{e}_n)\hat{\mathbf{h}}_{n-1}^T\} \\ &+ \left(\frac{1-\lambda}{1-\lambda^n}\right)^2\sigma^4\mathbf{R}E\{\psi(\mathbf{e}_n)\psi(\mathbf{e}_n)^T\}\mathbf{R}^T \end{aligned} \tag{4.29}$$

where the expectation is over both noise and channel estimation. Using (4.25) from previous section, the cross-correlation of the estimated channel gains and the output of the clipping function can be obtained as follows

$$\begin{aligned} E\{\psi(\mathbf{e}_n)\hat{\mathbf{h}}_{n-1}^T\} &= \frac{2\beta}{\sigma^2}E\Big\{\big(\tilde{\mathbf{P}}\tilde{\mathbf{h}} - \mathbf{P}\hat{\mathbf{h}}_{n-1}\big)\hat{\mathbf{h}}_{n-1}^T\Big\} \\ &= \frac{2\beta}{\sigma^2}\Big(\tilde{\mathbf{P}}\tilde{\mathbf{h}}E\{\hat{\mathbf{h}}_{n-1}^T\} - \mathbf{P}E\{\hat{\mathbf{h}}_{n-1}\hat{\mathbf{h}}_{n-1}^T\}\Big) \end{aligned} \tag{4.30}$$

where β is given by (4.26). The autocorrelation matrix of the output of the clipping function can be expressed as

$$E\{\psi(\mathbf{e}_n)\psi(\mathbf{e}_n)^T\} = \frac{4\beta^2}{\sigma^4}E\left\{\Delta\hat{\mathbf{h}}_{n-1}\Delta\hat{\mathbf{h}}_{n-1}^T\right\} + \frac{2\beta-4\beta^2}{\sigma^4}E\{\Omega\} + (\alpha_1+\alpha_2)\mathbf{I} \tag{4.31}$$

whose derivation is given in Appendix C. β in (4.31) is given by (4.26). Ω in (4.31) is a diagonal matrix whose diagonal elements are given by $\Omega_{mm} = \Delta\hat{\mathbf{h}}_{n-1}^2(m)$. α_1 and α_2 in (4.31) are defined to be

$$\begin{aligned} \alpha_1 &\triangleq \int_{-k\sigma^2}^{k\sigma^2}\frac{w_n^2(m)}{\sigma^4}f(w)dw \\ &= \frac{2(1-\epsilon)}{\sigma^2}\left[0.5 - Q(k\sigma) - \frac{k\sigma}{\sqrt{2\pi}}\exp\left(-\frac{k^2\sigma^2}{2}\right)\right] \\ &+ \frac{2\epsilon\kappa}{\sigma^2}\left[0.5 - Q\left(\frac{k\sigma}{\sqrt{\kappa}}\right) - \frac{k\sigma}{\sqrt{2\pi\kappa}}\exp\left(-\frac{k^2\sigma^2}{2\kappa}\right)\right] \end{aligned} \tag{4.32}$$

$$\alpha_2 \triangleq 2k^2\int_{k\sigma^2}^{\infty}f(w)dw = 2k^2\left[(1-\epsilon)Q(k\sigma) + \epsilon Q\left(\frac{k\sigma}{\sqrt{\kappa}}\right)\right]. \tag{4.33}$$

Assuming that off-diagonal elements of $E\{\Delta\hat{\mathbf{h}}_{n-1}\Delta\hat{\mathbf{h}}_{n-1}^T\}$ are negligible with respect to diagonal elements, (4.31) can be expressed as

$$E\{\psi(\mathbf{e}_n)\psi(\mathbf{e}_n)^T \mid \hat{\mathbf{h}}_{n-1}\} = \frac{2\beta}{\sigma^4}\Delta\hat{\mathbf{h}}_{n-1}\Delta\hat{\mathbf{h}}_{n-1}^T + (\alpha_1+\alpha_2)\mathbf{I} \tag{4.34}$$

using which and (4.30), the recursive relationship for the autocorrelation of the channel gains' estimate, i.e. (4.29), can be rewritten as

$$\begin{aligned} E\{\hat{\mathbf{h}}_n\hat{\mathbf{h}}_n^T\} &= \left[1 - 4\beta\frac{1-\lambda}{1-\lambda^n} + 2\beta\left(\frac{1-\lambda}{1-\lambda^n}\right)^2\right] E\{\hat{\mathbf{h}}_{n-1}\hat{\mathbf{h}}_{n-1}^T\} \\ &+ \frac{4\beta(1-\lambda)}{1-\lambda^n}\left(1 - \frac{1-\lambda}{1-\lambda^n}\right)(\mathbf{R}\tilde{\mathbf{P}}\tilde{\mathbf{h}})E\{\hat{\mathbf{h}}_{n-1}^T\} \\ &+ 2\beta\left(\frac{1-\lambda}{1-\lambda^n}\right)^2(\mathbf{R}\tilde{\mathbf{P}}\tilde{\mathbf{h}})(\mathbf{R}\tilde{\mathbf{P}}\tilde{\mathbf{h}})^T \\ &+ \left(\frac{1-\lambda}{1-\lambda^n}\right)^2\sigma^4(\alpha_1+\alpha_2)(\mathbf{P}^T\mathbf{P})^{-1}. \end{aligned} \tag{4.35}$$

Therefore, from (4.35), the asymptotic covariance matrix of TD channel estimate is found to be

$$\lim_{n\to\infty}\mathbf{K}_h^n = \frac{(1-\lambda)\sigma^4(\alpha_1+\alpha_2)}{2\beta(1+\lambda)}(\mathbf{P}^T\mathbf{P})^{-1} \tag{4.36}$$

where $\mathbf{K}_h^n = E\{\hat{\mathbf{h}}_n\hat{\mathbf{h}}_n^T\} - E\{\hat{\mathbf{h}}_n\}E\{\hat{\mathbf{h}}_n^T\}$ is the covariance matrix of the channel estimate. As it can be seen from (4.36), the channel correlation has an effect on the asymptotic covariance such that if the paths are correlated (resp. uncorrelated), their estimates are also correlated (resp. uncorrelated).

4.2.3. Robust TD Detection

In this section, we will consider the robust detection under the noise model given in (4.3). The subscripts of $\hat{\mathbf{h}}_n, \mathbf{y}_n$ and $\hat{\mathbf{g}}_n$ indicating the symbol number will be dropped for notational simplicity. The primary work considering robust detection is due to [62] where two hypotheses are assumed to have two distinct PDF families without any

overlap. The PDF family of each hypothesis is characterized by a dominating nominal PDF plus symmetric contaminations around the vicinity of the former. Then, a pair of PDFs, which are as close as possible in their shapes, i.e. has the minimum Kullback-Leibler divergence, is found and whose *likelihood-ratio* (LR) is shown to be robust in minimax sense.

However, some difficulties related with this method are reported in [63, 64]. First is that for weak-signal conditions, there may not exist such a pair. Second is that when detection is based on an observation vector rather than a single observation as in our case, for each sample of the observed vector, the pair of the PDFs should be found independently, possibly bringing about a computational load. Therefore, to overcome these difficulties, a solution has been proposed in [64] which mainly allows two PDF families to overlap by assuming that each hypothesis has the same PDF form differing in their means, only. Then, for the sake of robustness, the least favorable PDF of the family is used to form LR where the least favorable PDF is one with minimum Fisher information. Therefore to follow the approach in [64], first the following PDF family

$$\mathcal{F}_\epsilon = \left\{(1-\epsilon)g(x;0,\sigma^2) + \epsilon v(x); v(x) \text{ is a symmetric PDF } \right\} \tag{4.37}$$

will be considered to which (4.3) belongs. The least favorable PDF in this family is given by

$$f_{LF}(x) = \begin{cases} \frac{1-\epsilon}{\sqrt{2\pi}\sigma}\exp(-\frac{x^2}{2\sigma^2}) & \text{for } |x| \le k\sigma^2 \\ \\ \frac{1-\epsilon}{\sqrt{2\pi}\sigma}\exp(\frac{k^2\sigma^2}{2} - k|x|) & \text{for } |x| > k\sigma^2 \end{cases} \tag{4.38}$$

which obeys a Gaussian PDF at its center, then decays exponentially and k, ϵ, σ are related through

$$\frac{\phi(k\sigma)}{k\sigma} - Q(k\sigma) = \frac{\epsilon}{2(1-\epsilon)} \tag{4.39}$$

where $\phi(x) = \left(1/\sqrt{2\pi}\right)\exp\left(-x^2/2\right)$. Therefore, using (4.38), the robust test can be

given by

$$\sum_{m=0}^{N-1} T_{td,r}(m) \begin{array}{c} H_1 \\ > \\ < \\ H_0 \end{array} 0 \tag{4.40}$$

where $\{T_{td,r}(m)\}_{m=0}^{N-1}$ are the robust TD decision statistics which are given by

$$T_{td,r}(m) = \log\left(\frac{f_{LF}(\mathbf{y}(m) - \hat{\mathbf{g}}(m))}{f_{LF}(\mathbf{y}(m) + \hat{\mathbf{g}}(m))}\right) \tag{4.41}$$

and $\hat{\mathbf{g}} = \sum_{i=1}^{L} \hat{h}_i \mathbf{p}_i$ is the template for the detector. The decision statistics behave in a similar way to the clipping function given in (4.22) such that decision statistics are bounded by use of $f_{LF}(x)$. In the next section, we will present the performance analysis of this decision rule.

4.2.4. Performance Analysis of the TD Robust Detector

In this section, we will derive the probability of error for TD robust receiver incorporating channel estimation errors. For notational simplicity, the subscripts of $\hat{\mathbf{h}}_n, \Delta\hat{\mathbf{h}}_n, \mathbf{y}_n$ and $\hat{\mathbf{g}}_n$ indicating the symbol number will be dropped throughout this section. First, the mean and variance of the test statistics will be calculated. H_1 is assumed to be correct. Using (**A1**) stated in Section 4.2.2, decision statistic, i.e. $T_{td,r}(m)$, can be expressed as

$$T_{td,r}(m) = \begin{cases} \frac{2\hat{\mathbf{g}}(m)(\mathbf{g}(m)+\mathbf{w}(m))}{\sigma^2} & \text{if } \mid \mathbf{w}(m) \mid \leq k\sigma^2 \\ \\ 2k\hat{\mathbf{g}}(m)\text{sgn}(\mathbf{w}(m)) & \text{if } \mid \mathbf{w}(m) \mid > k\sigma^2 \end{cases} \tag{4.42}$$

from which mean of the sum of the decision statistics, i.e. mean of the *log-likelihood ratio* (LLR) is found to be

$$\mu_{td,r} = \sum_{m=0}^{N-1} E\{T_{td,r}(m)\} = \frac{4\beta}{\sigma^2}\sum_{m=0}^{N-1}\mathbf{g}(m)E\{\hat{\mathbf{g}}(m)\} = \frac{4\beta}{\sigma^2}(\tilde{\mathbf{P}}\tilde{\mathbf{h}})^T\mathbf{P}E\{\hat{\mathbf{h}}\}$$

where β is given by (4.26). Now, using (4.42), second moment of the decision statistic can be expressed as

$$\begin{aligned} E\{T_{td,r}^2(m)\} &= E\{\hat{\mathbf{g}}^2(m)\} \\ &\times \left[\frac{4}{\sigma^4}\mathbf{g}^2(m)\int_{-k\sigma^2}^{k\sigma^2} f(w)dw + \frac{4}{\sigma^4}\int_{-k\sigma^2}^{k\sigma^2} w^2 f(w)dw + 8k^2\int_{k\sigma^2}^{\infty} f(w)dw\right] \\ &= E\{\hat{\mathbf{g}}^2(m)\}\left[\frac{8\beta}{\sigma^4}\mathbf{g}^2(m) + 4(\alpha_1+\alpha_2)\right] \end{aligned} \quad (4.43)$$

where β, α_1 and α_2 are given by (4.26), (4.32) and (4.33), respectively. Using (4.43) and assuming that $T_{td}(m)$'s are uncorrelated, the variance of the LLR is found to be

$$\begin{aligned} \nu_{td,r}^2 &= \sum_{m=0}^{N-1} E\{T_{td,r}^2(m)\} - \sum_{m=0}^{N-1} E^2\{T_{td,r}(m)\} \\ &= \frac{8\beta}{\sigma^4}\mathrm{Tr}\left[\left(\mathbf{P}E\left\{\hat{\mathbf{h}}\hat{\mathbf{h}}^T\right\}\mathbf{P}^T\right)\odot\left(\mathbf{g}\mathbf{g}^T\right)\right] + 4(\alpha_1+\alpha_2)\mathrm{Tr}\left[\mathbf{P}E\left\{\hat{\mathbf{h}}\hat{\mathbf{h}}^T\right\}\mathbf{P}^T\right] \\ &- \frac{16\beta^2}{\sigma^4}\mathrm{Tr}\left[\left(\mathbf{P}E\left\{\hat{\mathbf{h}}\right\}E\left\{\hat{\mathbf{h}}^T\right\}\mathbf{P}^T\right)\odot\left(\mathbf{g}\mathbf{g}^T\right)\right] \end{aligned} \quad (4.44)$$

where Tr and $\odot$ denote the trace operator and Hadamard product, respectively. Therefore, using CLT and the symmetry between two hypotheses, the probability of error can be written as

$$P_{e,td}^r = Q\left(\frac{\mu_{td,r}}{\nu_{td,r}}\right) \quad (4.45)$$

for which the effect of noise on the test statistics is governed by β, α_1 and α_2, in contrary to TD matched filter for which this effect is governed directly by $E\{w^2\}$. This difference results from use of the robust detection rule. The probability of error of TD matched filter subject to both impulsive noise and channel estimation error is derived

in Appendix D.

4.3. Robust FD Channel Estimation and Detection for UWB Systems

4.3.1. Robust FD Channel Estimation

In this section, we will derive the robust FD channel estimator. The recursive channel estimation in FD can be carried out with usual methods, such as RLS, LMS. However both methods employ a quadratic cost function that is very sensitive to the tail behavior of the distribution (outliers). As a consequence they suffer from performance deterioration when the noise distribution is impulsive with a heavy tail. To obtain a robust estimator, the quadratic cost function should be replaced with one of the cost functions given in [60]. Therefore, following cost function

$$\rho(x) = \begin{cases} \frac{x^2}{2\sigma^2} & \text{for } |x| < k\sigma^2, \\ \\ \frac{k^2\sigma^2}{2} - k|x| & \text{for } |x| > k\sigma^2, \end{cases} \tag{4.46}$$

will be used which is the $M-$estimator for the PDF in (4.38). Since samples are independent, estimation of each frequency bin can be carried out separately. Using (4.46), cost function can be written as

$$J(\hat{\mathbf{G}}_n(m)) = \sum_{j=1}^{n} \lambda^{n-j} \rho\big(\mathbf{Y}_j(m) - \hat{\mathbf{G}}_n(m)\big) \tag{4.47}$$

where $\hat{\mathbf{G}}_n$ denotes the estimate of the aggregate channel response at nth iteration, i.e. using n symbols. The recursive solution to (4.47) can be written as [61]

$$\begin{aligned} \hat{\mathbf{G}}_n(m) &= \hat{\mathbf{G}}_{n-1}(m) + \frac{q\left(\mathbf{E}_n(m)\right)\mathbf{E}_n(m)}{z_n(m)} && (4.48) \\ z_n(m) &= \lambda z_{n-1}(m) + q(\mathbf{E}_n(m)) && (4.49) \\ \mathbf{E}_n(m) &= \mathbf{Y}_n(m) - \hat{\mathbf{G}}_{n-1}(m) = \Delta\hat{\mathbf{G}}_{n-1}(m) + \mathbf{W}_n(m) \end{aligned}$$

where $\mathbf{E}_n(m)$ is the composite error, i.e. channel estimation error plus noise. The channel estimation error at the nth step is given by $\mathbf{G}(m) - \hat{\mathbf{G}}_{n-1}(m) = \Delta\hat{\mathbf{G}}_{n-1}$. $q(x)$ is given by $q(x) = \psi(x)/x$ whose role in these equations is to detect the samples with noise coming through the impulsive component and to clip these outliers. In the subsequent section, we will investigate convergence properties of the algorithm.

4.3.2. Convergence Analysis of Robust FD Channel Estimation

In this section, we will analyze the convergence properties of robust FD channel estimation algorithm presented in the previous section. Although such an analysis has been conducted in [61], both the penalty function, $\rho(.)$, and the signal model in this work differ from the former requiring a new performance analysis. Generally speaking, an exact performance analysis of RLS-type algorithms are tedious, but under a few reasonable assumptions, a consistent analysis can be carried out. We use the following standard assumptions in convergence analysis of RLS-like algorithms

A2: that signal is ergodic [61] and,

A3: that for sufficiently large n, the channel estimation error, $\Delta\hat{\mathbf{G}}_n(m)$, is small compared to $\mathbf{W}_n(m)$ for $\forall m \in \{0, 1, \ldots, N-1\}$.

The third assumption, (**A3**), is analogous to (**A1**) stated in Section 4.2.2 which means that noise value determines the region of penalty function where the error, $\mathbf{E}_n(m)$, falls into, either quadratic or linear part. Before starting the convergence analysis of the mean, it should be noted that for sufficiently large n, using (**A2**), $z_n(m)$ can be approximated as

$$\begin{aligned} z_n(m) &= \sum_{i=1}^{n} \lambda^{n-i} q(\Delta\hat{\mathbf{G}}_{n-1}(m) + \mathbf{W}_i(m)) \\ &\approx \Big(\sum_{i=1}^{n} \lambda^{n-i}\Big) E\big\{q(\Delta\hat{\mathbf{G}}_{n-1}(m) + \mathbf{W}_i(m))\big\} \\ &\approx \Big(\sum_{i=1}^{n} \lambda^{n-i}\Big) E\big\{q(\mathbf{W}_i(m))\big\} = \overline{\lambda}(n)\gamma \end{aligned} \tag{4.50}$$

where $\overline{\lambda}(n) = \frac{1-\lambda^{n+1}}{1-\lambda}$, $\gamma = E\{q(\mathbf{W}_i(m))\}$. In the next two sections, the convergence analysis of robust FD channel estimator will be conducted using (4.50) and the assumptions (**A2**)-(**A3**).

4.3.2.1. Convergence of the Mean. In this section, convergence of the robust FD channel estimator's mean will be investigated. The recursive relationship for the mean of aggregate channel estimate is given by

$$E\{\Delta\hat{\mathbf{G}}_n(m)\} = E\{\Delta\hat{\mathbf{G}}_{n-1}(m)\} - \frac{1}{\overline{\lambda}(n)\gamma}E\{\psi(\mathbf{E}_n(m))\} \tag{4.51}$$

where the expectation is over both noise and the channel estimation error. Using (**A3**), the output of clipping function can be written as

$$\psi(\mathbf{E}_n(m)) = \begin{cases} \frac{\mathbf{E}_n(m)}{\sigma^2} & \text{if } \mid \mathbf{W}_n(m) \mid \leq k\sigma^2 \\ \\ k\ \text{sgn}(\mathbf{W}_n(m)) & \text{if } \mid \mathbf{W}_n(m) \mid > k\sigma^2. \end{cases} \tag{4.52}$$

which is a similar expression to (4.24) written for TD processing. Therefore, using (4.52), the expected value of the clipping function's output can be written as

$$\begin{aligned} E\{\psi(\mathbf{E}_n(m)) \mid \Delta\hat{\mathbf{G}}_{n-1}(m)\} &= \int_{-k\sigma^2}^{k\sigma^2} \frac{\Delta\hat{\mathbf{G}}_{n-1}(m) + \mathbf{W}_n(m)}{\sigma^2} f(w)dw \\ &= \frac{2\Delta\hat{\mathbf{G}}_{n-1}(m)\beta}{\sigma^2} \end{aligned} \tag{4.53}$$

where β is given in (4.26). Using (4.53) the recursive equation for the expected value of the channel estimation error, namely (4.51), can be expressed as

$$E\{\Delta\hat{\mathbf{G}}_n(m)\} = \left(1 - \frac{2\beta}{\overline{\lambda}(n)\gamma}\right) E\{\Delta\hat{\mathbf{G}}_{n-1}(m)\} \tag{4.54}$$

from which for the asymptotic mean of the channel estimation error, it can be concluded that

$$\lim_{n\to\infty} E\{\Delta\hat{\mathbf{G}}_n(m)\} = 0 \tag{4.55}$$

which implies that the robust FD channel estimator with the cost function defined in (4.46) is an asymptotically unbiased estimator. In the next section, the convergence of robust FD channel estimator's variance will be investigated.

4.3.2.2. Convergence of the Variance. In this section, we will consider the convergence of the variance of the robust FD channel estimator. The recursive equation for the second moment of the aggregate channel estimate can be written as

$$\begin{aligned} E\big\{\Delta\hat{\mathbf{G}}_n^2(m)\big\} &= E\big\{\Delta\hat{\mathbf{G}}_{n-1}^2(m)\big\} - \frac{2}{\overline{\lambda}(n)\gamma} E\big\{\Delta\hat{\mathbf{G}}_{n-1}(m)\psi(\mathbf{E}_n(m))\big\} \\ &+ \frac{1}{\overline{\lambda}^2(n)\gamma^2} E\big\{\psi^2(\mathbf{E}_n(m))\big\} \end{aligned} \tag{4.56}$$

where the expectations are over both noise and channel estimation error. First, the conditional expected value of the cross-correlation between the channel estimation error and the output of the clipping function in (4.56) will be evaluated which is

$$\begin{aligned} E\big\{\Delta\hat{\mathbf{G}}_{n-1}(m)\psi(\mathbf{E}_n(m)) \mid \Delta\hat{\mathbf{G}}_{n-1}\big\} &= \int_{-k\sigma^2}^{k\sigma^2} \frac{\Delta\hat{\mathbf{G}}_{n-1}(m)\mathbf{E}_n(m)}{\sigma^2} f(w)dw \\ &= \frac{2\Delta\hat{\mathbf{G}}_{n-1}^2(m)\beta}{\sigma^2} \end{aligned} \tag{4.57}$$

where the first equality is due to (4.52), and the second equality is due to fact that channel estimation error at the $(n-1)$th step, $\Delta\hat{\mathbf{G}}_{n-1}(m)$, is independent of the noise at the nth step, $\mathbf{W}_n(m)$. Secondly, the conditional second moment of the output of

the clipping function in (4.56) will be considered which is

$$\begin{aligned} E\{\psi^2(\mathbf{E}_n(m)) \mid \Delta\hat{\mathbf{G}}_{n-1}(m)\} &= \int_{-k\sigma^2}^{k\sigma^2} \frac{\mathbf{E}_n^2(m)}{\sigma^4} f(w)dw + 2k^2 \int_{k\sigma^2}^{\infty} f(w)dw \\ &= \int_{-k\sigma^2}^{k\sigma^2} \frac{\Delta\hat{\mathbf{G}}_{n-1}^2(m)}{\sigma^4} f(w)dw + \int_{-k\sigma^2}^{k\sigma^2} \frac{\mathbf{W}_n^2(m)}{\sigma^4} f(w)dw \\ &\quad +2k^2 \int_{k\sigma^2}^{\infty} f(w)dw \\ &= \frac{2\beta}{\sigma^4}\Delta\hat{\mathbf{G}}_{n-1}^2(m) + (\alpha_1 + \alpha_2) \end{aligned} \tag{4.58}$$

where we again used (4.52), and the independence of the channel estimation error at the $(n-1)$th step, $\Delta\hat{\mathbf{G}}_{n-1}(m)$, and the noise, $\mathbf{W}_n(m)$. Using (4.57) and (4.58), the recursive relationship for the second moment of the channel estimator, (4.56), is given by

$$E\{\Delta\hat{\mathbf{G}}_n^2(m)\} = E\{\Delta\hat{\mathbf{G}}_{n-1}^2(m)\}\left(1 - \frac{2\beta\big(2\overline{\lambda}(n)\gamma\sigma^2 - 1\big)}{\overline{\lambda}^2(n)\gamma^2\sigma^4}\right) + \frac{(\alpha_1+\alpha_2)}{\overline{\lambda}^2(n)\gamma^2} \tag{4.59}$$

from which for the asymptotic variance of the channel estimator, it can be concluded that

$$\lim_{n\to\infty} E\{\Delta\hat{\mathbf{G}}_n^2(m)\} = \frac{\sigma^4(\alpha_1+\alpha_2)}{2\beta\big(\frac{2\gamma\sigma^2}{1-\lambda} - 1\big)} \approx \frac{\sigma^2(1-\lambda)(\alpha_1+\alpha_2)}{4\beta\gamma} \tag{4.60}$$

which is smaller than the total noise variance, i.e. $(1-\epsilon+\kappa\epsilon)\sigma^2/2$, which is the noise floor induced by the RLS algorithm.

4.3.3. Robust FD Detection and the Performance Analysis

In this section, we will present the decision rule and derive the probability of error of the FD robust detector incorporating channel estimation errors. The subscripts of $\mathbf{Y}_n, \mathbf{W}_n, \Delta\hat{\mathbf{G}}_n, \mathbf{G}_n$ will be dropped for notational simplicity. The discussions carried out in Section 4.2.3 for TD detection holds for FD detection also. Therefore, using

least favorable PDF, (4.38), the robust detection rule is given by

$$\sum_{m=0}^{N-1} T_{fd,r}(m) \begin{array}{c} H_1 \\ > \\ < \\ H_0 \end{array} 0 \tag{4.61}$$

where $\{T_{fd,r}(m)\}_{m=0}^{N-1}$ are the robust FD decision statistics which are given by

$$T_{fd,r}(m) = \log\left(\frac{f_{LF}(\mathbf{Y}(m) - \hat{\mathbf{G}}(m))}{f_{LF}(\mathbf{Y}(m) + \hat{\mathbf{G}}(m))}\right) \tag{4.62}$$

H_1 is assumed to be correct, then using (**A3**) stated in Section 4.3.2, decision statistic in FD can be expressed as

$$T_{fd,r}(m) = \begin{cases} \frac{2(\mathbf{G}(m)+\mathbf{W}(n))(\mathbf{G}(m)-\Delta\hat{\mathbf{G}}(m))}{\sigma^2} & \text{if } \mid \mathbf{W}(m) \mid \leq k\sigma^2 \\ \\ 2k(\mathbf{G}(m) - \Delta\hat{\mathbf{G}}(m))\text{sgn}(\mathbf{W}(m)) & \text{if } \mid \mathbf{W}(m) \mid > k\sigma^2 \end{cases} \tag{4.63}$$

which is similar to its TD counterpart, i.e. (4.42), Therefore, the mean of $T_{fd,r}(m)$ under H_1 is given by

$$\mu_{fd,r}(m) \triangleq E\{T_{fd,r}(m)\} = \int_{-k\sigma^2}^{k\sigma^2} \frac{2\mathbf{G}^2(m)}{\sigma^2} f(w)dw = \frac{4\mathbf{G}^2(m)\beta}{\sigma^2} \tag{4.64}$$

where β is given in (4.26). The second moment of $T_{fd,r}(m)$ under H_1 is

$$\begin{aligned} E\{T_{fd,r}^2(m)\} &= E\left\{(\mathbf{G}(m) - \Delta\hat{\mathbf{G}}(m))^2\right\} \\ &\quad \times \left[\int_{-k\sigma^2}^{k\sigma^2} \frac{4}{\sigma^4}(\mathbf{G}(m) + \mathbf{W}(m))^2 f(w)dw + \int_{k\sigma^2}^{\infty} 8k^2 f(w)dw\right] \\ &= 4\left(\mathbf{G}^2(m) + E\left\{\Delta\hat{\mathbf{G}}^2(m)\right\}\right)\left[\frac{2\mathbf{G}^2(m)}{\sigma^4}\beta + (\alpha_1 + \alpha_2)\right] \end{aligned} \tag{4.65}$$

where $\beta, \alpha_1, \alpha_2$ are given in (4.26), (4.32), (4.33), respectively. Therefore, the variance of $T_{fd,r}(m)$ is defined to be

$$\nu^2_{fd,r}(m) \;=\; E\left\{T^2_{fd,r}(m)\right\} - E^2\left\{T_{fd,r}(m)\right\} \tag{4.66}$$

from which using the CLT and the symmetry between two hypotheses, the probability of error is given by

$$P^r_{e,fd} = Q\left(\frac{\sum_{m=0}^{N-1}\mu_{fd,r}(m)}{\sqrt{\sum_{m=0}^{N-1}\nu^2_{fd,r}(m)}}\right) \tag{4.67}$$

for which the effect of noise on the test statistics is governed by β, α_1 and α_2, in contrary to FD matched filter for which this effect is governed directly by $E\{w^2\}$.

Table 4.1. Computational Load of Channel Estimation

	Multiplications	Summations
FD	$3N$	$4N$
TD	$2NL$	$2NL + L$

4.4. Complexity Analysis and Comparison

In this section, we will discuss advantages and disadvantages of TD and FD processing starting with the computational complexity. The exact number of operations for one update of path estimates is given in Table 4.1. But these complexities does not take the load induced by FFT or by inversion of $\mathbf{R}$ into account. Therefore, since an N-point FFT is $\mathcal{O}(N\log(N))$ and the inversion of an L by L matrix is $\mathcal{O}(L^3)$, the overall complexities of TD and FD processing are $\mathcal{O}(L^3 + LN)$ and $\mathcal{O}(N\log(N))$, respectively which implies the efficiency of FD processing for multipath channels. As in [26, 27, 28, 29], if the paths are assumed to be uncorrelated resulting in $\mathbf{P}^T\mathbf{P} = \mathbf{I}$, the computational complexity of TD channel estimation boils down to $\mathcal{O}(LN)$ which can be still higher than the FD's depending on the number of paths. Therefore, it is

straightforward to deduce that if the number of multipath components of a channel is high, then FD processing is more suitable. Since, even for LOS UWB channel, number of significant paths (number of paths to capture 85% energy) is about 20-25, FD processing of UWB is computationally efficient. It should be noted that we have only addressed the computational complexity of channel estimation because in both TD and FD, detection is $\mathcal{O}(N)$ which is negligible with respect to computations mentioned above.

The advantages and disadvantages of two approaches can be summarized as follows:

1. In TD, time-delays of all multipath components should be known (or estimated), however, in FD, only the delay of the first path is sufficient. Moreover, for TD estimation, number of paths should be known in contrary to FD which does not require such an information.
2. FD processes each frequency bin independently, therefore it does not employ fading correlation between path gains of channel response, however TD exploits this knowledge. However as in [26, 27, 28, 29], if the signal echoes are assumed to be uncorrelated, then TD does not exploit fading correlation, also. However, in UWB, multipath components arrive the receiver in terms of clusters with non-resolvable rays, therefore the validity of this assumption becomes questionable. Also it should be noted that as in [78], structured FD channel estimation algorithms can be derived to improve the performance exploiting the correlation of the paths.
3. FD robust channel estimator is asymptotically unbiased independent of the channel structure, however biasedness of the TD channel estimator depends on the channel structure. If paths are correlated and only a number of paths are estimated, then TD channel estimator is biased, otherwise not.
4. Comparing (4.36) and (4.60) reveals that TD channel estimates can be correlated depending on the correlation of the paths, but FD channel estimates are uncorrelated.

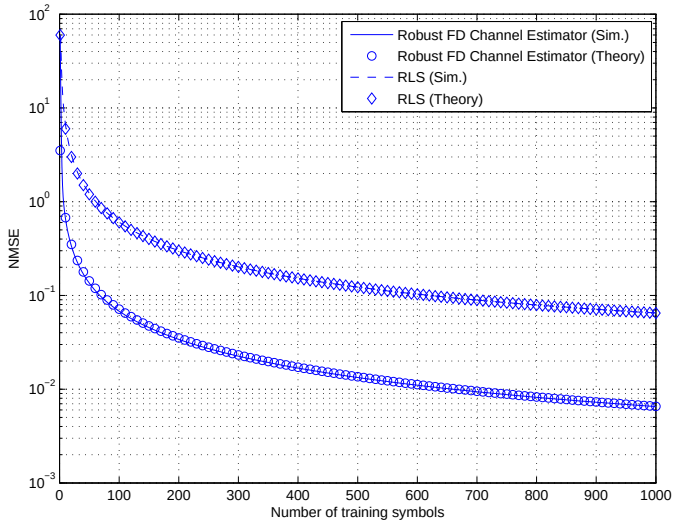

Figure 4.1. MSE of FD Channel Estimation under CM1 Channel, when $\epsilon = 0.01$, $\kappa = 1000$ and SNR=10 dB.

4.5. Simulation Results

In this section, we tested the performances of channel estimation and detection. The pulse is selected as second derivative of the Gaussian function with duration $T_p = 1$ ns. The frame duration is selected to be 20 ns. Each symbol consists of $N_f = 15$ frames resulting in $T_s = 300$ ns. $N_G = 5$ guard frames are employed for FD processing. The chip duration is chosen as $T_c = 1$ ns and the TH codes are randomly generated from a uniformly distributed set of $\{0, 1, \ldots, N_c - 1\}$. In all graphs, SNR value is calculated by E_s/N_0, where $(1-\epsilon)\,\sigma^2 + \epsilon\kappa\sigma^2 = N_0/2$ denotes the total noise variance at the input of the receiver, i.e. not only considering the variance of the nominal (thermal) noise but also taking into account the variance of the contamination. Moreover, in all simulations, the forgetting factor, λ, is set to 0.999 and the threshold parameter, k, of (4.46) is adjusted according to (4.39). For illustrative purposes, we employed CM1 and CM4 channel models in [23] where the former is a *line-of-sight* (LOS) channel, whereas the latter is NLOS channel with an extreme delay spread. We have chosen these two channels specifically, because although Rake receiver perform well in a LOS channel with a reasonable number of finger, its performance is unsatisfactory in NLOS channels with severe multipath delay spread.

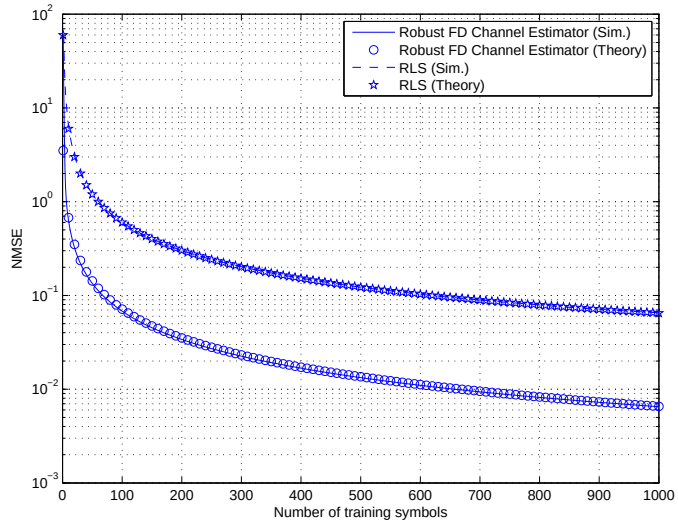

Figure 4.2. MSE of FD Channel Estimation under CM4 Channel, when $\epsilon = 0.01$, $\kappa = 1000$ and SNR=10 dB.

First we analyzed the performance of robust FD channel estimator. For channel estimation, the NMSE is used as performance measure which is explicitly given by

$$\text{NMSE}(\hat{\mathbf{G}}) = \frac{\text{E}\left\{ || \mathbf{G} - \hat{\mathbf{G}} ||^2 \right\}}{\text{E}\left\{ || \mathbf{G} ||^2 \right\}}. \tag{4.68}$$

The optimal training sequences for FD channel estimation should have flat spectrum through all frequencies of interest. However, in [34], the effect of optimal training symbols on the performance of NMSE has been investigated and it has been shown that difference between NMSEs of channel estimation with optimal and non-optimal (random) sequences is not significant. Therefore, we use +1s as training symbols in all simulations. In Figures 4.1-4.2, learning curves of robust FD channel estimator and RLS algorithm are plotted. In both cases, RLS converges to total SNR whereas in robust FD channel estimation algorithm, NMSE converges to nominal SNR value due to elimination of impulsive noise components, i.e. outliers, with the nonlinearity given in (4.46). Moreover, although channel statistics and characteristics are totally different, in both channels, FD estimation yield approximately same results which has been previously stated in [33]. This evidence implies that robust FD channel estimation is inherently robust to channel statistics. Since in minimax sense robust designs,

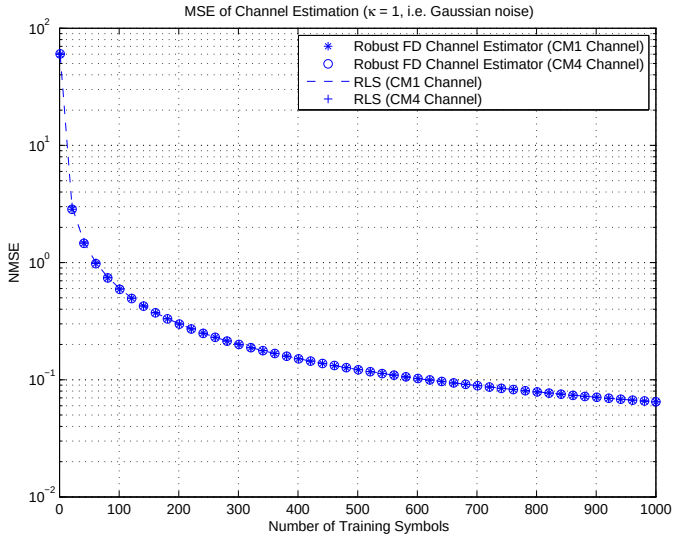

Figure 4.3. MSE of FD Channel Estimation under AWGN and SNR=10 dB.

worst case performance is optimized, a performance loss is expected in nominal case. To evaluate the channel estimation performance of robust FD channel estimator in nominal, AWGN case, we tested both robust FD channel estimator and RLS algorithm in AWGN. The resulting learning curves of both method are plotted in Figure 4.3 from which it can be concluded that robust method does not incur a significant performance loss in nominal situation. Moreover, in all of these graphs theoretical learning curves are also plotted and it can be seen that agreement between theoretical, (4.59), and numerical results are perfect.

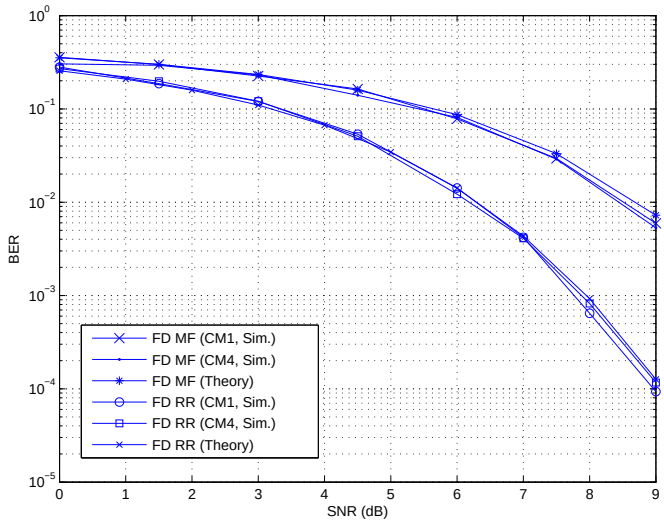

Figure 4.4. BER performance of FD processing when $\epsilon = 0.01$, $\kappa = 100$.

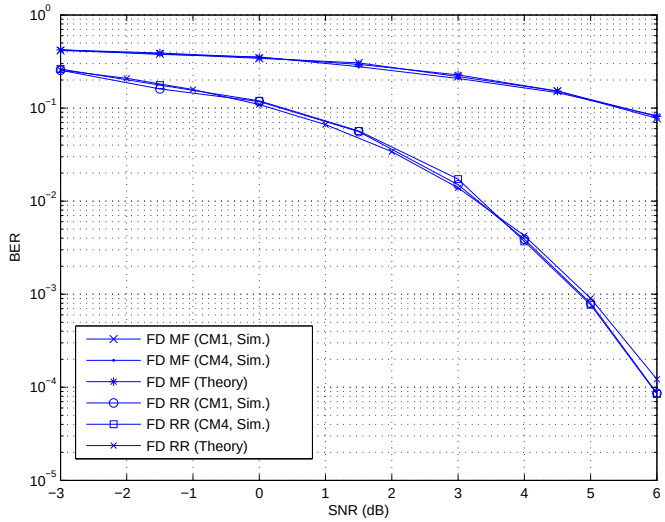

Figure 4.5. BER performance of FD processing when $\epsilon = 0.01$, $\kappa = 300$.

Next, we started to test the robust receivers, i.e. channel estimation plus detector. For channel estimation, each packet is sent with a training sequence of length 100 symbols which are all +1s. Although the receivers can be employed in decision-directed mode, i.e. after transmission of training sequence, the estimated channel responses can be updated in conjunction with the previously detected information symbols, we do not invoke this method. In Figure 4.4, we plotted BER performance of robust FD receiver and FD matched filter when $\epsilon = 0.01, \kappa = 100$. As it can be seen from Figure 4.4, both robust methods have approximately same performance which substantially outperform the matched filter. Moreover, as in robust FD channel estimation, robust FD receivers have the same performance in both CM1 and CM4 channels, despite their totally different characteristics. Then in Figure 4.5, we increased the impulsiveness of the noise, and as we expected performance gap between robust and conventional methods increases. Theoretically, this stems from that the asymptotic variance of robust methods are decreasing functions of either ϵ or κ when one of them is kept fixed whereas in linear methods, asymptotic variance of the estimators are almost invariant to changes in either κ or ϵ when one of them is kept fixed. Lastly, we tested both methods under AWGN, and from Figure 4.6, it can be concluded that there does not exist any serious performance loss in robust methods under nominal situation. Again, as in channel estimation, theoretical results are also plotted which are in a good agreement with simulations.

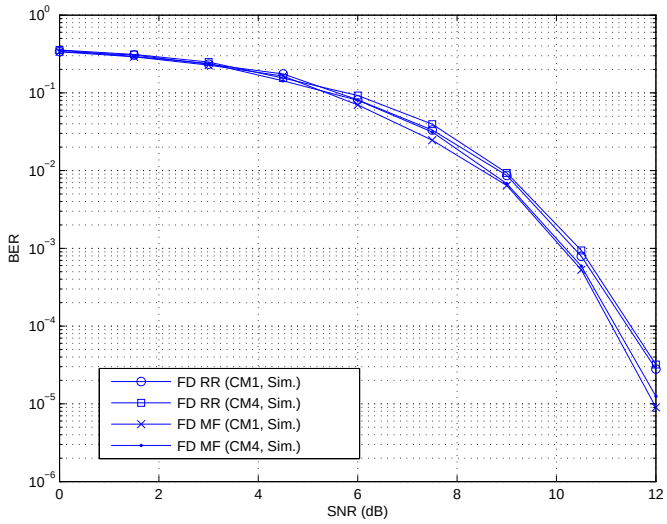

Figure 4.6. BER performance of FD processing when noise is AWGN.

Then we tested the robust TD receivers, i.e. robust TD channel estimation plus robust TD detection. Again, we used 100 training symbols for each packet. In Figure 4.7, BER performance robust TD receiver and TD matched filter in CM1 channel are plotted. Although robust receiver outperforms its linear counterpart, the performance is very sensitive to the number of paths estimated. Since an increase in the number of paths estimated, or combined, results in an increase in the received energy decreasing effective SNR, the performance of robust TD receiver increases directly with L. Although for CM1 channel, the performance of TD robust receiver with this complexity is at an acceptable level, for CM4 channel, the same conclusion cannot hold. Although in CM4 channel, robust TD channel estimator outperforms its linear counterpart, its performance is very poor with respect to its FD counterpart which can be seen in Figure 4.8. Comparison of these two figures, Figure 4.7 and Figure 4.8, reveals that in a LOS channel, TD channel estimation can provide good performances with an acceptable complexity due to the fact that in LOS channel, most of energy lies in a limited number of paths. However, in a NLOS channel, TD channel estimation that yields a satisfactory performance can be prohibitively complex due to homogenous energy spread over a lot of multipath components. These two observations lead to the conclusion that the performance of TD receivers is very sensitive to the channel statistics.

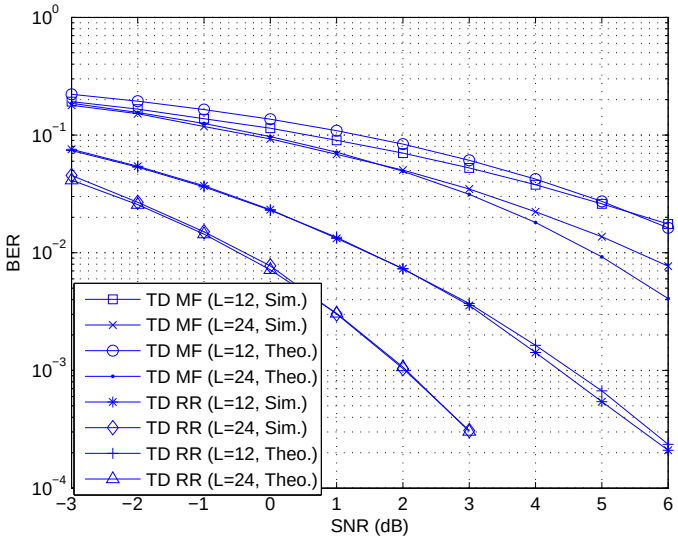

Figure 4.7. BER performance of TD processing under CM1 channel when $\epsilon = 0.01$, $\kappa = 300$.

Lastly, for comparison purposes, we plotted the BER performances of TD and FD robust receivers together in Figure 4.9 and Figure 4.10. The TD result for $L = 12$ is selected because when L in on the order of 10, both of the receivers have the same complexity since complexities of TD and FD processing are $\mathcal{O}(NL)$ and $\mathcal{O}(N \log N)$, respectively. As it can be seen from Figure 4.10, for NLOS channel, performance gain of robust FD receiver over robust TD receiver is substantial for the same computational complexity. But the differences are not so clear for CM1 channel. At low SNRs, TD processing performs better than FD processing due to fact that channel estimation is more accurate in TD than in FD at low SNRs. Because the concentrated energy of LOS channel is spreaded over a broad frequency range, the SNR of each sample in FD is smaller than L path gains' in TD where each have a sufficient amount of energy. But, at high SNR regime, the accuracy of these path gains' estimate does not increase as much as accuracy of FD estimation because of the frequency diversity of the latter. A similar observation was noticed in [35]. In the light of these, it can be claimed that robust FD processing is preferable over robust TD processing especially for NLOS channels, due to its lower computational complexity.

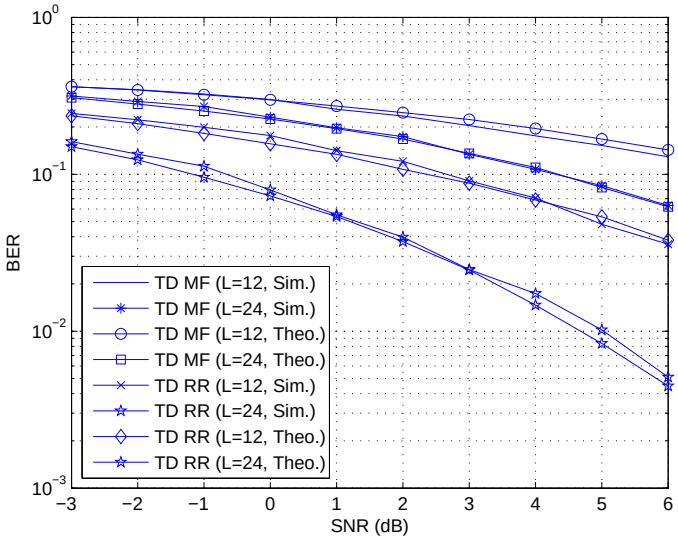

Figure 4.8. BER performance of TD processing under CM4 channel when $\epsilon = 0.01$, $\kappa = 300$.

4.6. Discussions

In this chapter, we proposed robust channel estimation and detection algorithms in both FD and TD. Theoretical convergence analysis and theoretical BER calculations are carried out for both methods and verified via simulations. For comparison purposes, BER performances of TD and FD matched filter subject to combined effect of non-Gaussian noise and channel estimation error are also evaluated both theoretically and via simulations. In the light of these, it has been shown that both robust methods provide substantial performance gains with respect to their linear counterparts, i.e. systems designed to be optimum under AWGN. But, despite their superiority over linear methods, also there exists significant differences between FD and TD robust algorithms in terms of both complexity and performance. The most striking difference is that although FD channel estimation has same complexity and performance irrespective of the number of paths and channel statistics, the performance and the complexity of the TD robust channel estimation highly depends on these parameters. For example, in LOS channels, i.e. CM1, both methods provide approximately same performance with the same complexity due to concentrated energy spread of such channels, i.e.

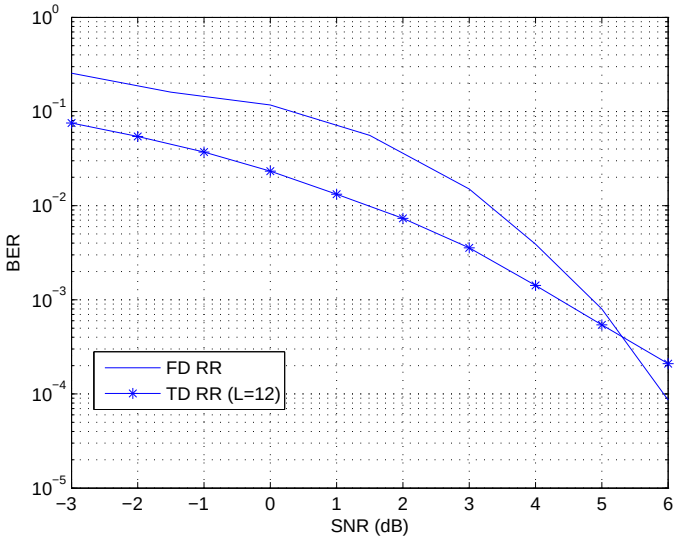

Figure 4.9. Comparison of BER performances of FD and TD processing when $\epsilon = 0.01$, $\kappa = 300$ and channel is CM1.

number of paths that yield sufficient energy ratio is rather low. However, in NLOS channels, i.e. CM4, there is a significant performance gap between FD and TD robust receivers in the favor of FD processing. Therefore, the main conclusion of this work is that in both FD and TD, robust methods outperform their linear counterparts. Moreover, FD channel estimation is inherently more robust to the channel statistics than the TD channel estimation and stands as a lower complexity solution than the TD channel estimation.

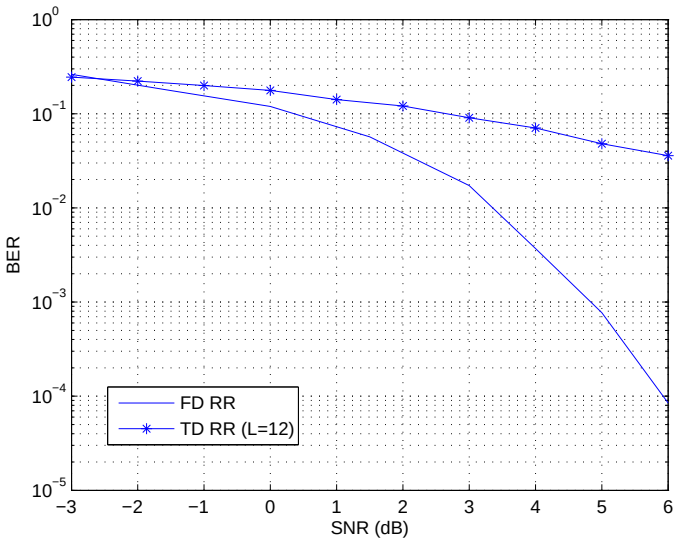

Figure 4.10. Comparison of BER performances of FD and TD processing when $\epsilon = 0.01$, $\kappa = 300$ and channel is CM4.

5. CONCLUSIONS

In this thesis, three problems are considered and brief overviews of the proposed methods are presented at the end of each chapter. In this chapter, we will briefly outline the further research directions related with these problems:

- **Robust acquisition of UWB signals under non-Gaussian noise**: The proposed method comes up with substantial performance gains but noise samples are assumed to be i.i.d in the receiver design. However, typical duration of a noise burst is on the order of microseconds which is much larger than the typical symbol durations in UWB systems. Therefore, it is expected that a noise burst can prevent detection of many samples. However, this point is left for a future research.
- **Iterative multiuser synchronization under ISI**: Although proposed algorithm's performance is very satisfactory, it can be further improved. First improvement is that to embed a channel estimation algorithm to alleviate need for channel knowledge. But this seems to be a simple extension especially the work in [81] is considered which proposes a channel estimator using the soft information. Second is to allow time-delays of paths to be non-integer multiples of chip duration. However, this does not seem to be as simple as the first improvement because of that it requires a new design. But, by such a design, timing jitter problem can also be alleviated.
- **Channel estimation:** Although FD channel estimation seems to be an attractive approach because of its lower complexity than TD channel estimation and its inherently robustness to channel statistics, there still exists problems to be handled. First is that channel estimation and equalization algorithms for ISI channels should be designed immediately, especially if one considers the extreme delay spread and resolvability of UWB channels. Second is that multiuser channel estimation algorithms should be proposed. Although this topic is widely investigated for CDMA systems, most of these works basically depend on subspace techniques. However, it takes long observation times to form reliable estimates

via subspace techniques because of large dimensions of the matrices involved.

APPENDIX A: PDF OF THE NOISE AT THE CORRELATOR OUTPUT

In this Appendix, the noise PDFs of the successive sampling and averaged template, (2.8) and (2.23), are derived. The noise term in successive sampling, $\omega_{ss}(m)$, consists of three parts such that

$$\omega_{ss}(m) = \omega_{ss,1}(m) + \omega_{ss,2}(m) + \omega_{ss,3}(m) \tag{A.1}$$

where $\omega_{ss,1}(m), \omega_{ss,2}(m)$ and $\omega_{ss,3}(m)$ are given by

$$\omega_{ss,1}(m) = \int_0^{T_s} r_s(t + mT_s)w(t + (m+1)T_s)dt, \tag{A.2}$$

$$\omega_{ss,2}(m) = \int_0^{T_s} r_s(t + (m+1)T_s)w(t + mT_s)dt, \tag{A.3}$$

$$\omega_{ss,3}(m) = \int_0^{T_s} w(t + mT_s)w(t + (m+1)T_s)dt, \tag{A.4}$$

respectively, where $r_s(t + mT_s) = b(m-1)p_r(t + T_s - \tau_1) + b(m)p_r(t - \tau_1)$. The autocorrelation function and the PDF of $\omega_{ss}(m)$ are derived in [39] for Gaussian $w(t)$ and it is shown that PDF of $w_{ss}(m)$ is Gaussian, as well. Here, following the same approach, the PDF of $\omega_{ss}(m)$ is derived for the case where $w(t)$ is modelled by a Gaussian-mixture. The autocorrelation function of $\omega_{ss}(m)$ is given by

$$\begin{aligned} R_{ss}(\tau) &= E\{\omega_{ss}(T_s)\omega_{ss}(T_s - \tau)\} \\ &= E\left\{\left(\sum_{i=1}^{3}\omega_{ss,i}(T_s)\right)\left(\sum_{i=1}^{3}\omega_{ss,i}(T_s - \tau)\right)\right\} \end{aligned} \tag{A.5}$$

Because the PDF of $w(t)$ is sum of two Gaussians, it can be decomposed as $w(t) = w_B(t) + w_I(t)$ where $w_B(t)$ is thermal noise with Gaussian PDF and $w_I(t)$ is shot noise with a PDF of the form, $f_I(x) = (1-\epsilon)\delta(x) + \epsilon g(x; \mu, \sigma^2)$ which can be approximated as a Gaussian PDF under certain conditions [82]. In four of nine terms in (A.5), there is the multiplication of $\omega_{ss,3}(m)$ with either $\omega_{ss,1}(m)$ or $\omega_{ss,2}(m)$. Since third moment

of a jointly Gaussian process is zero, (A.5) reduces to

$$\begin{aligned} R_{ss}(\tau) &= E\{\omega_{ss,1}(T_s)\omega_{ss,1}(T_s-\tau)\} + E\{\omega_{ss,2}(T_s)\omega_{ss,2}(T_s-\tau)\} \\ &\quad + E\{\omega_{ss,3}(T_s)\omega_{ss,3}(T_s-\tau)\} + E\{\omega_{ss,1}(T_s)\omega_{ss,2}(T_s-\tau)\} \\ &\quad + E\{\omega_{ss,2}(T_s)\omega_{ss,1}(T_s-\tau)\} \end{aligned} \tag{A.6}$$

where the cross-terms between $\omega_{ss,1}$ and $\omega_{ss,2}$ are explicitly given by

$$\begin{aligned} &E\{\omega_{ss,1}(T_s)\omega_{ss,2}(T_s-\tau)\} = \\ &\quad \int_0^{T_s}\int_{-\tau}^{T_s-\tau} E\{r_s(t+mT_s)r_s(u+(m+1)T_s)\}E\{w(t+(m+1)T_s)w(u+mT_s)\}dtdu. \end{aligned} \tag{A.7}$$

The autocorrelation of signal parts in the integrand of (A.7) is a function of $(t-u-T_s)$ whereas the autocorrelation of the noise parts in the integrand of (A.7) is a function of $(t-u+T_s)$, i.e. two expectations don't line up, in other words, mainlobe of one autocorrelation function is multiplied by the sidelobe of the other. Therefore, if T_s is large enough, the cross-terms between $\omega_{ss,1}$ and $\omega_{ss,2}$ have small contributions which is negligible [39]. Then, the autocorrelation function of $\omega_{ss}(m)$ becomes

$$\begin{aligned} R_{ss}(\tau) &\approx E\{\omega_{ss,1}(T_s)\omega_{ss,1}(T_s-\tau)\} \\ &\quad + E\{\omega_{ss,2}(T_s)\omega_{ss,2}(T_s-\tau)\} + E\{\omega_{ss,3}(T_s)\omega_{ss,3}(T_s-\tau)\} \end{aligned} \tag{A.8}$$

which implies that $\omega_{ss,1}(m), \omega_{ss,2}(m), \omega_{ss,3}(m)$ can be assumed to be uncorrelated and since their PDFs are sum of two Gaussian PDFs, also independent. The autocorrelation function of $\omega_{ss,1}$, or equivalently of $\omega_{ss,2}$, is given by

$$\begin{aligned} &E\{\omega_{ss,1}(T_s)\omega_{ss,1}(T_s-\tau)\} \\ &= \int_0^{T_s}\int_{-\tau}^{T_s-\tau} E\{r_s(t+mT_s)r_s(u+mT_s)\}E\{w(t+mT_s)w(u+mT_s)\}dtdu \\ &= \int_0^{T_s}\int_{-\tau}^{T_s-\tau} E\{r_s(t+mT_s)r_s(u+mT_s)\}\big(R_B(t-u)+R_I(t-u)\big)dtdu \end{aligned} \tag{A.9}$$

where $R_B(t-u)$ and $R_I(t-u)$ are the autocorrelation functions of $w_B(t)$ and $w_I(t)$, respectively. From (A.9), it can be deduced that $\omega_{ss,1}(m), \omega_{ss,2}(m)$ are also Gaussian-mixtures because their autocorrelation functions are sum of two autocorrelation functions, one for nominal (thermal) noise and one for impulsive one. Therefore, variances and the PDFs of $\omega_{ss,1}(m)$ and $\omega_{ss,2}(m)$ are given by

$$E\big\{\omega_{ss,1}^2(m)\big\} = E\big\{\omega_{ss,2}^2(m)\big\} = C_g N_f\big(\sigma^2 + \kappa\sigma^2\big) \tag{A.10}$$

$$f_{ss,1}(x) = f_{ss,2}(x) = (1-\epsilon)g(x;0,C_g N_f\sigma^2) + \epsilon g(x;0,C_g N_f\kappa\sigma^2). \tag{A.11}$$

Now, autocorrelation function of $\omega_{ss,3}$ will be investigated which is given by

$$E\big\{\omega_{ss,3}(T_s)\omega_{ss,3}(T_s-\tau)\big\} = \int_0^{T_s}\int_{-\tau}^{T_s-\tau} E\Big\{w(t+mT_s)w\big(t+(m+1)T_s\big)w(u+mT_s)w\big(u+(m+1)T_s\big)\Big\}dt. \tag{A.12}$$

Using the facts that $w_B(t)$ and $w_I(t)$ are uncorrelated, and third moment of a jointly Gaussian process is zero, integrand in (A.12) reduces to

$$\begin{aligned} & E\Big\{w(t+mT_s)w\big(t+(m+1)T_s\big)w(u+mT_s)w\big(u+(m+1)T_s\big)\Big\} \\ = \;& E\Big\{w_B(t+mT_s)w_B\big(t+(m+1)T_s\big)w_B(u+mT_s)w_B\big(u+(m+1)T_s\big)\Big\} \\ & + E\Big\{w_I(t+mT_s)w_I\big(t+(m+1)T_s\big)w_I(u+mT_s)w_I\big(u+(m+1)T_s\big)\Big\} \\ & + 2R_B(T_s)R_I(T_s) + 2R_B(t-u)R_I(t-u) \\ & + R_B(t-u+T_s)R_I(u-t+T_s) + R_B(u-t+T_s)R_I(t-u+T_s) \end{aligned} \tag{A.13}$$

where $R_B(T_s)$ and $R_I(T_s)$ are quite small if T_s is large enough and last two terms can be neglected because the autocorrelation functions of $w_B(t)$ and $w_I(t)$ do not line up

[39]. Therefore, integrand in (A.12) can be expressed as

$$\begin{aligned} & E\Big\{w(t+mT_s)w\big(t+(m+1)T_s\big)w(u+mT_s)w\big(u+(m+1)T_s\big)\Big\} \\ &= E\Big\{w_B(t+mT_s)w_B\big(t+(m+1)T_s\big)w_B(u+mT_s)w_B\big(u+(m+1)T_s\big)\Big\} \\ &\quad +E\Big\{w_I(t+mT_s)w_I\big(t+(m+1)T_s\big)w_I(u+mT_s)w_I\big(u+(m+1)T_s\big)\Big\} \\ &\quad +2R_B(t-u)R_I(t-u). \end{aligned} \tag{A.14}$$

Moreover, using the fact that $E\{abcd\} = E\{ab\}E\{cd\} + E\{ac\}E\{bd\} + E\{ad\}E\{bc\}$, if a, b, c, d are jointly Gaussian, fourth moments of $w_B(t)$ and $w_I(t)$ can be written as

$$E\Big\{w_B(t+mT_s)w_B\big(t+(m+1)T_s\big)w_B(u+mT_s)w_B\big(u+(m+1)T_s\big)\Big\} \approx 2R_B^2(t-u) \tag{A.15}$$

$$E\Big\{w_I(t+mT_s)w_I\big(t+(m+1)T_s\big)w_I(u+mT_s)w_I\big(u+(m+1)T_s\big)\Big\} \approx 2R_I^2(t-u) \tag{A.16}$$

using which the autocorrelation function of $\omega_{ss,3}$ is found to be

$$\begin{aligned} E\big\{\omega_{ss,3}(T_s)\omega_{ss,3}(T_s-\tau)\big\} &= \int_0^{T_s}\int_{-\tau}^{T_s-\tau} 2R_B^2(t-u)dtdu \\ &\quad + \int_0^{T_s}\int_{-\tau}^{T_s-\tau} 2R_I^2(t-u)dtdu \\ &\quad + \int_0^{T_s}\int_{-\tau}^{T_s-\tau} 2R_B(t-u)R_I(t-u)dtdu \end{aligned} \tag{A.17}$$

where with respect to first two integrals, the last one can be eliminated [39] resulting in

$$E\{\omega_{ss,3}(T_s)\omega_{ss,3}(T_s-\tau)\} = 2\int_0^{T_s-|\tau|}\int_{-\infty}^{\infty}\big\{R_B^2(y)+R_I^2(y)\big\}dydx. \tag{A.18}$$

Therefore, $\omega_{ss,3}$ is also a Gaussian-mixture because its autocorrelation function is sum of two autocorrelation functions, one for nominal and one for impulsive noise. The

variance and the PDF of $\omega_{ss,3}$ is given by

$$E\{\omega_{ss,3}^2\} = 4T_s W\sigma^2\big(\sigma^2 + \kappa^2\sigma^2\big) \tag{A.19}$$

$$f_{ss,3}(x) = (1-\epsilon)g(x;0,4T_s W\sigma^4) + \epsilon g(x;0,4T_s W\kappa^2\sigma^4) \tag{A.20}$$

where W is the bandwidth of the front-end filter employed in the receiver and can be approximated as $W \approx 1/T_p$, pulse duration [19]. Since $\omega_{ss} = \omega_{ss,1} + \omega_{ss,2} + \omega_{ss,3}$, the density of ω_{ss} is given by $f_{ss} = f_{ss,1} * f_{ss,2} * f_{ss,3}$, where $*$ denotes linear convolution, which results in (2.8). The noise PDF for averaged template-based acquisition, i.e. (2.23), can be obtained with similar arguments.

APPENDIX B: PDF OF THE OVERALL DISTURBANCE

Here, the variance of the MUI term and the PDF given in (2.42) and (2.43), respectively, will be derived. First, MUI term will be written as

$$\omega_{mui}(m) \triangleq \xi_1(m) + \xi_2(m) \tag{B.1}$$

where $\xi_1(m)$ and $\xi_2(m)$ are given by

$$\begin{aligned}
\xi_1(m) &= \frac{2}{N_t}\int_0^{T_s}\left[\sum_{\substack{u=1\\u\neq d}}^{N_u} b_u(m-1)p_{u,r}(t+T_s-\tau_1^u)+b_u(m)p_{u,r}(t-\tau_1^u)\right] \\
&\quad\times\left[\sum_{l=1}^{N_u}\sum_{i=0}^{N_t/2-1} b_l(i-1)p_{l,r}(t+T_s-\tau_1^l)+b_l(i)p_{l,r}(t-\tau_1^l)\right]dt \qquad \text{(B.2)}\\
\xi_2(m) &= \frac{2}{N_t}\int_0^{T_s}\left[p_{d,r}(t+T_s-\tau_1^d)+p_{d,r}(t-\tau_1^d)\right] \\
&\quad\times\left[\sum_{\substack{l=1\\l\neq d}}^{N_u}\sum_{i=0}^{N_t/2-1} b_l(i-1)p_{l,r}(t+T_s-\tau_1^l)+b_l(i)p_{l,r}(t-\tau_1^l)\right]dt. \qquad \text{(B.3)}
\end{aligned}$$

Since asynchronous interfering users are transmitting i.i.d. data symbols, their mean and cross-correlation are zero, i.e.

$$E\{\xi_1(m)\} = E\{\xi_2(m)\} = E\{\xi_1(m)\xi_2(m)\} = 0 \tag{B.4}$$

using which variance of the MUI term can be expressed as

$$\sigma_{mui}^2(m) = E\{\xi_1^2(m)\} + E\{\xi_2^2(m)\} \tag{B.5}$$

where the second moments of $\xi_1(m)$ and $\xi_2(m)$ are given by

$$\begin{aligned} E\{\xi_1^2(m)\} &= \frac{2}{N_t}\sum_{\substack{u=1\\u\neq d}}^{N_u}\sum_{l=1}^{N_u}\Bigg\{\left[\int_0^{\tau_1^u} p_{u,r}(t+T_s-\tau_1^u)p_{l,r}(t+T_s-\tau_1^l)dt\right]^2 \\ &\quad+\left[\int_{\tau_1^u}^{\tau_1^l} p_{u,r}(t-\tau_1^u)p_{l,r}(t+T_s-\tau_1^l)dt\right]^2 \\ &\quad+\left[\int_{\tau_1^l}^{T_s} p_{u,r}(t-\tau_1^u)p_{l,r}(t-\tau_1^l)dt\right]^2\Bigg\}, \end{aligned} \tag{B.6}$$

$$\begin{aligned} E\{\xi_1^2(m)\} &= \frac{2}{N_t}\sum_{\substack{l=1\\l\neq d}}^{N_u}\Bigg\{\left[\int_0^{\tau_1^d} p_{d,r}(t+T_s-\tau_1^d)p_{l,r}(t+T_s-\tau_1^l)dt\right]^2 \\ &\quad+\left[\int_{\tau_1^d}^{\tau_1^l} p_{d,r}(t-\tau_1^d)p_{l,r}(t+T_s-\tau_1^l)dt\right]^2 \\ &\quad+\left[\int_{\tau_1^l}^{T_s} p_{d,r}(t-\tau_1^d)p_{l,r}(t-\tau_1^l)dt\right]^2\Bigg\}. \end{aligned} \tag{B.7}$$

Therefore, using (B.6) and (B.7), variance of the MUI can be expressed as

$$\sigma_{mui}^2(m) \approx \frac{2}{N_t}\sum_{\substack{u=1\\u\neq d}}^{N_u} E_{u,r}^2 + \frac{2}{N_t}\sum_{u=1}^{N_u}\sum_{\substack{l=1\\l\neq u}}^{N_u}\Theta_{u,l}^2 \tag{B.8}$$

where $\Theta_{u,l}$ is the cross-correlation between uth and lth users' received symbol-length waveforms which is given by

$$\begin{aligned} \Theta_{u,l} &= \int_0^{\tau_1^u} p_{u,r}(t+T_s-\tau_1^d)p_{l,r}(t+T_s-\tau_1^l)dt + \int_{\tau_1^d}^{\tau_1^l} p_{d,r}(t-\tau_1^d)p_{u,r}(t+T_s-\tau_1^l)dt \\ &\quad+\int_{\tau_1^l}^{T_s} p_{d,r}(t-\tau_1^d)p_{u,r}(t-\tau_1^l)dt \end{aligned} \tag{B.9}$$

which is negligible with respect to first term in (B.8). Therefore, variance of the MUI can be approximated as

$$\sigma^2_{mui}(m) \approx \frac{2}{N_t}\sum_{\substack{u=1\\u\neq d}}^{N_u} E^2_{u,r}. \tag{B.10}$$

Now, PDF of the overall disturbance, noise plus MUI, will be derived. First consider the noise which consists of three parts as in previous cases, namely

$$\omega_{ma}(m) = \omega_{ma,1}(m) + \omega_{ma,2}(m) + \omega_{ma,3}(m) \tag{B.11}$$

which are explicitly given by

$$\omega_{ma,1}(m) = \sum_{u=1}^{N_u}\int_0^{T_s} \left[b_u(m-1)p_{u,r}(t+T_s-\tau_1^u) + b_u(m)p_{u,r}(t-\tau_1^u)\right]\bar{w}(t)dt \tag{B.12}$$

$$\omega_{ma,2}(m) = \frac{2}{N_t}\sum_{u=1}^{N_u}\sum_{i=0}^{N_t/2-1}\int_0^{T_s} \big[b_u(i-1)p_{u,r}(t+T_s-\tau_1^u) + b_i(m)p_{u,r}(t-\tau_1^u)\big]w(t)dt \tag{B.13}$$

$$\omega_{ma,3}(m) = \int_0^{T_s}\bar{w}(t)w(t)dt. \tag{B.14}$$

Using the analysis carried out in Appendix A, it can be shown that these noise samples are independent and their PDFs are also given by Gaussian mixture model with zero mean and variances

$$E\{\omega^2_{ma,1}(m)\} = E_{T,r}\left(2\frac{\sigma^2}{N_t} + 2\kappa\frac{\sigma^2}{N_t}\right) \tag{B.15}$$

$$E\{\omega^2_{ma,2}(m)\} = E_{d,r}(\sigma^2 + \kappa\sigma^2) \tag{B.16}$$

$$E\{\omega^2_{ma,3}(m)\} = 4T_sW\left(\frac{\sigma^4}{N_t} + \kappa^2\frac{\sigma^2}{N_t}\right) \tag{B.17}$$

where $E_{T,r} = \sum_{u=1}^{N_u} E_{u,r}$ is the sum of received energies of the all users. By approximating MUI term by a Gaussian PDF using CLT and by defining the PDFs of $\omega_{ma,1}(m), \omega_{ma,2}(m)$ and $\omega_{ma,3}(m)$ as $f_{ma,1}(x), f_{ma,2}(x)$ and $f_{ma,3}(x)$, the overall PDF of the all disturbances, noise plus MUI, can be found by $f_{ma}(z) = g(z; 0, \sigma^2_{mui}) * f_{\omega_{ma,1}}(z) * f_{\omega_{ma,2}}(z) * f_{\omega_{ma,3}}(z)$ which results in (2.43).

APPENDIX C: DERIVATION OF AUTOCORRELATION MATRIX

In this Appendix, the autocorrelation matrix of the clipping function's output, i.e. (4.31), will be derived. Using the independence of the noise samples, the cross-correlation of the output of the clipping function conditioned on the estimated path gains is given by

$$\begin{aligned} & E\big\{\psi(\mathbf{e}_n(m))\psi(\mathbf{e}_n(l)) \mid \hat{\mathbf{h}}_{n-1}\big\} \\ &= \begin{cases} E\big\{\psi(\mathbf{e}_n(m)) \mid \hat{\mathbf{h}}_{n-1}\big\}E\big\{\psi(\mathbf{e}_n(l)) \mid \hat{\mathbf{h}}_{n-1}\big\} & \text{if } m \neq l \\ \\ E\big\{\psi^2(\mathbf{e}_n(m)) \mid \hat{\mathbf{h}}_{n-1}\big\} & \text{if } m = l, \end{cases} \end{aligned} \tag{C.1}$$

from which, for $m \neq l$, the cross-correlation conditioned on the estimated path gains can be obtained as

$$E\big\{\psi(\mathbf{e}_n(m))\psi(\mathbf{e}_n(l)) \mid \hat{\mathbf{h}}_{n-1}\big\} = \frac{4\beta^2}{\sigma^4}\Delta\hat{\mathbf{h}}_{n-1}(m)\Delta\hat{\mathbf{h}}_{n-1}(l), \tag{C.2}$$

using (4.25). For $m = l$, using (4.24), the second moment of the output of the clipping function conditioned on the estimated channel gains can be obtained as

$$\begin{aligned} E\{\psi^2(\mathbf{e}_n(m)) \mid \hat{\mathbf{h}}_{n-1}\} &= \frac{\Delta\hat{\mathbf{h}}^2_{n-1}(m)}{\sigma^4}\int_{-k\sigma^2}^{k\sigma^2} f(w)dw + \int_{-k\sigma^2}^{k\sigma^2}\frac{w^2}{\sigma^4}f(w)dw \\ &\quad + \int_{k\sigma^2}^{\infty} 2k^2 f(w)dw \\ &= \frac{2\beta}{\sigma^4}\Delta\hat{\mathbf{h}}^2_{n-1}(m) + (\alpha_1 + \alpha_2), \end{aligned} \tag{C.3}$$

where α_1, α_2 are given by (4.32) and (4.33), respectively. Combining (C.2)-(C.3), the cross-correlation of the output of the clipping function conditioned on the estimated

path gains, i.e. (C.1), can be obtained as follows:

$$E\{\psi(\mathbf{e}_n(m))\psi(\mathbf{e}_n(l)) \mid \hat{\mathbf{h}}_{n-1}\} = \begin{cases} \frac{4\beta^2}{\sigma^4}\Delta\hat{\mathbf{h}}_{n-1}(m)\Delta\hat{\mathbf{h}}_{n-1}(l) & \text{if } m \neq l \\ \\ \frac{2\beta}{\sigma^4}\Delta\hat{\mathbf{h}}^2_{n-1}(m) + (\alpha_1 + \alpha_2) & \text{if } m = l. \end{cases}$$

from which (4.31) can be concluded.

APPENDIX D: PERFORMANCE OF TD MATCHED FILTER

In this Appendix, the probability of error of the TD matched filter will be derived taking both impulsive noise and the channel estimation error into account. For TD matched filter, decision is given via

$$T_{td,m} = \hat{\mathbf{g}}_{td,m}^T \mathbf{y} \underset{H_0}{\overset{H_1}{\gtrless}} 0 \tag{D.1}$$

where $T_{td,m}$ is the output of the matched filter and the $\hat{\mathbf{g}}_{td,m}$ denotes the linear estimate of the aggregate channel response. H_1 is assumed to be correct. Then, the mean of the decision statistic is given by

$$\mu_{td,m} = E\left\{T_{td,m}\right\} = \left(\mathbf{P}E\left\{\hat{\mathbf{h}}_{td,m}\right\}\right)^T \mathbf{g} \tag{D.2}$$

where $\hat{\mathbf{h}}_{td,m}$ denote the linear estimate of the channel response, i.e. $\mathbf{P}\hat{\mathbf{h}}_{td,m} = \hat{\mathbf{g}}_{td,m}$. The variance of the decision statistic is given by

$$\begin{aligned}
\nu_{td,m}^2 &= E\left\{T_{td,m}^2\right\} - E^2\left\{T_{td,m}\right\} \\
&= \left(\tilde{\mathbf{P}}\tilde{\mathbf{h}}\right)^T \left(\mathbf{P}E\left\{\hat{\mathbf{h}}_{td,m}\hat{\mathbf{h}}_{td,m}^T\right\}\mathbf{P}^T\right)\left(\tilde{\mathbf{P}}\tilde{\mathbf{h}}\right) + E\left\{\mathbf{w}^T\left(\mathbf{P}\hat{\mathbf{h}}_{td,m}\hat{\mathbf{h}}_{td,m}^T\mathbf{P}^T\right)\mathbf{w}\right\} \\
&\quad - \left(\tilde{\mathbf{P}}\tilde{\mathbf{h}}\right)^T \left(\mathbf{P}E\{\hat{\mathbf{h}}_{td,m}\}E\{\hat{\mathbf{h}}_{td,m}\}^T\mathbf{P}^T\right)\left(\tilde{\mathbf{P}}\tilde{\mathbf{h}}\right) \\
&= \left(\tilde{\mathbf{P}}\tilde{\mathbf{h}}\right)^T \left(\mathbf{P}\mathbf{K}_{h,td}\mathbf{P}^T\right)\left(\tilde{\mathbf{P}}\tilde{\mathbf{h}}\right) \\
&\quad + E\left\{w^2\right\}\mathrm{Tr}\left[\mathbf{P}(\mathbf{K}_{h,td} + E\{\hat{\mathbf{h}}_{td}\}E\{\hat{\mathbf{h}}_{td}\}^T)\mathbf{P}^T\right]
\end{aligned} \tag{D.3}$$

where $\mathbf{K}_{h,td}$ is the covariance matrix of the linear channel estimate, i.e. $\mathbf{K}_{h,td} = E\left\{\hat{\mathbf{h}}_{td,m}\hat{\mathbf{h}}_{td,m}^T\right\} - E\left\{\hat{\mathbf{h}}_{td,m}\right\}E\{\hat{\mathbf{h}}_{td,m}^T\}$. It should be noted that $\mathbf{K}_{h,td}$ and $E\left\{\hat{\mathbf{h}}_{td,m}\right\}$ can be calculated from their robust counterparts, i.e. $\mathbf{K}_h^n$ and $E\{\hat{\mathbf{h}}\}$ via setting $k = \infty$.

Therefore, using CLT and symmetry between two hypotheses, probability of error of TD matched filter can be written as

$$P_{e,td}^{m} = Q\left(\frac{\mu_{td,m}}{\nu_{td,m}}\right) \tag{D.4}$$

for which although mean of the test statistic, (D.2), is not affected by the impulsive noise, there is an increase in the variance of the test statistic, (D.3), with respect to nominal case, due to impulsive noise. Moreover, both from (D.2) and (D.3), it can be seen that correlation structure of the channel has an impact on the performance of the TD matched filter.

APPENDIX E: PERFORMANCE OF FD MATCHED FILTER

In this Appendix, the probability of error of the FD matched filter under impulsive noise will be derived incorporating channel estimation errors. In the FD matched filter, detection is based on the test

$$\sum_{l=0}^{N-1} T_{fd,m}(l) \underset{H_0}{\overset{H_1}{\gtrless}} 0 \tag{E.1}$$

where $T_{fd,m}(l) = \hat{\mathbf{G}}_{fd,m}(l)\mathbf{Y}(l)$ where $\hat{\mathbf{G}}_{fd,m}$ denotes the linear estimate of the aggregate channel response. H_1 is assumed to be correct, then the mean and the variance of $T_{fd,m}(l)$ are given by

$$\begin{aligned} \mu_{fd,m}(l) &= E\{T_{fd,m}(l)\} = E\{\hat{\mathbf{G}}_{fd,m}(l)\mathbf{Y}(l)\} \\ &= E\{\hat{\mathbf{G}}_{fd,m}(l)(\mathbf{G}(l) + \mathbf{W}(l))\} = \mathbf{G}^2(l), \end{aligned} \tag{E.2}$$

$$\begin{aligned} \nu^2_{fd,m}(l) &= E\left\{T^2_{fd,m}(l)\right\} - E^2\left\{T_{fd,m}(l)\right\} \\ &= E\left\{\hat{\mathbf{G}}^2_{fd,m}(l)\left(\mathbf{G}(l) + \mathbf{W}(l)\right)^2\right\} - \mathbf{G}^4(l) \\ &= E\left\{\left(\mathbf{G}(l) - \Delta\hat{\mathbf{G}}_{fd,m}(l)\right)^2\left(\mathbf{G}(l) + \mathbf{W}(l)\right)^2\right\} - \mathbf{G}^4(l) \\ &= \mathbf{G}^2(l)E\left\{\Delta\hat{\mathbf{G}}_{fd,m}(l)^2\right\} + E\left\{\mathbf{W}^2(l)\right\}\left(\mathbf{G}^2(l) + E\left\{\Delta\hat{\mathbf{G}}_{fd,m}(l)^2\right\}\right) \end{aligned} \tag{E.3}$$

where $\Delta\hat{\mathbf{G}}_{fd,m}(l)$ is the error of the linear estimate of the aggregate channel response which can be calculated from its robust counterpart, i.e. $\Delta\hat{\mathbf{G}}_{fd,m}(l)$, via setting $k = \infty$. Therefore, using CLT and symmetry between two hypotheses, the probability of error is given by

$$P_{e,fd}^{m} = Q\left(\frac{\sum_{m=0}^{N-1}\mu_{fd,m}(m)}{\sqrt{\sum_{m=0}^{N-1}\nu_{fd,m}^{2}(m)}}\right) \tag{E.4}$$

for which although mean value of the test statistic, (E.2), is not affected by the impulsive noise, there has been a serious increase in the variance of the test statistic, (E.3), with respect to nominal case, due to impulsive noise.

REFERENCES

1. Roy, S., J. F. Foerster, V. S. Somayazulu, and D. G. Leeper, "Ultrawideband radio design: The promise of high-speed, short-range wireless connectivity", *Proceedings of IEEE*, Vol. 92, No. 2, pp. 295-311, February 2004.

2. Yang, L. and G. B. Giannakis, "Ultra wideband communications: An idea whose time has come", *IEEE Signal Processing Magazine*, Vol. 21, No. 6, pp. 26-54, November 2004.

3. "FCC notice of proposed rule making, revision of part 15 of the commission's rules regarding ultra-wideband transmission systems", Federal Communications Commission, Washington, DC, ET-Docket 98-153.

4. *IEEE Conference on Ultra Wideband Systems on Technologies.*

5. "Ultra wideband radio in multiaccess wiresless communications," *IEEE Journal on Selected Areas of Communication*, Vol. 20, No. 12, December 2002.

6. "Ultra wideband wireless communications: Theory and applications", *IEEE Journal on Selected Areas of Communication,* Vol. 24, No. 4, April 2006.

7. "Special issue on ultra wideband", *IEEE Transactions on Microwave Theory and Techniques*, April 2006.

8. "Special issue on ultra wideband radio", *Eurasip Journal on Applied Signal Processing*, Vol. 3, No. 3, March 2005.

9. Taylor, J. D., *Introduction to Ultra Wideband Radar Systems*, Boca Raton, FL: CRC, 1995.

10. Scholtz, R. A., "Multiple access with time-hopping impulse modulation", *Conference on Military Communications,* Bedford, MA, 1993.

11. Vijayakumaran, S., T. F. Wong and S. R. Aedudodla, "On the asymptotic performance of threshold-based acquisition systems in multipath fading channels", *IEEE Transactions on Information Theory,* Vol. 51, No. 11, pp. 3973-3986, November 2005.

12. Homier, E. A. and R. A. Scholtz, "Rapid acquisition of ultra wideband signals in dense multipath", *Proceedings of Conference on Ultra Wideband Systems and Technologies*, pp. 105-110, Baltimore, MD, May 2002.

13. Homier E. A. and R. A. Scholtz, "Hybrid fixed dwell-time search techniques for rapid acquisition of ultra wideband signals in dense multipath", *International Workshop on UWB Systems*, Oulu, Finland, June 2003.

14. Homier, E. A. and R. A. Scholtz, "A generalized signal flowgraph approach for hybrid acquisition for ultra-wideband signals", *International Journal on Wireless Information Networks*, pp. 179-191, October 2003.

15. Vijayakumaran, S. and T. F. Wong, "Best permutation search strategy for ultra wideband signal acquisition", *Proceedings of IEEE Vehicular Technology Conference,* September 2004.

16. Gezici, S., E. Fishler, H. Kobayashi, H. V. Poor, and A. Molisch, "A rapid acquisition techniques for impulse radio", *Proceedings of 2003 IEEE Pacific-Rim Conference on Communations, Computers and Signal Processing,* pp. 627-630, August 2003.

17. Aedudodla, S. R., S. Vijayakumaran, and T. F. Wong, "Ultra-wideband signal acquisition with hybrid DS-TH spreading", *IEEE Transactions on Wireless Communications,* Vol. 5, No. 9, pp. 2504-2515, September 2006.

18. Tian, Z. and G. B. Giannakis, "A GLRT approach to data-aided timing acquisition in UWB radios - part I: Algorithms", *IEEE Transactions Wireless Communications*, Vol. 4, No. 6, pp. 2956-2967, November 2005.

19. Yang, L. and G. B. Giannakis, "Timing UWB signals with dirty template," *IEEE Transactions on Communications*, Vol. 53, No. 11, pp. 1952-1963, November 2005.

20. Franz, S., C. Carbonelli and U. Mitra, "Semi-blind ML synchronization for UWB signals," *Proceedings of 42th Allerton Conference on Communication, Control, and Computing*, Monticello, IL, September 2004.

21. Yang, L., Z. Tian and G. B. Giannakis, "Non-data aided timing acquisition of ultra wideband transmissions using cyclostationary", in *Proceedings of International Conference on Acoustics, Speech, and Signal Processing*, pp. 121-124, Hong Kong, April 2003.

22. Maravic, I., J. Kusuma and M. Vetterli, "Low-sampling rate UWB channel characterization and synchronization", *Journal on Communication Networks*, Vol. 5, pp. 319-327, 2003.

23. Foerster, J. R., "Channel modeling sub-committee report (final)", Tech. Rep. P802.15-02 / 368r5-SG3a, IEEE P802.15 Working Group for Wireless Personal Area Networks (WPANs), December 2002.

24. Simon, M. K., J. K. Omura, R. A. Scholtz and B. K. Levitt, *Spread Spectrum Communications: Volume III.* Rockville, MD: Computer Science, 1985.

25. Aedudodla, S., S. Vijayakumaran and T. F. Wong, "Timing acquisition in ultra-wideband communication systems", *IEEE Transactions on Vehicular Technology*, Vol. 54, No. 5, pp. 1570-1583, September 2005.

26. Lottici, V., A. D'Andrea, and U. Mengali, "Channel estimation for ultra-wideband communications", *IEEE Journal on Selected Areas of Communications*, Vol. 20,

No. 9, pp. 1638-1645, December 2002.

27. Win, M. Z. and R. A. Scholtz, "Characterization of Ultra-Wide bandwidth wireless indoor channels: a communication theoretic view", *IEEE Journal on Selected Areas of Communications*, Vol. 20, No. 9, pp. 1613-1627, December 2002.

28. Li, Y., A. F. Molisch and J. Zhang, "Channel estimation and signal detection for UWB", *Proceedings of International Symposium on Wireless Personal Multimedia Communications*, 2003.

29. Mielczarek, B., M. Wessman and A. Svensson, "Performance of coherent UWB RAKE receivers with channel estimators", *Proceedings of Vehicular Technology Conference*, October 2003.

30. Saberinia, E., A. Tewfik, J. Tang and K. Parhi, "Pulsed OFDM modulation for Ultra wideband Communications", *IEEE International Symposium On Circuits and Systems,* Vancouver, B.C., Canada, May 2004.

31. Tewfik, A. and E. Saberinia, "System aspects of multi-band UWB-OFDM: status and optimal design rules", *IEEE Radio and Wireless Conference, UWB Technology Components, Systems, and Architectures Workshop,* Atlanta, GA, September 2004.

32. Batra, A., J. Balakrishnan, G. R. Aiello, J. R. Foerster and A. Dabak, "Design of a multiband OFDM system for realistic UWB channel environments", *IEEE Transactions on Microwave Theory and Techniques*, Vol. 52, No. 9, pp. 2123-2138, September 2004.

33. Wang, Y., X. Dong, P. H. Wittke and S. Mo, "Cyclic prefixed single carrier transmission in UWB communications", *Proceedings of IEEE International Conference on Communications*, Vol. 4, pp. 2862-2866, 2005.

34. Wang, Y. and X. Dong, "Frequency domain channel estimation for SC-FDE in

UWB communications", *Proceedings of IEEE Global Telecommunications Conference*, Vol. 6, pp. 3654-3658, 2005.

35. Sato, H. and T. Ohtsuki, "Performance evaluation of frequency domain equalization and channel estimation for direct sequence-ultra wideband (DS-UWB) system", *Proceedings of IEEE Vehicular Technology Conference*, Vol. 1, pp. 481-485, 2005.

36. Tonello, A. M. and R. Rinaldo, "A time-frequency domain approach to synchronization, channel estimation, and detection for DS-CDMA impulse-radio systems", *IEEE Transactions on Wireless Communications*, Vol. 4, No. 6, pp. 3005-3017, November 2005.

37. Batra, A. "TI physical layer proposal for IEEE 802.15 task group 3a", IEEE P802.15-03/142r2-TG3a, March 2003.

38. Batra, A. "Multi-band OFDM physical layer proposal", IEEE P802.15-03/268r0-TG3a, July 2003.

39. Hoctor, R. T. and H. W. Tomlinson, "An overview of delay-hopped transmitted-reference RF communications", G. E. Research and Development Center, Technical Information Series, pp. 1-29, 2002.

40. Chao, Y. and R. A. Scholtz, "Optimal and suboptimal receivers for ultra wideband transmitted reference systems", *Proceedings of Global Telecommunications Conference*, pp. 744-748, San Fransisco, CA, 2003.

41. Yang, L. and G. B. Giannakis, "Optimal pilot waveform assisted modulation for ultra wideband communications", *IEEE Transactions on Wireless Communications,* Vol. 3, No. 4, pp. 1236-1249, July 2004.

42. Zhang, H. and D. K. Goeckel, "Generalized transmitted-reference UWB systems", *Proceedings of Conference on Ultra Wideband Systems and Technologies,* pp. 147-

151, Reston, VA, 2003.

43. Franz, S. and U. Mitra, "Generalized UWB transmitted-reference systems", *IEEE Journal on Selected Areas of Communications,* Vol. 24, No. 6, pp. 780-786, April 2006.

44. Ho, M., V. Somayazulu, J. Foerster and S. Roy, "A differential detector for an ultra wideband communications system", *Proceedings of Vehicular Technology Conference,* pp. 1896-1900, Birmingham, AL, 2002.

45. Yang, L., G. B. Giannakis, and A. Swami, "Noncoherent ultra wideband radios", *Proceedings of Military Communications Conference,* Monterey, CA, 2004.

46. Blackard, K. L., T. S. Rappaport, and C. W. Bostian, "Measurements and models of radio frequency impulsive noise for indoor wireless communications", *IEEE Journal on Selected Areas in Communications*, Vol. 11, pp. 991-1001, September 1993.

47. Kassam, S. A. and H. V. Poor, "Robust techniques for signal processing: a survey", *Proceedings of the IEEE*, Vol. 73, No. 3, March 1985.

48. Djapic, R., G. Leus, A. Trindade, and A. J. van der Veen, "Blind synchronization in multiuser transmit-reference UWB systems", *Proceedings of the European Signal Processing Conference*, Antalya, Turkey, September 2005.

49. Luo, X. and G. B. Giannakis, "Low-complexity blind synchronization and demodulation for (ultra-) wideband multi-user ad hoc access", *IEEE Transactions on Wireless Communications*, Vol. 5, No. 7, pp. 1930-1941, July 2006.

50. Mahadevappa, R. H. and J. G. Proakis, "Mitigating multiple access interference and intersymbol interference in uncoded CDMA systems with chip-level interleaving", *IEEE Transactions on Wireless Communications*, Vol. 1, No. 4, pp. 781-792, October 2002.

51. Li, K., X. Wang, G. Yue, and L. Ping, "A low rate code-spread and chip-interleaved time-hopping UWB system", *IEEE Journal on Selected Areas of Communications*, Vol. 24, No. 4, pp. 864-870, April 2006.

52. Douillard, C., M. Jezequel, C. Berrou, A. Picart, P. Didier, and A. Glavieux, "Iterative correction of intersymbol interference: Turbo equalization", *European Transactions on Telecommunications*, Vol. 6, pp. 507-511, September- October 1995.

53. Tuchler, M., R. Koetter, and A. Singer, "Turbo equalization: Principles and new results", *IEEE Transactions on Communications* , Vol. 50, pp. 754-767, May 2002.

54. Wang, X. and H. V. Poor, "Iterative (turbo) soft interference cancellation and decoding for coded CDMA", *IEEE Transactions on Communications*, Vol. 47, pp. 1046-1061, July 1999.

55. Noels, N., V. Lottici, A. Dejonghe, H. Steendam, M. Moeneclay, M. Luise, L. Vandendorpe, "A theoretical framework for soft-information-based synchronization in iterative (turbo) receivers", *Eurasip Journal on Wireless Communication Networks* , Vol. 2, pp. 117-129, 2005.

56. Lottici, V. and M. Luise, "Embedding carrier phase recovery into iterative decoding of turbo-coded linear modulations", *IEEE Transactions on Communications,* Vol. 52, No. 4, pp. 661-669, April 2004.

57. Burr, A. and L. Zhang, "A novel carrier phase recovery method for turbo-coded QPSK system", *Proceedings of European Wireless 2002*, pp. 817-821, Florence, Italy, February 2002.

58. Morlet, C., I. Buret, and M. -L. Boucheret, "A carrier phase estimator for multimedia satellite payloads suited to RSC coding schemes", *Proceedings of IEEE International Conference on Communications,* vol. 1, pp. 455-459, New Orleans,

LA, USA, June 2000.

59. Langlais, C. and M. Helard, "Phase carrier for turbo codes over a satellite link with the help of tentative decisions", *2nd International Symposium on Turbo Codes and Related Topics,* Vol. 5, pp. 439-442, Brest, France, September 2002.

60. Huber, P. J., *Robust Statistics*, New York: Wiley, 1981.

61. Chan, S. C. and Y. X. Zou, "A recursive least M-estimate algorithm for robust adaptive filtering in impulsive noise: fast algorithm and convergence analysis", *IEEE Transactions on Signal Processing*, Vol. 52, No. 4, pp. 975-991, April 2004.

62. Huber, P. J., "A Robust version of the probability ratio test", *Annals of Mathematics and Statistics,* vol. 36, pp. 1753-1758, 1965.

63. Martin, R. D. and S. C. Schwartz, "Robust detection of a known signal in nearly Gaussian noise", *IEEE Transactions on Information Theory*, Vol. IT-17, pp. 50-56, January 1971.

64. El-Sawy, A. H. and V. D. Vandelinde, "Robust detection of known signals", *IEEE Transactions on Information Theory*, Vol. IT-23, No. 6, pp. 722-727, November 1977.

65. Tian, Z. and G. B. Giannakis, "BER sensitivity to mistiming in ultra wideband communications, part 1: Nonrandom Channels," *IEEE Trans. Signal Processing*, Vol. 53, No. 4, pp. 1550-1560, April 2005.

66. Middleton, D., "Statistical-physical models of electromagnetic interference," *IEEE Transactions on Electromagnetic Compatibility*, Vol. EC-19, No. 8, pp. 106-127, August 1977.

67. Vastola, K. S., "Threshold detection in narrowband non-Gaussian noise," *IEEE Transactions on Communications*, Vol. COM-32, No. 2, pp.134-139, February 1984.

68. Wang, X. and H. V. Poor, "Robust multiuser detection in non-Gaussian channels", *IEEE Transactions on Signal Processing,* Vol. 47, No. 2, pp. 289-305, February 1999.

69. Barry, J. R., A. Kavcic, S. W. McLaughlin, A. Nayak, and W. Zeng, "Iterative timing recovery", *IEEE Signal Processing Magazine*, Vol. 20, pp. 89-102, January 2004.

70. Bahl, L. R., J. Cocke, F. Jelinek, and J. Raviv, "Optimal decoding of linear codes for minimizing symbol error rate", *IEEE Transactions on Information Theory*, Vol. 20, pp. 284-287, March 1974.

71. Proakis, J. G., *Digital Communications*, 3rd ed. , New York: McGraw-Hill, 1995.

72. Gezici, S., H. Kobayashi, H. V. Poor, A. F. Molisch, "Performance evaluation of impulse radio UWB systems with pulse-based polarity randomization", *IEEE Transactions on Signal Processing*, Vol. 53, No. 7, July 2005.

73. Poor, H. V. and S. Verdu, "Probability of error in MMSE multiuser detection," *IEEE Transactions on Information Theory,* Vol. IT-43, pp. 858-871, May 1997.

74. Guney, N., Hakan Deliç, and M. Koca, "Robust detection of UWB signals in non-Gaussian noise," *IEEE Transactions on Microwave Theory and Techniques*, Vol. 54, No. 4, pp. 1724-1731, April 2006.

75. Falconer, D., S. L. Ariyavisitakul, A. Benyamin-Seeyar, and B. Eidson, "Frequency-domain equalization for single-carrier broadband wireless systems", *IEEE Communications Magazine*, Vol. 40, No. 6, pp. 58-66, April 2002.

76. Clark, M. V., "Adaptive frequency-domain equalization and diversity combining for broadband wireless communications", *IEEE Journal on Selected Areas of Communications*, Vol. 16, No. 8, pp. 1385-1395, October 1998.

77. Sari, H., G. Karam, and I. Jeanclaude, "Frequency domain equalization of mobile radio and terrestrial broadcast channels", *Proceedings of IEEE Global Telecommunications Conference*, pp. 1-5, San Francisco, CA, November-December 1994.

78. Morelli, M., L. Sanguinetti, and U. Mengali, "Channel estimation for adaptive frequency-domain equalization", *IEEE Transactions on Wireless Communications*, Vol. 4, No. 5, pp. 2508-2518, September 2005.

79. Shynk, J. J., "Frequency-domain and multirate adaptive filtering", *IEEE Signal Processing Magazine*, Vol. 9, No. 1, pp. 14-35, January 1992.

80. Hocanın, A. and Hakan Deliç, "Robust detection in DS-CDMA", *IEEE Transactions on Vehicular Technology*, Vol. 51, No. 1, pp. 155-170, January 2002.

81. Kobayashi, M., J. Boutros, and G. Caire, "Successive interference cancellation with SISO decoding and EM channel estimatin", *IEEE Journal on Selected Areas of Communications,* Vol. 19, No. 8, pp. 1450-1460, August 2001.

82. Larson, H. J. and B. O. Shubert, *Probabilistic models in engineering sciences*, Malabar, Fla. : R.E. Krieger Pub. Co., 1989.